The roles of BRCA2 in chromosome integrity

by

Florian Joseph Groelly

A thesis submitted for the degree of

Doctor of Philosophy



St Cross College, University of Oxford

Hilary Term 2021

The roles of BRCA2 in chromosome integrity

A thesis submitted to the University of Oxford
for the degree of *Doctor of Philosophy*
Florian Joseph Groelly
St Cross College, Hilary term 2021

High frequency of fork stalling and fork degradation are associated with DNA damage accumulation and represent key replication pathologies in cells lacking BRCA2. As a consequence, these cells enter mitosis with under-replicated DNA, which leads to interlinks between sister chromatids in anaphase. Failure to resolve these interlinks causes chromosome mis-segregation, aneuploidy and micronuclei. Here we show that BRCA2 loss leads to micronuclei formation, which triggers an innate immune response signalling via activation of the cGAS-STING pathway. However, cleavage of these interlinks by the MUS81 endonuclease activates mitotic DNA synthesis (MiDAS), thereby completing genome replication and ensuring correct chromosome segregation. Which genomic loci require BRCA2 for their replication and therefore become unstable upon BRCA2 inactivation remains unknown. Here we label mitotic nascent DNA and perform EdU-seq to monitor at high-resolution sites where MiDAS occurs in absence of BRCA2. Our findings reveal that loss of BRCA2 triggers MiDAS at 150 genomic loci, which map within regions replicating in early S phase and are therefore distinct from aphidicolin-induced common fragile sites. Our results suggest that BRCA2 inactivation causes replication failure at early-replicating genomic regions, a subset of which completes replication during mitosis.

Acknowledgements

I would like to thank Madalena Tarsounas for welcoming and advising me throughout my DPhil. Not only did I benefit from her scientific guidance, but I was also able to gain precious communication, responsibility, leadership and teamworking experience.

I also would like to thank Thanos Halazonetis for hosting me in his laboratory. Many thanks to Frank, Jeltje, Pauline and Elena for organising my secondment at Merck KGaA. Whilst the work performed during these 2 months is not directly described in this thesis, I had an exceptional first touch of the contribution of Medical Affairs.

Thank you to my colleagues, Rebecca, Giuliana, Angelina, Timo, Hugo, Emilia, Yanti, Pia, Yuri, Sophie, Anastasiya and Irene, for the great moments shared inside and outside of the lab. In particular, thank you to Rebecca for teaching me a plethora of molecular and cell biology techniques, and to Timo for the fruitful teamwork as well as for commenting on this thesis.

To my dearest housemates, Ashwin, Charlotte, Luana, Sergio, Nico, and Gabriele: what great times we had. Thank you for your support, for picking (not only) the best movies and for experimenting my cuisine.

Thank you to all my dearest friends and all the people who made my Oxford experience exceptional: Timo, Hugo, Ashwin, Luana, Asmita, Maria, Viviana, Giovanna, Angela, Andrea, Prashanti, Gerardo, Simone, Sophie, Egon, Manon, Niloufar, Jakob, Javier, Sam, Shudong, John, Tiffany, Christie, Giacomo, Tzveta, Salomé, Shahd, Jack, James, Xiaoning, Hongbin, Lottie, Tobias and many others.

I would like to thank all members of the SYNTRAIN network for the great collaborations, training and outcomes. In particular thank you to all the fellows for the great atmosphere: Giacomo, Giorgos, Christos, Nibal, Ana, Mariana, Luka, Karolin, Nanda, Bishoy, Aleks, Anna, Jemina, and Timo.

Thank you who were not here but supported nonetheless: Charlotte, Eileen, Pierre-Louis, Cédric, Émilie, Stéphanie, Aurélia, Maxime, Dario, Michael, Hugo, Johanna, and many others. A special note also goes to my parents, Patrick and Christine, as well as to my siblings, Nicolas and Marie.

Declaration of authorship

I confirm that this thesis I am submitting is wholly my own work except where otherwise indicated. Part of this thesis was published in peer-reviewed journals (Reisländer *et al.*, 2019; Reisländer, Groelly and Tarsounas, 2020).

The cells for RNA-sequencing were grown by Timo Reisländer and differential gene expression was analysed by Emilia Puig Lombardi. Quantitative reverse transcription PCR (RT-qPCR) was performed by Timo Reisländer, using sample prepared together. Analysis of the EdU-sequencing data was done with help from Emilia Puig Lombardi.

Funding

The work presented here was performed at the Department of Oncology, University of Oxford and has received funding from the European Union's Horizon 2020 research and innovation programme under the Marie Skłodowska-Curie grant agreement number 722729.

Table of contents

The roles of BRCA2 in chromosome integrity ..... **II**

Acknowledgements ..... **III**

Declaration of authorship ..... **V**

Funding ..... **V**

Table of contents ..... **VI**

List of tables ..... **X**

List of figures ..... **XI**

List of abbreviations ..... **XIII**

Chapter 1 Introduction **16**

1.1 DNA damage, DNA repair pathways and genome stability 17

1.1.1 DNA as the molecular basis of genetic information 17

1.1.2 Damage of nucleic bases and repair 18

1.1.3 Mechanisms of SSB repair 20

1.1.4 Mechanisms of DSB repair 21

1.2 Stalled replication forks as a source of genomic instability 25

1.2.1 Functions of BRCA2 at stalled replication forks 25

1.2.2 Restart of stalled replication forks in BRCA2-deficient cells 30

1.3 Chromosome fragility 32

1.3.1 Common fragile sites 32

1.3.2 Other fragile sites 34

1.3.3 Mitotic DNA synthesis (MiDAS) 34
1.3.4 BRCA2 inactivation in chromosome fragility and instability 38
1.4 Research aims 38

Chapter 2 Material and methods 40
2.1 Cell lines and cell culture 41
2.2 RNA-sequencing (RNA-seq) 42
2.3 RNA-seq data processing 42
2.4 Differential gene expression analysis 43
2.5 Quantitative RT-PCR 43
2.6 Western blotting 44
2.7 Resazurin-based viability assay 45
2.8 Flow cytometry-based assays 46
2.8.1 Detection of EdU and Histone H3 (S10) 46
2.8.2 Cell cycle analysis 46
2.8.3 S phase entry 47
2.8.4 S-to-M progression 47
2.8.5 DNA content analysis 47
2.9 Drug treatment 47
2.10 Cell synchronization for mitotic EdU-seq 48
2.11 EdU-seq 48
2.12 EdU-seq data processing 50
2.13 Analysis of MiDAS peaks 50
2.14 Analysis of the replication timing 51
2.15 Assignment of genic and intergenic regions 51
2.16 Statistical analyses 51

Chapter 3 BRCA2 abrogation activates the cGAS-STING-IRF3 and JAK-STAT pathways to promote expression of interferon-stimulated genes ... 52

3.1 Introduction ... 53

3.2 Characterisation of the inducible models for BRCA2 inactivation ... 54

3.3 Long-term BRCA2 abrogation triggers innate immune response signalling ... 57

3.4 Long-term BRCA2 abrogation activates the cGAS-STING-IRF3 and the JAK-STAT pathways ... 59

3.5 PARP inhibitors enhance the type I innate immune response in BRCA2-deficient cells ... 65

3.6 DNA damaging agents targeting BRCA2-deficiency trigger a type I IFN response ... 69

3.7 Functional up-regulation of ISG15 and its ISGylation activity ... 71

3.8 Discussion ... 73

Chapter 4 Protocols for high-resolution detection of mitotic DNA synthesis (MiDAS) using mitotic EdU-seq. ... 79

4.1 Introduction ... 80

4.2 Synchronous S phase progression ... 80

4.3 Cell synchronisation in G2/M ... 83

4.4 Protocol for detection of MiDAS under untreated conditions using mitotic EdU-seq ... 83

4.5 Low dose aphidicolin delays S phase progression ... 85

4.6 Protocol for detection of MiDAS events induced by low dose aphidicolin 88

4.7 Discussion ... 90

Chapter 5 High-resolution detection of MiDAS upon BRCA2 abrogation . 93

5.1 Introduction 94

5.2 Detection of aphidicolin-induced MiDAS at common fragile sites..... 95

5.3 Detection of MiDAS in BRCA2-deficient cells..... 99

5.4 BRCA2 abrogation does not activate MiDAS at common fragile sites .. 101

5.5 BRCA2 abrogation activates MiDAS within genomic regions that replicate during early S phase..... 101

5.6 Resemblance between the aphidicolin-induced MiDAS pattern in BRCA2-proficient and BRCA2-deficient cells..... 105

5.7 Discussion..... 107

Chapter 6 Discussion and conclusion..... 111

6.1 Micronuclei formation and innate immune response signalling 112

6.2 Replication defects and mitotic DNA synthesis (MiDAS) 114

6.3 The role of BRCA2 for genome and chromosome stability 116

References 117

Appendix..... 150

List of tables

Table 2.1. Primer pairs used for RT-qPCR. 43

Table 2.2. Primary antibodies used for immunoblotting. 45

Table 2.3. Secondary antibodies used for immunoblotting. 45

List of figures

Fig. 1.1. Repair pathway for SSBs. 21

Fig. 1.2. Repair pathways for DSBs. 29

Fig. 1.3. Mechanisms of stabilisation and restart of stalled replication forks. 32

Fig. 1.4. Model of MiDAS at under-replicated loci. 37

Fig. 2.1. Strategy for high-resolution detection of nascent DNA using EdU-seq 49

Fig. 3.1. Time-dependent activation of the cGAS-STING-IRF3 and JAK-STAT pathways upon BRCA2 depletion. 56

Fig. 3.2. RNA-seq analysis reveals upregulation of immune response signalling upon long-term BRCA2 depletion. 58

Fig. 3.3. Time-dependent expression of interferon-stimulated genes (ISGs) upon BRCA2 depletion. 61

Fig. 3.4. Time-dependent activation of the cGAS-STING-IRF3 and JAK-STAT pathways upon BRCA2 depletion. 64

Fig. 3.5. Olaparib-treatment affects growth and survival of BRCA2-deficient H1299+sh*BRCA2*^{DOX} cells..... 67

Fig. 3.6. Olaparib-treatment activates the cGAS-STING-IRF3 and JAK-STAT pathways in BRCA2-deficient H1299+sh*BRCA2*^{DOX} cells. 68

Fig. 3.7. DNA damaging agents activate the cGAS-STING-IRF3 and JAK-STAT pathways in BRCA2-deficient H1299+sh*BRCA2*^{DOX} cells. 70

Fig. 3.8. Functional expression of ISG15 upon BRCA2 depletion and Olaparib treatment. 72

Fig. 3.9. Interplay between the DNA damage response and the innate immune response for cancer (immuno-)therapy. 78

Fig. 4.1. Cell cycle progression after thymidine block and release. 82
Fig. 4.2. RO-3306-induced G2 block does not stop S phase progression. ... 85
Fig. 4.3. Mitotic EdU-seq protocol for H1299+sh*BRCA2*^{DOX} cells. 86
Fig. 4.4. S phase progression upon aphidicolin treatment. 87
Fig. 4.5. Mitotic EdU-seq protocol for aphidicolin-treated H1299+sh*BRCA2*^{DOX} cells. 90
Fig. 5.1. Detection of MiDAS in BRCA2-proficient H1299+sh*BRCA2*^{DOX} treated or not with aphidicolin. 96
Fig. 5.2. MiDAS upon aphidicolin treatment takes place at known common fragile sites. 98
Fig. 5.3. Detection of MiDAS in BRCA2-deficient H1299+sh*BRCA2*^{DOX} cells. 100
Fig. 5.4. BRCA2 inactivation and aphidicolin-treatment trigger MiDAS at distinct genomic regions 102
Fig. 5.5. BRCA2 inactivation triggers MiDAS at early S phase replicating domains. 104
Fig. 5.6. Comparison of aphidicolin-induced MiDAS in BRCA2-proficient and BRCA2-deficient cells. 106

List of abbreviations

%	Percent
ºC	Celsius degree
DNA	Deoxyribonucleic acid
A	Adenosine
BER	Base-excision repair
BIR	Break-induced repair
C	Cytosine
cDNA	Complementary DNA
D-loop	Displacement loop
Da	Dalton(s)
DDR	DNA damage response
DMEM	Dulbecco's Modified Eagle's Medium
DMSO	Dimethyl sulfoxide
DOX	Doxycycline
DSB	Double-strand break
DSBR	Double-strand break repair
DTT	Dithiothreitol
EDTA	Ethylenediaminetetraacetic acid
EdU	5-Ethynyl-2´-deoxyuridine
EdU-seq	EdU-sequencing
ERFS	Early replicating fragile sites
FBS	Foetal bovine serum
FDR	False discovery rate
Fig.	Figure

FISH	Fluorescence in situ hybridization
G	Guanine
GO	Gene Ontology
h	Hour(s)
HR	Homologous recombination
HRP	Horseradish peroxidase
HU	Hydroxyurea
IFN	Interferon
IR	Ionising radiation
ISG	Interferon-stimulated gene
ISRE	IFN-stimulated response elements
M	Molar
MiDAS	Mitotic DNA synthesis
min	Minute(s)
MMR	Mismatch repair
mtDNA	Mitochondrial DNA
NER	Nucleotide excision repair
NHEJ	Non-homologous end joining
PAR	Poly [ADP-ribose]
PARG	PAR glycohydrolase
PARP	PAR polymerase
PBS	Phosphate saline buffer
PBST	0.05% Tween 20 in PBS
PCR	Polymerase chain reaction
QIBC	Quantitative image-based cytometry

RNA	Ribonucleic acid
RNA-seq	RNA-sequencing
ROS	Reactive oxygen species
RT-qPCR	Quantitative reverse transcription PCR
SDS	Dodecyl sulfate-polyacrylamide
SDSA	Synthesis-dependent strand annealing
shRNA	Short hairpin RNA
siRNA	Small interfering RNA
SSA	Single-strand annealing
SSB	Single-strand break
ssDNA	Single-stranded DNA
T	Thymidine
UV	Ultra-violet
V	Volt

Chapter 1

Introduction

1.1 DNA damage, DNA repair pathways and genome stability

1.1.1 DNA as the molecular basis of genetic information

The human genome consists of linear arrays of nucleotides forming double-stranded DNA (deoxyribonucleic acid) molecules assembled into 23 pairs of chromosomes within the nucleus (Gartler, 2006). A fraction of the genetic information is also stored on circular DNA within mitochondria (Taanman, 1999), known as mitochondrial DNA (mtDNA). The human genome is highly conserved among the population, with variations randomly distributed across the genome (Genomes Project *et al.*, 2010; Genomes Project *et al.*, 2015). Because DNA is duplicated in a semi-conserved manner (Meselson and Stahl, 1958), all of an individual's nucleated cells should, in theory, contain the same genetic information. There are, however, specific cellular contexts that can lead to programmed changes in the genetic information. Prominent examples are lymphocytes undergoing V(D)J recombination (Roth and Craig, 1998; Schatz and Ji, 2011) and gametes undergoing meiosis (Marston and Amon, 2004). Importantly, spontaneous changes in the nucleotide sequence can occur as a consequence of inaccurate DNA replication (e.g., nucleotide mismatch) or of inaccurate repair of DNA damage (Abbotts and Wilson, 2017; Tubbs and Nussenzweig, 2017).

DNA damage can arise spontaneously, as a result of cellular metabolism, or can be caused by exposure to exogenous genotoxic agents. DNA damage can interfere with DNA replication and transcription and can trigger cellular senescence or apoptosis. If incorrectly repaired, DNA damage can lead to mutations, such as point mutations, insertion and deletions (indels), chromosome rearrangements and chromosome fusions (Abbotts and Wilson, 2017; Tubbs and

Nussenzweig, 2017). Of note, a DNA alteration, which is highly relevant in the context of cancer, is DNA methylation (Ehrlich, 2002; Das and Singal, 2004). It however does not alter nucleotide sequences, but impacts on DNA transcription: promoter hypermethylation can result in loss of gene expression. DNA methylation is, however, part of the cell's epigenome, which is beyond the scope of this thesis.

1.1.2 Damage of nucleic bases and repair

Spontaneous DNA damage often affects nucleic bases, through deamination of cytosine, guanine or adenine that can negatively impact on genome stability (Abbotts and Wilson, 2017). Deamination of cytosine or adenine does not directly impact on the Watson-Crick base pairing. However, deamination of methylated cytosine (5-methylcytosine) produces thymidine, which can result in a C-to-T mutation. This DNA lesion is repaired by the base-excision repair (BER) pathway (Abbotts and Wilson, 2017; Wu and Zhang, 2017), which requires the G/T mismatch-specific thymine DNA glycosylase and produces an abasic sites. Such sites can also result from the spontaneous cleavage of the covalent bound between the deoxyribose and an adenine or guanine base. Repair of abasic sites requires the recruitment of the apurinic/apyrimidinic endonucleases APE1 or APE2, which leads to the formation of a DNA single-strand break (SSB; see below).

Replication of damaged nucleic bases can also lead to mismatched Watson-Crick bases. DNA polymerases are error-prone enzymes with an error rate ranging from 10^{-3} to 10^{-7}. The high-fidelity polymerases, including DNA polymerase δ or ε, replicate most of the human genome and exhibit a proofreading exonuclease activity (Kunkel, 2004; Kunkel and Erie, 2015; Liu,

Keijzers and Rasmussen, 2017). In contrast, low fidelity DNA polymerases including polymerase tetha (POLQ), are usually required for translesion synthesis and lack the proof-reading mechanism, inserting errors at a rate of 10^{-3} (Arana *et al.*, 2008). Whilst mismatches do not represent DNA damage *per se*, they can be mutagenic and alter gene expression and therefore their detection by the DNA mismatch repair (MMR) pathway is critical for genome stability. MMR activation leads to the excision of several hundred nucleotides surrounding the mismatch, followed by pol δ/ε-dependant DNA re-synthesis and ligation (Kunkel and Erie, 2015; Hsieh and Zhang, 2017).

Nucleic bases can also be damaged by endogenous and exogenous agents, including reactive oxygen species (ROS) or ultra-violet (UV) light, respectively. For example, exposure to UV light catalyses the formation of pyrimidine dimers between two consecutive thymidine or cytosine bases (Rastogi *et al.*, 2010; Abbotts and Wilson, 2017). Failure to repair pyrimidine dimers causes increased frequency of C-to-T substitutions and DNA deletions (Sale, 2013). Studies into the genetic and molecular defects underlying the Cockayne syndrome or xeroderma pigmentosum disorders, led to the discovery of specific repair mechanisms for bulky DNA lesions, such as UV-induced pyrimidine dimers (Cleaver, Lam and Revet, 2009; Vaisman and Woodgate, 2017). Indeed, Cockayne syndrome patients suffer from photosensitivity and neurological disorders caused by deleterious mutations in the *ERCC6* (sometimes referred to as *CSB*) or *ERCC8* (or *CSA*) genes, whose products are essential for nucleotide excision repair (NER) (Cleaver, Lam and Revet, 2009). The NER pathway detects bulky DNA lesions and promotes the excision of 22-32 nucleotides around the lesion, which results in a single-stranded DNA gap. Subsequently,

DNA polymerases and ligases are required to re-synthesise DNA and complete the repair.

1.1.3 Mechanisms of SSB repair

SSBs are obligate intermediates in several repair pathways, including BER, NER and MMR. Oxidative attack of the deoxyribose constitutive of the DNA backbone by ROS represent a well-characterised source of SSBs. Importantly, direct sugar disintegration leads to lesions of the 5'-phosphate or 3'-hydroxyl groups, which are particularly cytotoxic (Kathe, Shen and Wallace, 2004). SSBs are deleterious lesions because they can cause replication fork stalling (see below) or can be converted to DNA double-strand breaks (DSBs).

SSB repair pathways are essential for the repair of SSBs arising during BER or NER and resembles the repair of direct SSBs (Caldecott, 2008; Abbotts and Wilson, 2017). Consequently, these different repair mechanisms are considered to be sub-pathways of SSB repair pathway (Caldecott, 2008). Four steps define the SSB repair pathway: 1) SSB detection and signalling; 2) 5'- and 3'-termini processing; 3) DNA gap filling; 4) DNA ligation. For example, ROS-induced SSBs are detected by members of the poly [ADP-ribose] (PAR) polymerase (PARP) family, which conjugate PAR units to proteins present at the break, including itself, in a process known as PARylation. Conversely, dePARylation is mediated by the PAR glycohydrolase (PARG). PARylation and dePARylation events facilitate the recruitment of the SSB repair protein XRCC1, which acts as a scaffold for the recruitment and assembly of further SSB repair factors. Amongst those, DNA end processing enzymes, such as DNA polymerase β, FEN-1 or APE1, are required to remove damaged 5'- or 3'-flaps, thus allowing access of DNA polymerases, for instance the previously mentioned Pol δ/ε, to fill

the DNA gap, and of DNA ligases to covalently attach the newly synthesis DNA to the original DNA strand.

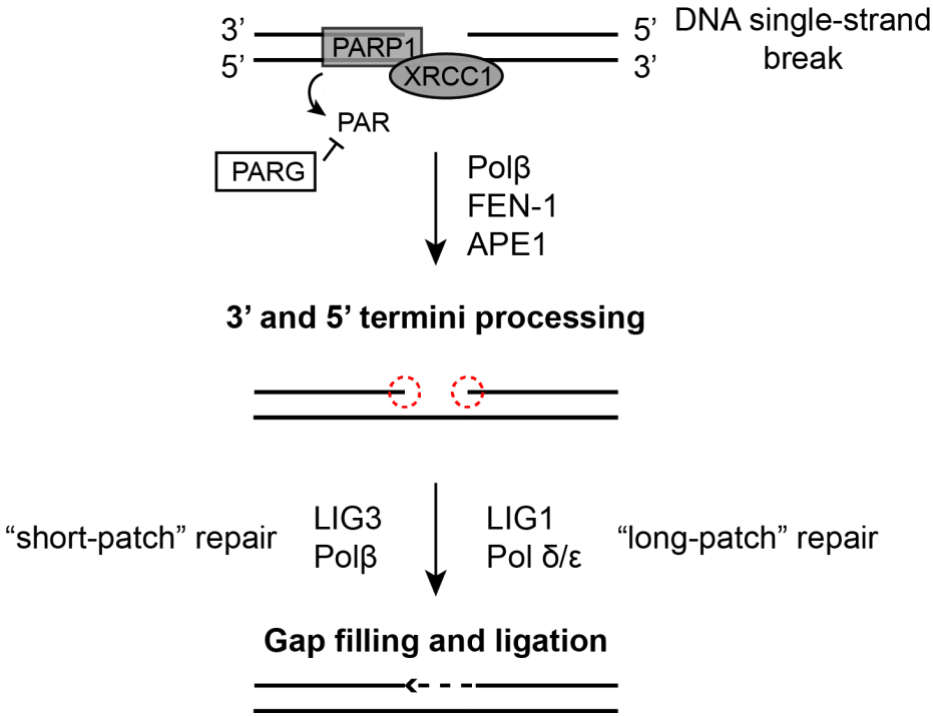


Fig. 1.1. Repair pathway for SSBs.

SSBs are detected by PARP1, which PARylation activity is counteracted by PARG. These events trigger the recruitment of downstream repair factors, including the XRCC1 scaffold protein. Next, damaged DNA ends are processed by Polβ, FEN-1 or APE1 in preparation for DNA gap filling and ligation. Upon short-patch repair. Polβ and LIG3 are responsible for the synthesis of the missing nucleotide and its ligation, respectively. Upon long-patch repair, Pol δ/ε synthesise 2–12 nucleotides and LIG1 catalyses DNA ligation.

1.1.4 Mechanisms of DSB repair

DSBs may arise from unrepaired SSB, from exposure to DNA damaging agents, such as the TOP1 poison etoposide, ionising radiation (IR) or crosslinking agents including platinum drugs, or from the collapse of stalled replication forks (Chang *et al.*, 2017; Scully *et al.*, 2019). DSBs are less frequent, yet more cytotoxic than SSBs (Abbotts and Wilson, 2017; Chang *et al.*, 2017). Moreover, these lesions

are highly mutagenic as illustrated by increased tumorigenesis onset after exposure to IR (Gilbert, 2009), a source of DSBs routinely used in the clinic for cancer treatment (Baskar *et al.*, 2012). DSB detection by the heterotrimeric complex MRN, formed by MRE11, RAD50 and NBS1, stimulates ATM, which initiates the cellular DNA damage response (DDR,(Abbotts and Wilson, 2017; Blackford and Jackson, 2017; Chang *et al.*, 2017)). ATM kinase activity is required to orchestrate DSB repair and/or to phosphorylate p53, which arrests cell cycle progression (Banin *et al.*, 1998; Canman *et al.*, 1998).

ATM activation triggers two main DNA DSB repair pathways: non-homologous end joining (NHEJ) and homologous recombination (HR). Alternative end-joining (sometimes referred to as microhomology-mediated end joining) and single-strand annealing (SSA) rely on the annealing of short homologous sequences and are considered to be backup repair pathways (Ceccaldi, Rondinelli and D'Andrea, 2016; Chang *et al.*, 2017; Scully *et al.*, 2019). Whilst NHEJ is active both in interphase, HR repair is restricted to S and G2 phases, where a sister chromatid is available as a template for repair (Hustedt and Durocher, 2016). Because it uses an intact DNA molecule as template, HR is considered the most accurate DSB repair pathway. Whether NHEJ is indeed mutagenic is still unclear, as increasing evidence suggests that either failed NHEJ or its illegitimate activation can lead to toxic DSB repair (Zong *et al.*, 2015; Balmus *et al.*, 2019).

The choice of DNA repair pathway at a given DSB is not only regulated by the cell cycle stage, but also by the type of DNA ends. Blunt or short single-stranded DNA ends are preferentially repaired by NHEJ, whilst long single-stranded DNA ends favour HR (Chang *et al.*, 2017; Scully *et al.*, 2019).

Consistently, 53BP1 (Bunting *et al.*, 2010), RIF1 (Chapman *et al.*, 2013; Di Virgilio *et al.*, 2013; Escribano-Diaz *et al.*, 2013; Zimmermann *et al.*, 2013) and REV7 (also known as MAD2L2; (Boersma *et al.*, 2015; Xu *et al.*, 2015)) act together to counteract DNA end resection at DSBs and promote NHEJ. Recent studies showed that SHLD3 binds to RIF1 to recruit REV7 to DSBs. REV7 and SHLD3 interact with SHLD1-SHLD2 to form the Shieldin complex (Dev *et al.*, 2018; Ghezraoui *et al.*, 2018; Gupta *et al.*, 2018; Mirman *et al.*, 2018; Noordermeer *et al.*, 2018). Upon its recruitment, SHLD2 is believed to bind to ssDNA at the DSB and protect DNA ends from resection. Whether ssDNA is required for the assembly of the Shieldin complex and which factors promote the formation of ssDNA at Shieldin-protected DSBs remain unknown (Noordermeer and van Attikum, 2019). The heterotrimeric CST complex, formed by CTC1, STN1 and TEN1, also impact on DSB repair pathway choice by counteracting resection. Indeed, the CST complex interacts with the Shieldin complex and is recruited to DSBs (Mirman *et al.*, 2018), where it promotes Pol α-mediated fill-in DNA synthesis of resected ends (Barazas *et al.*, 2018; Mirman *et al.*, 2018). Consistent with their functions at DSBs, loss of 53BP1, RIF1 or of members of the Shieldin or CST complexes restores HR and causes resistance to PARP inhibitors in BRCA1-deleted cells (Noordermeer and van Attikum, 2019).

The recruitment of the heterodimeric Ku70-Ku80 complex to each DNA end constitutes the first step of DSB repair by NHEJ. Next, two DNA-PKcs molecules interact with the Ku heterodimers to form the DNA-PK complex. Bridging of the broken ends through the DNA-PK complex creates a “long-range” synaptic complex (Scully *et al.*, 2019). The recruitment of XRCC4, LIG4, XLF and PAXX (Tadi *et al.*, 2016) permits the alignment of broken DNA ends and the

formation of a “short-range” synaptic complex (Scully *et al.*, 2019). ATM-mediated DNA-PKcs phosphorylation is required to recruit Artemis and specialised DNA polymerases to process DNA ends. Finally, DNA-PKcs autophosphorylation promotes DNA end ligation (Jiang *et al.*, 2015).

DSB repair by HR requires formation of long single-strand DNA overhangs at the DSB site (Chang *et al.*, 2017; Scully *et al.*, 2019). Whilst the importance of BRCA1 in promoting DNA end resection is yet unclear (Tarsounas and Sung, 2020), the nucleolytic activity of the MRN complex and the CtIP protein are required to initiate resection (Sartori *et al.*, 2007). Other factors further promote long-range DNA resection, including the EXO1 and DNA2 nucleases, as well as the BLM helicase (Scully *et al.*, 2019). The newly generated single-stranded DNA is rapidly coated by the heterotrimeric RPA complex, which prevents its degradation or annealing to another single-stranded DNA. Next, the BRCA1-BARD1 complex (Tarsounas and Sung, 2020) cooperates with PALB2 (Xia *et al.*, 2006; Zhang *et al.*, 2009; Zong *et al.*, 2019; Belotserkovskaya *et al.*, 2020) and the BRCA2-DSS1 complex (Pellegrini *et al.*, 2002; Yang *et al.*, 2002) to promote the exchange of RPA with RAD51 on single-stranded DNA (Ogawa *et al.*, 1993; Sung, 1994). BRCA1-BARD1 (Zhao *et al.*, 2017) and RAD54 (Petukhova, Stratton and Sung, 1998; Mazina and Mazin, 2004) stimulate RAD51-mediated invasion the sister chromatid and homology search (Petukhova, Stratton and Sung, 1998) (Bugreev and Mazin, 2004; Xu *et al.*, 2017b). Annealing of the RAD51-nucleoprotein filament to a complementary sequence within the homologous sister chromatid strand displaces the non-complementary strand, to form a displacement loop (D-loop). The second RAD51 nucleofilament anneals to the displaced strand and generates a four-way

branched DNA structure called double Holliday junction. Alternatively, synthesis-dependent strand annealing (SDSA) promotes the re-annealing of the invading strand with the non-invading, second DSB DNA end. The invaded strand serves as a template for pol δ-dependant DNA synthesis. Subsequent gap filling and ligation complete DNA repair (Scully *et al.*, 2019).

Double-strand break repair (DSBR) promote the formation of double Holliday junction, where both DSB DNA ends anneal to their complementary sister chromatid strand. Two distinct pathways may promote resolution of the double Holliday junction, which is required to complete of HR repair (Figure 2 (Li and Heyer, 2008; Tarsounas and Sung, 2020)). Resolution of double Holliday junctions by the scaffold protein complex SLX1-SLX4 and nucleases such as MUS81 or GEN1 can lead to chromosomal crossover. In contrast, non-crossover dissolution of double Holliday junctions requires the interaction of BLM, TOPIIIα, RMI1 and RMI2. It is noteworthy that a break-induced replication (BIR), which has been described as a third pathway for D-loop resolution in yeast, is involved in the repair of collapsed replication forks in human cells (Costantino *et al.*, 2014; Sotiriou *et al.*, 2016). In this pathway, the invading strand uses the sister chromatid to replicate the entire distal part of the chromosome.

1.2 Stalled replication forks as a source of genomic instability

1.2.1 Functions of BRCA2 at stalled replication forks

Replication fork barriers, such as DNA crosslinks, DNA-protein crosslinks, 3' adducts or abasic sites, impede the progression of the replisome, leading to replication fork stalling. This is caused by uncoupling of the helicase and polymerase activities and leads to accumulation of single stranded DNA (Byun *et*

al., 2005; Saldivar, Cortez and Cimprich, 2017; Berti, Cortez and Lopes, 2020). Several pathways have been shown to act at stalled replication forks to promote their restart and stabilisation, and to prevent DNA damage (Saldivar, Cortez and Cimprich, 2017; Berti, Cortez and Lopes, 2020). For example, transcription-replication conflicts have been shown to cause replication fork stalling (Hamperl *et al.*, 2017; Macheret and Halazonetis, 2018; Chappidi *et al.*, 2020) and underlie oncogene-induced replication stress. Similarly, spontaneous or chemically-induced stabilisation of the topoisomerase-1 or topoisomerase-2 complexes prevents replication fork progression. Whilst BRCA2 protects stalled replication forks (see below), the SPRTN or FAM111A proteases orchestrate the resolution of the DNA-protein crosslink (Ruggiano and Ramadan, 2021). BRCA1 has also been proposed to act with MRE11 as an alternative pathway for the resolution of topoisomerase-2-DNA adducts (Aparicio *et al.*, 2016; Sasanuma *et al.*, 2018).

BRCA2 acts at stalled replication forks, thereby preventing DNA damage accumulation (Lomonosov *et al.*, 2003). BRCA2 also interacts with RAD51 nucleoprotein filament assembled at stalled forks to prevent the nucleolytic degradation of nascent DNA (Schlacher *et al.*, 2011; Schlacher, Wu and Jasin, 2012). It was later shown that BRCA2 acts downstream of fork remodelling, where the classic three-branch fork is converted into a four-branch structure, called reversed fork (sometimes referred as “chicken foot” structure). This process requires RAD51 (Zellweger *et al.*, 2015; Bhat and Cortez, 2018) but here RAD51 loading is independent of BRCA2. Instead, the DNA translocases HLTF (Kile *et al.*, 2015; Bai *et al.*, 2020), SMARCAL (Couch *et al.*, 2013), ZRANB3 (Ciccia *et al.*, 2012; Weston, Peeters and Ahel, 2012; Vujanovic *et al.*, 2017) or the DNA helicase FBH1 (Fugger *et al.*, 2015) have been shown to promote

reversal of stalled replication forks. BRCA2, however, stabilises the RAD51 nucleofilament on reversed forks to prevents their nucleolytic degradation (Kolinjivadi *et al.*, 2017; Mijic *et al.*, 2017; Taglialatela *et al.*, 2017). Fork reversal therefore generates a structure vulnerable to fork degradation in BRCA2-deficient cells, and suppression of fork remodelling restores fork stability, thus leading to therapy resistance (Kolinjivadi *et al.*, 2017; Mijic *et al.*, 2017; Schlacher, 2017; Taglialatela *et al.*, 2017; Noordermeer and van Attikum, 2019).

RECQ1 restores the classical three-branch structure in a process call branch migration (Berti, Cortez and Lopes, 2020) and permits to restart reversed forks following the repair of the replication fork barrier. BRCA2 may also promote the restart of stalled replication forks via template switch, which resembles the strand invasion step of HR repair reactions (Fig. 1.2). Indeed, Brh2, a yeast (*Ustilago maydis*) ortholog of human BRCA2, has been shown to promote template switch both *in vivo* (Mazloum and Holloman, 2009) and *in vitro* (Giannattasio *et al.*, 2014). Other studies showed that RAD51 promotes the restart of stalled replication forks in human cells (Lambert *et al.*, 2010; Petermann *et al.*, 2010; Zimmer *et al.*, 2016). Whilst fork restart results in double Holliday junctions, it is unclear whether template switch is initiated at intact stalled replication forks or after MUS81-dependent cleavage of the stalled fork (Hanada *et al.*, 2007; Petermann *et al.*, 2010). Moreover, recent evidence suggest that template switch follows re-priming-mediated lesion by-pass (Fig. 1.3 ; (Berti, Cortez and Lopes, 2020)).

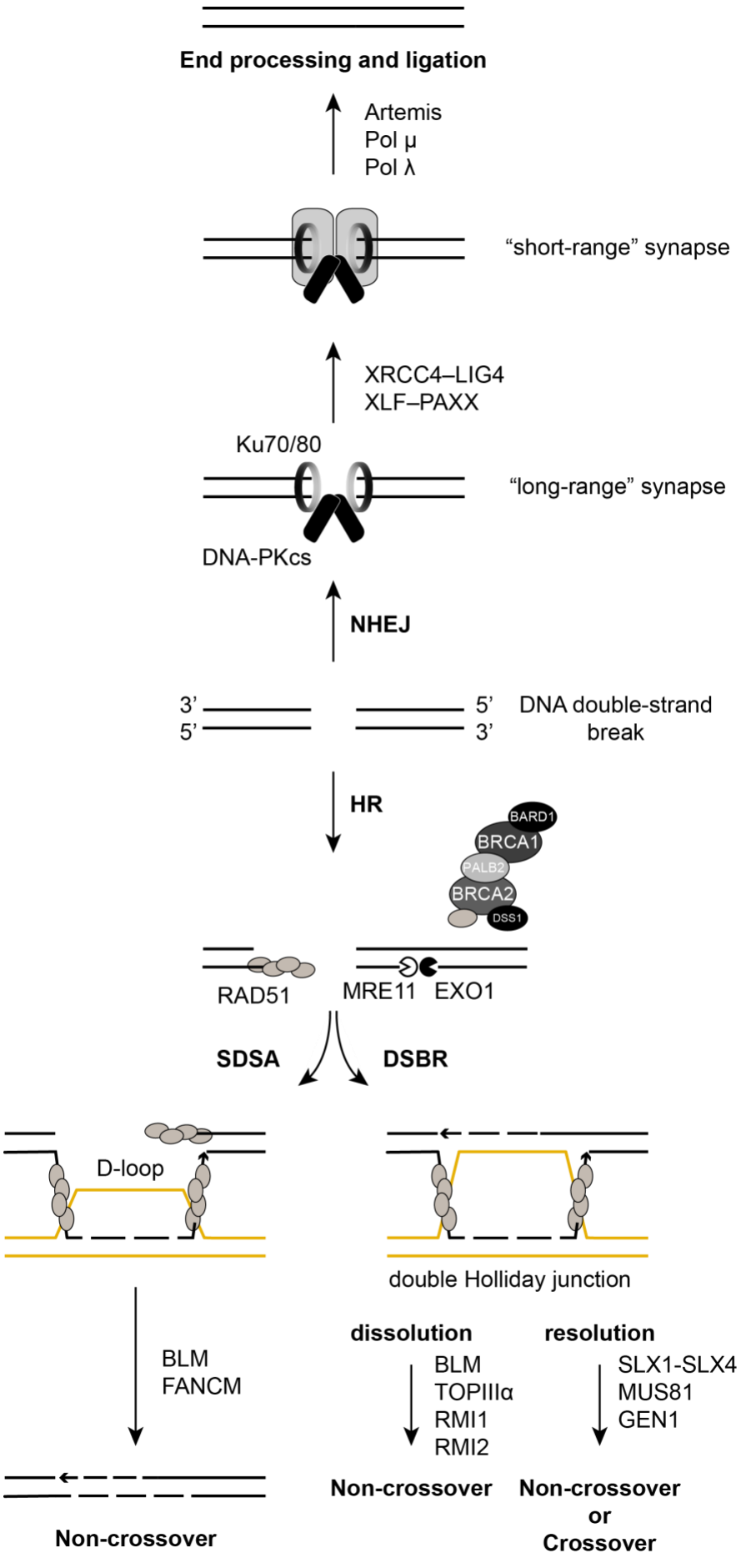

End processing and ligation
Artemis
Pol μ
Pol λ
"short-range" synapse
XRCC4–LIG4
XLF–PAXX
Ku70/80
"long-range" synapse
DNA-PKcs
NHEJ
3'
5'
5'
3'
DNA double-strand break
HR
BARD1
BRCA1
PALB2
BRCA2
DSS1
RAD51
MRE11
EXO1
SDSA
DSBR
D-loop
double Holliday junction
BLM
FANCM
dissolution
resolution
BLM
TOPIIIα
RMI1
RMI2
SLX1-SLX4
MUS81
GEN1
Non-crossover
Non-crossover
Non-crossover
or
Crossover

Fig. 1.2. Repair pathways for DSBs.

DSBs are detected by the MRN complex which recruits ATM to orchestrate DSB repair (not shown). **Top**: Non-homologous end-joining (NHEJ) is initiated by the binding of Ku70/80 to DNA ends, which promotes the recruitment of DNA-PKcs to form a “long-range” synaptic complex. The recruitment of XRCC4-LIG4 and XLF-PAXX brings DNA ends together to form a “short-range” synaptic complex. The nuclease Artemis acts with Pol λ and Pol μ to process DNA ends. Finally, DNA-PKcs autophosphorylation promotes end-joining. **Bottom**: Schematic representation of the homologous recombination (HR) repair pathway. The endonuclease activity of MRE11 initiates DNA resection and its exonuclease activity promote short-range (3’-5’) resection. EXO1 and DNA2 promote long-range (5’-3’) resection. BRCA1, PALB2 and BRCA2 target RAD51 to ssDNA, where it displaces RPA (not shown). Invasion of the sister chromatid by the RAD51 nucleofilament results in the formation of a D-loop (left). Capture of the displaced strand generate a double Holliday junction (right). Disassembly of the D-loop leads is a non-crossover pathway. “Dissolution” or “resolution” of double Holliday junctions are non-crossover or crossover pathways, respectively. Sister chromatids are shown in yellow. Newly synthesised DNA is shown as dashed lines. SDSA: synthesis-dependent strand annealing; DSBR: double-strand break repair.

An alternative fork restart pathway requires PrimPol-mediated re-priming downstream of the DNA lesions (Mouron *et al.*, 2013). Because re-priming does not require fork remodelling (Bai *et al.*, 2020; Quinet *et al.*, 2020), PrimPol has been associated with increased fork stability and therapy resistance in BRCA2-deficient cells (Quinet *et al.*, 2020). PrimPol-mediated fork restart is, however, associated with ssDNA gaps (Piberger *et al.*, 2020; Quinet *et al.*, 2020), which undergo post-replicative repair (Berti, Cortez and Lopes, 2020). Whilst the exact function of BRCA2 at these sites is not clearly established, a recent study

reported a DSB-independent role of HR in ssDNA gap-filling (Piberger *et al.*, 2020). This suggests that BRCA2 may not only act at stalled replication forks, but is also required to promote genome stability downstream, following BRCA2-independent fork restart.

1.2.2 Restart of stalled replication forks in BRCA2-deficient cells

In addition to PrimPol-mediated DNA re-priming, translesion DNA synthesis represents another tolerance mechanism, which requires specific polymerases, such a DNA polymerase eta (Pol η). These low-fidelity polymerases are specialised in the replication of damaged nucleic bases (Sale, 2013; Vaisman and Woodgate, 2017).

Additionally, MUS81 is known to promote fork restart by creating a substrate to initiate HR in a BRCA2-dependent manner (Hanada *et al.*, 2007; Petermann *et al.*, 2010). However, recent reports proposed a role of MUS81 in BRCA2-independent fork restart (Lemacon *et al.*, 2017; Rondinelli *et al.*, 2017). Cleavage of stalled replication forks by MUS81 rescues nascent DNA degradation and activates a break-induced repair (BIR)-like repair, which requires POLD3 (Lemacon *et al.*, 2017). It is noteworthy that MUS81 is involved in mitotic BIR mechanisms following replication stress. Indeed, MUS81 activates mitotic DNA synthesis (MiDAS) at under-replicated loci (Minocherhomji *et al.*, 2015), including in the context of BRCA2 deficiency (see below; (Feng and Jasin, 2017; Lai *et al.*, 2017).

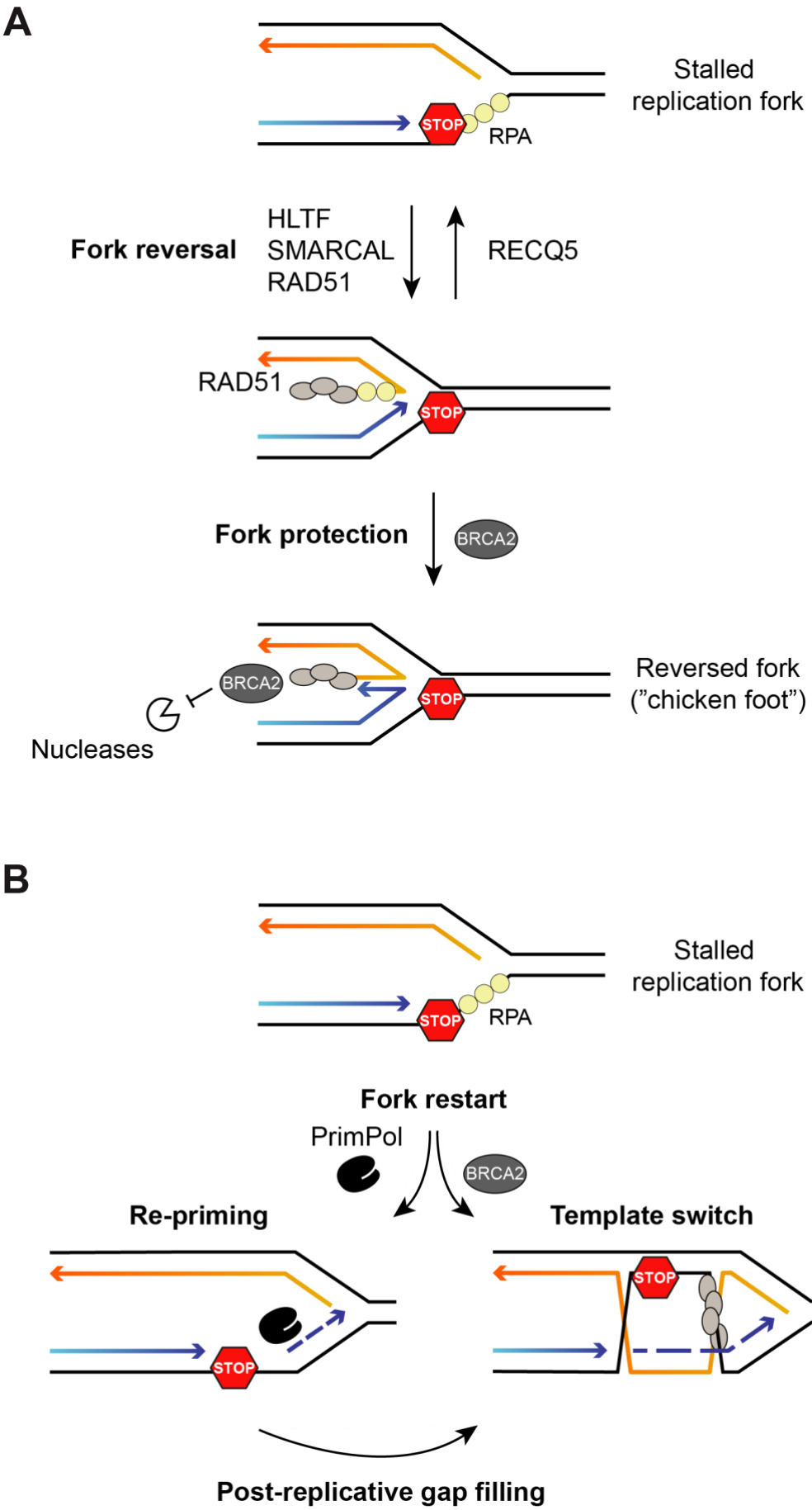

A
Stalled
replication fork
STOP
RPA
Fork reversal
HLTF
SMARCAL
RAD51
RECQ5
RAD51
STOP
Fork protection
BRCA2
BRCA2
STOP
Reversed fork
("chicken foot")
Nucleases
B
Stalled
replication fork
STOP
RPA
Fork restart
PrimPol
BRCA2
Re-priming
Template switch
STOP
STOP
Post-replicative gap filling

Fig. 1.3. Mechanisms of stabilisation and restart of stalled replication forks.

Replication fork barriers cause helicase-polymerase uncoupling and accumulation of RPA-coated ssDNA. (**A**) Schematic representation of fork reversal and protection. RAD51 monomers compete with RPA for binding at ssDNA and form transient, unstable filaments. The recruitment of DNA translocases promotes fork reversal, whilst RECQ5 counteracts it. BRCA2 stabilises RAD51 nucleofilaments on ssDNA, which protects reversed forks from nucleolytic degradation. (**B**) Schematic representation of fork restart. During template switch (right), RAD51 loading onto the ssDNA promotes the annealing of the parental strands and allows the replication to resume using the nascent strand (orange strand) as a template for DNA synthesis. Alternatively, PrimPol-mediated re-priming (left) promotes DNA synthesis downstream of the replication fork barrier. The ssDNA gap can be refilled by translesion DNA synthesis (not shown) or template switch reactions. Newly synthesised DNA is shown as dashed lines.

1.3 Chromosome fragility

1.3.1 Common fragile sites

Cytogeneticists identified gaps or breaks within condensed mitotic chromosome (Glover *et al.*, 1984; Sutherland, 2003). In particular, treatment with aphidicolin revealed the presence of chromosome gaps at non-random loci, termed common fragile sites (Glover *et al.*, 1984). To date, 86 common fragile sites have been identified by cytogenetics studies (Wilson *et al.*, 2015). These sites correlate with chromosome rearrangements in cancers and thus, common fragile sites have been associated with tumorigenesis (Glover, Wilson and Arlt, 2017; Debatisse and Rosselli, 2019).

Common fragile sites map to late replicating regions (Le Beau *et al.*, 1998; Debatisse and Rosselli, 2019). Given that premature mitotic entry recapitulated

aphidicolin-induced breaks at common fragile sites (El Achkar *et al.*, 2005), it was suggested that common fragile sites correspond to under-replicated genomic regions upon mitotic entry. Indeed, under-replicated DNA was observed at fragile sites, including common fragile sites, in the form of DNA bridges in anaphase, which are flanked by FANCD2 foci (Chan *et al.*, 2009; Naim and Rosselli, 2009). The recruitment of structure-specific nucleases MUS81-EME1 and XPF-ERCC1 to these anaphase bridges promotes their cleavage and faithful chromosome segregation (Naim *et al.*, 2013; Ying *et al.*, 2013; Duda *et al.*, 2016; Lai *et al.*, 2017). The Bloom syndrome helicase BLM has also been shown to be essential for this process (Chan, North and Hickson, 2007; Chan *et al.*, 2009; Naim *et al.*, 2013; Chan, Fugger and West, 2018). It was therefore proposed that mitotic chromosome breakage followed by MiDAS is a controlled mechanism, which prevents chromosome mis-segregation, cytokinesis failure or micronucleation at under-replicated regions, including common fragile sites.

Unresolved anaphase bridges are visible as 53BP1 nuclear bodies in subsequent G1 phase (Harrigan *et al.*, 2011; Lukas *et al.*, 2011). In particular, treatment with low dose aphidicolin leads to the formation of 53BP1 nuclear bodies at common fragile sites. A recent report proposed that these lesions are repaired in the subsequent S phase, in a RAD52-dependent manner (Spies *et al.*, 2019).

The mechanisms underlying genome under-replication at common fragile sites have been extensively studied yet have only been partially uncovered (Glover, Wilson and Arlt, 2017; Debatisse and Rosselli, 2019). In addition to being late replicating, common fragile sites often map to large, actively transcribed genes (Helmrich, Ballarino and Tora, 2011; Okamoto *et al.*, 2018; Pentzold *et al.*,

2018; Macheret *et al.*, 2020). The paucity of replication origins also governs common fragile site expression (Le Tallec *et al.*, 2011; Letessier *et al.*, 2011). Finally, several reports linked chromosome fragility, including at common fragile sites, to replication fork stalling (Ozeri-Galai *et al.*, 2011; Tubbs *et al.*, 2018).

1.3.2 Other fragile sites

Aphidicolin-induced common fragile sites have been extensively studied, yet chromosome fragility at other sites have also been described. For example, folate-sensitive regions are fragile sites and were describe even before common fragile sites (Sutherland, 2003). These sites lie within micro- or mini-satellites repeats acquiring unusual structures, such as hairpins (Zlotorynski *et al.*, 2003).

More recently, early replicating fragile sites (ERFSs) have been identified upon hydroxyurea (HU)-induced replication in murine B lymphocytes (Barlow *et al.*, 2013). The presence of repetitive deoxyadenosine and deoxythymidine (poly(dA:dT)) tracts may promote replication fork stalling and obstruct their restart (Tubbs *et al.*, 2018). Similar to common fragile sites, ERFSs also correlate with transcription and are sensitive to ATR inhibition (Barlow *et al.*, 2013).

1.3.3 Mitotic DNA synthesis (MiDAS)

EdU foci were detected in mitosis in asynchronous U2OS cells treated with low-dose aphidicolin and pulse-labelled with EdU. Because the duration of the EdU pulse was relatively short compared to the rate of mitotic progression following its onset, it was suggested that the presence of EdU foci in anaphase is unlikely to result from DNA synthesis in interphase. This shed light on MiDAS as compensatory mechanism activated at under-replicated loci in cells exposed to replication stress (Minocherhomji *et al.*, 2015).

Following release from CDK1 inhibitor (RO-3306)-mediated G2 arrest, mitotic EdU foci were detected at FANCD2-labelled common fragile sites. Indeed, MiDAS occurred at apparent chromosome gaps and at known common fragile sites, as shown by fluorescence in situ hybridization (FISH) experiments (Minocherhomji *et al.*, 2015). The authors showed that activation of MiDAS depended on the SLX4 scaffold protein-mediated recruitment of MUS81-EME1 (Minocherhomji *et al.*, 2015) and RAD52 (Bhowmick, Minocherhomji and Hickson, 2016). MUS81 and RAD52 were also required for the recruitment of POLD1 and POLD3, the catalytic and non-catalytic subunits of Pol δ, respectively. Importantly, POLD3 co-localised with EdU foci and its depletion abrogated MiDAS (Minocherhomji *et al.*, 2015). A recent study in *Caenorhabditis elegans* showed that the recruitment of FANCD2 and of MiDAS-promoting factors at under-replicated loci follows TRAIP-mediated replisome disassembly (Sonneville *et al.*, 2019).

Because studies on MiDAS often uses CDK1 inhibition as a mean to reversibly block cells in G2, it remains unclear whether high CDK1 activity alone or whether mitotic entry elicits the detection of under-replicated loci remains unclear. Indeed, CDK1 activity promotes the phosphorylation and activation of MUS81 and EME1 (Duda *et al.*, 2016; Palma *et al.*, 2018). Moreover, mitotic kinases are required for the TRAIP-catalysed ubiquitination of MCM7 by and its subsequent disassembly (Deng *et al.*, 2019; Priego Moreno *et al.*, 2019; Sonneville *et al.*, 2019). However, Minocherhomji and colleagues showed that depletion of SMC2, and thus abrogation of chromosome condensation, prevented MiDAS in aphidicolin-treated cells released from G2 block. Whether common

fragile expression caused by premature chromosome condensation (El Achkar *et al.*, 2005) is associated with activation of MiDAS has yet not been tested.

Because RAD52 and POLD3 are involved in BIR of stalled replication forks (Costantino *et al.*, 2014; Sotiriou *et al.*, 2016), it has been hypothesised that MiDAS acts as a BIR pathway occurs via conservative DNA synthesis (Minocherhomji *et al.*, 2015; Bhowmick, Minocherhomji and Hickson, 2016; Macheret *et al.*, 2020).

Inactivation of MiDAS caused by MUS81, RAD52 or POLD3 depletion, or by chemical inhibition of RAD52 or of DNA synthesis with high-dose aphidicolin lead to increase 53BP1 nuclear bodies in the subsequent G1, micronuclei formation and reduced survival (Minocherhomji *et al.*, 2015; Bhowmick, Minocherhomji and Hickson, 2016). Moreover, error in the repair of under-replicated loci via activation of MiDAS has been proposed to promote genomic duplications at common fragile sites (Macheret *et al.*, 2020). The exact consequences of MiDAS on chromosome fragility, replication stress tolerance and genomic instability are yet not fully understood.

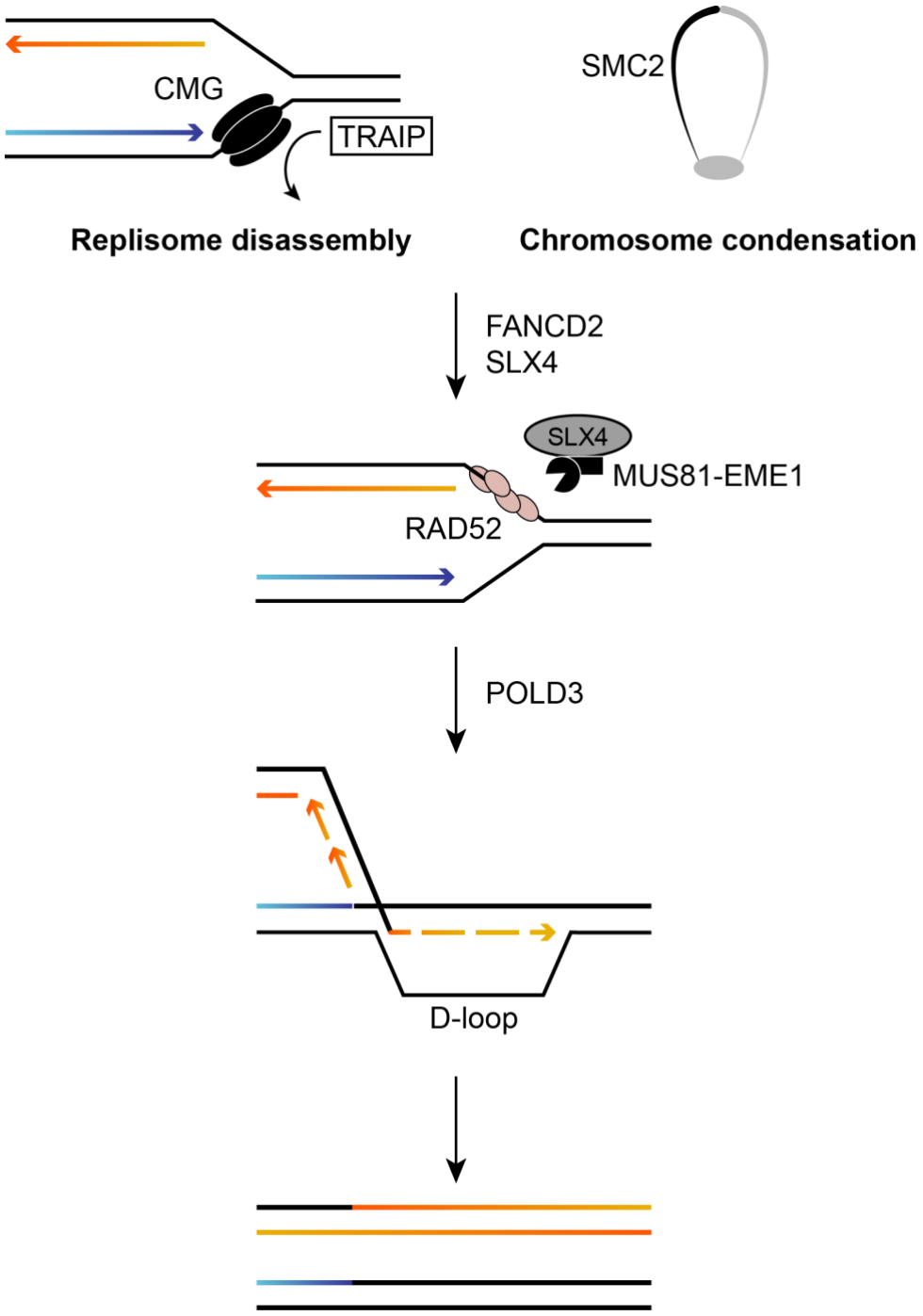


Fig. 1.4. Model of MiDAS at under-replicated loci.

Upon mitotic entry, TRAIP-mediated ubiquitination of the CMG (Cdc45-MCM-GINS) helicase triggers its disassembly whilst SMC2 promotes chromosome condensation. This exposes replication forks at under-replicated loci which are marked by FANCD2 and the SLX4 scaffold protein. SLX4 recruits RAD52 and MUS81-EME1 leading to fork

cleavage, D-loop formation and POLD3-mediated conservative DNA synthesis. Newly synthesised DNA is shown as dashed lines.

1.3.4 BRCA2 inactivation in chromosome fragility and instability

BRCA2-deficient cells were shown to exhibit mitotic abnormalities comparable to those caused by aphidicolin-treatment, suggesting that BRCA2 functions in preventing chromosome fragility. In particular, BRCA2 abrogation leads to anaphase bridges, chromosome mis-segregation and 53BP1 nuclear bodies (Feng and Jasin, 2017; Lai *et al.*, 2017). BRCA2 abrogation also triggers spontaneous MiDAS at FANCD2-labelled sites (Feng and Jasin, 2017; Lai *et al.*, 2017; Graber-Feesl *et al.*, 2019), suggesting that MiDAS plays a key role in maintaining chromosome integrity in the absence of BRCA2.

BRCA2 has also been proposed to activate the spindle assembly checkpoint by facilitating the acetylation of BUBR1 (Ehlen *et al.*, 2021). More recently, BRCA2 has been shown to promote proper chromosome alignment in metaphase and, thus preventing chromosome mis-segregation (Ehlen *et al.*, 2020). Indeed, phosphorylated BRCA2 interacts with PLK1, BUBR1 and the PP2A phosphatase, which activity counteracts Aurora B-mediated destabilisation of kinetochore-microtubule attachment. This suggests that BRCA2 function in chromosome integrity is not only dependant on its role in interphase but also to its DDR-independent mitotic activity (Ehlen *et al.*, 2021).

1.4 Research aims

The research presented here provides a better understanding of the causes and consequences of the chromosome instability cause by BRCA2 abrogation. In a

first part, we aim to elucidate the transcriptional adaptation caused by BRCA2 abrogation and their implication on cellular signalling (Chapter 3). In a second part, we provide new insights into the mechanisms underlying mitotic abnormalities, in particular MiDAS activation, caused by BRCA2 abrogation.

Chapter 2

Material and methods

2.1 Cell lines and cell culture

Cell lines were cultivated at 37˚C in 5% CO_2. Human non-small-cell lung carcinoma H1299 and invasive ductal breast cancer MDA-MB-231 cells carrying a doxycycline (DOX)-inducible shRNA against BRCA2 (H1299+sh*BRCA2*^{DOX} and MDA-MB-231+sh*BRCA2*^{DOX}) cells were grown as monolayer in Dulbecco's Modified Eagle's Medium (DMEM) supplemented with 10% foetal bovine serum (FBS), certified tetracycline-free. Expression of shRNA against BRCA2 was induced by adding 2 µg/mL DOX in the growth medium. The shRNA-expressing cell lines were previously established (Zimmer et al 2016). In brief, the shRNA sequence (GAG AAU GUC UCA CAA AUA A) was cloned into pLKO-Tet-On and introduced into cells using lentiviral infection.

H1299 cells harbour *TP53* deletion and heterozygous *NRAS* (NRAS Q61K) mutation, which increased signalling activates the MAPK pathway to enhance cell proliferation and motility (Song, Liu and Zhang, 2017). MDA-MB-231 cells harbour homozygous gain-of-function mutation in *TP53* (p53 R280K (Ghosh *et al.*, 2021)), MAPK pathway activation via KRAS (G13D) and BRAF (G464V) mutations (Hollestelle *et al.*, 2010; Bracht *et al.*, 2019; McFall *et al.*, 2020) and *CDKN2A* deletion (Hollestelle *et al.*, 2010).

For the 28-day time course, 500'000 cells were seeded in a T75 in order to establish a mass cell culture for each condition (H1299+sh*BRCA2*^{DOX} and MDA-MB-231+sh*BRCA2*^{DOX}, ±DOX). Cells were passaged every fourth day using trypsin, and 500'000 cells were seeded in the same flask, to maintain the mass cell culture. 1'300'000 and 500'000 cells were seeded in a T75 and were collected for Western Blotting two (e.g., at day 2, 6, 10, etc. of the 28-day period) or four days later (e.g., at day 4, 8, 12, etc. of the 28-day period), respectively.

160’000 and 60’000 cells were seeded in a 6-well and were collected for quantitative RT-PCR two or four days later, respectively. Passaged cells were grown in fresh medium and DOX was added where appropriate.

2.2 RNA-sequencing (RNA-seq)

RNA was extracted using the RNeasy Mini Kit (Qiagen) according to the manufacturer’s instructions and quantified using RiboGreen (Invitrogen) on the FLUOstar OPTIMA plate reader (BMG Labtech). Input material was normalized to 1 µg prior to library preparation. The TruSeq Stranded mRNA kit (Illumina) was used according to the manufacturer’s instructions for poly(A) transcript enrichment and strand specific library preparation. Libraries were amplified on a Tetrad (Bio-Rad) and individual libraries were normalized using Qubit. Individual libraries were pooled together. Each library aliquot was denatured and further diluted prior to loading on the sequencer. Paired-end sequencing was performed using a HiSeq4000 75 base pair platform (Illumina), generating a raw read count of > 22 million reads per sample.

2.3 RNA-seq data processing

RNA-seq reads were aligned to the human reference genome (GRCh37) using HISAT245 and duplicate reads removed using the Picard MarkDuplicates tool (Broad Institute). Reads mapping uniquely to Ensembl-annotated genes were summarised using featureCounts. The R/BioConductor environment for analysis of the raw count gene matrix. Genes with less than 10 reads in more than three samples were removed and sets of 14,000–15,000 genes remained for differential gene expression analysis.

2.4 Differential gene expression analysis

The analyses were carried out using the R package DESeq2. Differentially expressed genes were identified based on their false discovery rate (FDR) using Benjamini-Hochberg adjusted p-values <0.05 and absolute value of Log_2(Fold change). Absolute value of Log_2(Fold change) > 0.5 was used to determine differentially expressed genes expression between H1299+sh*BRCA2*^{DOX} treated with DOX or not (+DOX vs -DOX) or MDA-MB-231+sh*BRCA2*^{DOX} treated with DOX or not (+DOX vs -DOX). Absolute value of Log_2(Fold change) > 0.3 was used to determine differentially expressed genes common to both cell lines.

2.5 Quantitative RT-PCR

Cells were grown in the presence or absence of DOX for a 28-day period and were passaged every four days in order to be 70-90% confluent two or four days later. RNA was extracted using TRIzol reagent and the SYBR Green cells-to-CT kit (Thermo Fisher Scientific) was used according to the manufacturer's instruction to generate complementary DNA (cDNA). The SensiMix SYBR No-ROX kit (Bioline) was used to prepare 10 µL reactions using 0.2 µL of cDNA and 10 µM forward and reverse primers. Quantitative PCR was performed in 384-well plates using the QuantStudio 5 Real-Time PCR System (Thermo Fisher Scientific). Gene expression was normalised to housekeeping genes *ACTB* and expressed relative to day 2 of treatment using the Livak $2^{-\Delta\Delta CT}$ method.

Table 2.1. Primer pairs used for RT-qPCR.

Target	Forward primer	Reverse primer
ACTB	5'- ATTGGCAATGAGCGGTTC	5'- GGATGCCACAGGACTCCAT
IFI6	5'- TCGCTGATGAGCTGGTCTGC	5'- ATTACCTATGACGACGCTGC
IFIT1	5'- TACCTGGACAAGGTGGAGAA	5'- GTGAGGACATGTTGGCTAGA
IFIT2	5'- TGTGCAACCTACTGGCCTAT	5'- TTGCCAGTCCAGAGGTGAAT

ISG15	5'- GCGAACTCATCTTTGCCAGTA	5'- CCAGCATCTTCACCGTCAG
OAS1	5'- CGCCTAGTCAAGCACTGG TA	5'- CAGGAGCTCAGGGCATA
OAS2	5'- TCCAGGGAGTGGCCATAG	5'- TCTGATCCTGGAATTGTTTTAAGTC

2.6 Western blotting

Cells were lysed using loading buffer (0.16 M Tris pH 8, 4% sodium dodecyl sulfate-polyacrylamide (SDS), 20% glycerol, 0.01% bromophenol blue) supplemented with 100 mM dithiothreitol (DTT), and protease and phosphatase inhibitor cocktails (Roche). Samples were sonicated for 3 sec on ice, heated at 70ºC for 10 min and centrifuged at >20'000 g for 7 min. The protein concentration was quantified using a NanoDrop-1000 spectrophotometer. Equal amounts of protein were loaded on 4-12% Bis-Tris, 10% Bis-Tris or 3-8% Tris-acetate gels (Thermo Fisher Scientific). Bis-Tris gels were run in MOPS buffer and Tris-acetate gels in Tris-acetate buffer (Thermo Fisher Scientific) at 100-180 V until the desired separation was achieved. PageRuler prestained protein ladder (Thermo Fisher Scientific) and HiMark prestained protein standard (Thermo Fisher Scientific) were used as molecular weight markers. Protein transfer onto a nitrocellulose membrane was run in transfer buffer supplemented with 10% methanol (Thermo Fisher Scientific) at 30 V for 100 min. The membranes were subsequently blocked in 5% skimmed milk dissolved in 0.05% Tween 20 (also known as polysorbate 20) in PBS (hereafter PBST). Membranes were incubated with primary antibodies diluted in 2% bovine serum albumin and 0.05% azide in PBST over-night at 4ºC and with horseradish peroxidase (HRP)-conjugated secondary antibodies diluted in 5% skimmed milk in PBST for 1h at room-temperature. Detection was achieved by enhanced chemiluminescence detected on X-ray films.

Table 2.2. Primary antibodies used for immunoblotting.

Specificity	Host	Provider	Catalogue Number	Dilution
BRCA2	Mouse	Calbiochem	OP95	1:1'000
Cyclin B	Mouse	Cell Signaling Technology	4135	1:1'000
GAPDH	Mouse	Novus Biologicals	6C5	1:30'000
HERC5	Rabbit	Thermo Fisher Scientific	703675	1:1'000
Histone H3	Mouse	Thermo Fisher Scientific	865R2	1:1'000
Histone H3 (S10)	Rabbit	Abcam	AB5176	1:1'000
IRF3	Rabbit	Abcam	AB76409	1:1'000
IRF3 (S386)	Rabbit	Abcam	AB76493	1:1'000
ISG15	Rabbit	Cell Signaling Technology	2743	
KAP1	Rabbit	Bethyl Laboratories	A300-274A	1:5'000
KAP1 (S824)	Rabbit	Bethyl Laboratories	A300-767A	1:1'000
SMC1	Rabbit	Bethyl Laboratories	A300-055A	1:5'000
STAT1	Rabbit	Cell Signaling Technology	9175	1:1'000
STAT1 (Y701)	Rabbit	Cell Signaling Technology	9167	1:1'000
STING	Rabbit	Cell Signaling Technology	13647	1:1'000
USP18	Rabbit	Cell Signaling Technology	4813	1:1'000

Table 2.3. Secondary antibodies used for immunoblotting.

Specificity	Host	Provider	Catalogue Number	Dilution
Mouse	Goat	Dako	P0447	1:5'000
Rabbit	Goat	Dako	P0448	1:5'000

2.7 Resazurin-based viability assay

Where indicated, DOX was added to the grow medium four days before the start of the experiment. A range of 250-750 H1299+sh*BRCA2*^{DOX} cells or 375-1000 MDA-MB-231+sh*BRCA2*^{DOX} cells were seeded in 96-well plates in order for the untreated cells to reach 80-90% confluency at the end of the assay The following day, cells were treated with olaparib or talazoparib at indicated concentration. Six days later, cells were grown in medium supplemented with 10 µg/mL resazurin for 2 h. Cell viability was determined by fluorescence (590 nm) using a plate

reader (POLARstar, Omega). Cell viability was expressed relative to cells mock-treated cells.

2.8 Flow cytometry-based assays

2.8.1 Detection of EdU and Histone H3 (S10)

Cells were collected using trypsin and fixed in 90% ice-cold methanol overnight. Cells were then processed using the Click-iT EdU Alexa Fluor 647 flow cytometry assay kit (Thermo Fisher Scientific) according to manufacturer's instructions. They were permeabilised using a saponin-based buffer. For EdU detection, a Click-iT reaction was performed according to the manufacturer's instructions. For detection of phosphorylated Histone H3 (S10), cells were washed with 2% FBS in PBS and incubated with mouse anti-Histone H3 (S10) antibody (Cell Signaling Technology #9701) diluted in 2% FBS in PBS (1:50) for 90 min at room temperature. They were subsequently washed with 2% FBS in PBS and incubated with goat anti-mouse AlexaFluor488 (Life Technologies A-10667) diluted in 2% FBS in PBS (1:200) for 1 h at room temperature. Finally, cells were washed in 2% FBS in PBS and resuspended in PBS containing 20 µg/mL propidium iodide and 400 µg/ml RNaseA. A total of 5'000 to 10'000 events per condition were recorded using a FACS Calibur flow cytometer. Flow cytometry data were analysed with the FlowJo software.

2.8.2 Cell cycle analysis

Asynchronous cells were pulse-labelled with 25 µM EdU for 30 min and processed as described above.

2.8.3 S phase entry

Cells were blocked in G2 with 9 µM RO-3306 for 16 h and subsequently released in a medium containing 100 ng/ml nocodazole for 2h. Mitotic cells were harvested by mitotic shake-off and released in fresh medium supplemented with 25 µM EdU. The percentage of EdU-labelled cells was determined as described above.

2.8.4 S-to-M progression

Asynchronous cells were pulse-labelled with 10 µM EdU for 1 h and subsequently allowed to grow for 7 h. Cells were then processed as mentioned above. The percentage of Histone H3 (S10)-positive cells amongst the EdU-positive cells is reported.

2.8.5 DNA content analysis

Cells were incubated in 1.5 mM thymidine for 16 h and released in fresh medium. At indicated timepoints after the release, cells were collected using trypsin and fixed in 90% ice-cold methanol overnight. Fixed cells were washed with PBS, resuspended in PBS containing 20 µg/mL propidium iodide and 400 µg/mL RNaseA and processed as described above.

2.9 Drug treatment

Cells were grown in the presence or absence of DOX for 3 days and seeded in order to reach 70-90% confluency at the end of the experiment (160’000 cells in 6-cm dish, or 60’000 cells in 6-well respectively). The following day cells were treated as indicated. Mock-treated cells were treated with equal volume of vehicle (DMSO for Olaparib, H_2O for pyridostatin, and ethanol for chlorambucil).

2.10 Cell synchronization for mitotic EdU-seq

Cells were seeded in order to reach 70-80% confluence at the end of the experiment (1’800’000 cells per T175 flask, 10-25 flasks per condition) and DOX was added where indicated. After 12 h, cells were treated with 1.5 mM thymidine for 16 h. To detect MiDAS under untreated conditions, cells were released in fresh medium containing 6 µM RO-3306 for 10.5 h. To detect aphidicolin-induced MiDAS, cells were released in fresh medium containing 6 µM RO-3306 and 0.2 µM aphidicolin. For both protocols, cells were then washed three times with warm medium and released in medium containing 100 ng/ml nocodazole and 10 µM EdU. 2 mM HU was added during the final 3 h of treatment.

2.11 EdU-seq

Mitotic cells were harvested by mitotic shake-off and fixed with 90% ice-cold methanol. Cells were washed with PBS and permeabilised with 0.2% Triton-X in PBS. A cleavable biotin linker (Azide-PEG(3+3)-S-S-biotin, Jena Biosciences) was attached to the EdU using the Click-It kit described above. The DNA was isolated by phenol-chloroform extraction and precipitated in ethanol. Isolated DNA was resuspended in TE buffer and sonicated to 100-500 nucleotide-long fragments. Dynabeads MyOne streptavidin C1 (Invitrogen) were used to purify Edu-labelled DNA fragments. The beads were washed three times, resuspended in 5 mM Tris-HCl, pH 7.5, 0.5 mM EDTA, 1 M NaCl, 0.5% Tween 20 (buffer A) containing the sonicated DNA and incubated on a rotating wheel for 15 min at room temperature. The beads were washed three times with buffer A and once with Tris-EDTA buffer. The EdU-labelled DNA fragments were eluted with 2% β-mercaptoethanol in Tris-EDTA buffer for 1h at room temperature. Purified EdU-labelled DNA was used for libraries preparation (TruSeq ChIP Library Preparation

Kit, Illumina) and high-throughput 100-base-pair single-end sequencing was performed on Illumina Hi-Seq 4000 sequencer.

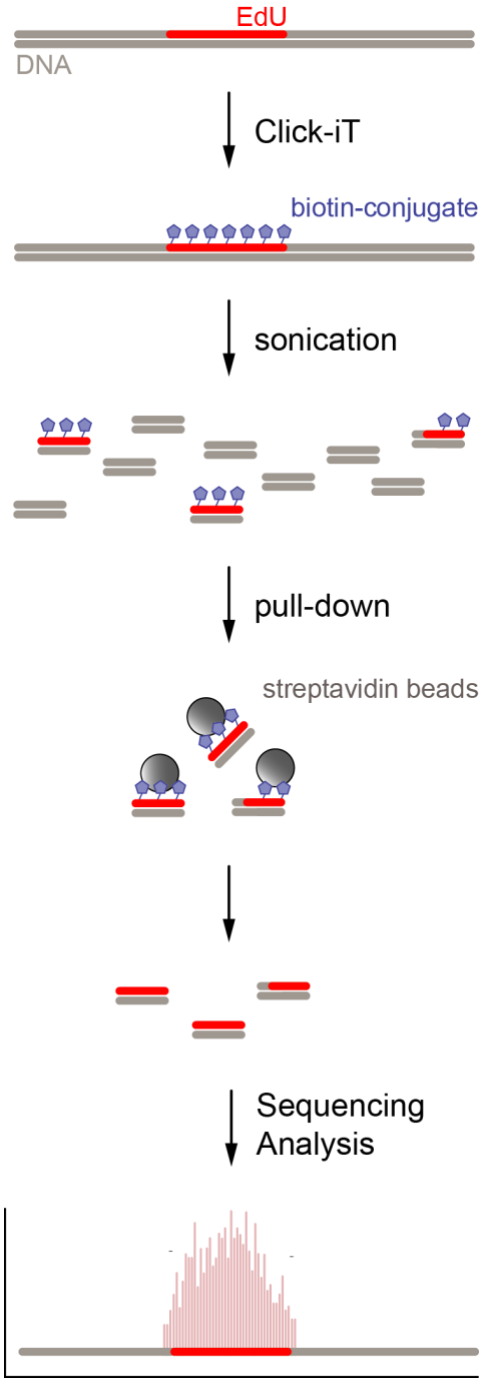


Fig. 2.1. Strategy for high-resolution detection of nascent DNA using EdU-seq

2.12 EdU-seq data processing

Sequencing reads were aligned on the masked human genome assembly (GRCh37/hg19) using the Burrows-Wheeler Aligner software and reads with quality score below 60 were removed. Custom scripts were used to assign the aligned reads to 10 kb genomic bins. The normalised number of reads per genomic bin was calculated by dividing the number of EdU-seq reads per genomic bin by the number of reference reads for the same genomic bin. Here the reference reads were obtained from high-coverage sequencing of genomic DNA. Finally, sigma values were calculated as the normalised number of reads per bin divided by its standard deviation (Macheret and Halazonetis, 2018).

2.13 Analysis of MiDAS peaks

For plots showing individual genomic regions, the EdU-seq data were plotted using sigma values, which corrects for systemic biases in high throughput sequencing data. Custom scripts were used to identify sites (peaks) with sigma values significantly higher than background signal (local maxima) within a 2 Mb-long region. MiDAS peaks were plotted, validated manually and subsequently classified as single- or multiple-peaks manually. The maximal sigma value of each individual MiDAS site is indicated in the figure legend. The “was used to generate BigWig files using BAM files aligned as described above. were used to generate average plots and heatmaps across multiple regions. Genome-wide averages of all MiDAS sites were plotted using the “computeMatrix” and “plotHeatmap” functions of deepTools (Ramirez *et al.*, 2016) using BigWig files generated with the “bamCoverage” function.

2.14 Analysis of the replication timing

REPLI-seq data were previously generate in asynchronous U2OS cells (Macheret and Halazonetis, 2018).

2.15 Assignment of genic and intergenic regions

Ensembl gene annotations (v99 for GRCh37/hg19) were used to list the genomic position of all human genes. Genomic bins that mapped entirely within genes were defined as genic. Genomic bins that mapped entirely within intergenic regions were defined as intergenic. Genomic bins that contained both genic and intergenic regions were classified as mixed genic/intergenic.

2.16 Statistical analyses

Statistical analyses were performed using GraphPad Prism. For comparison of means, unpaired two-tailed Student's t-test was applied. The interpretation of the p-value is described in the figure legends.

Chapter 3

BRCA2 abrogation activates the cGAS-STING-IRF3 and JAK-STAT pathways to promote expression of interferon-stimulated genes

3.1 Introduction

BRCA2 plays major roles in the maintenance of genome stability. It facilitates DNA replication by protecting stalled replication forks from nucleolytic degradation and promoting their restart via template switch reactions (Saldivar, Cortez and Cimprich, 2017; Berti, Cortez and Lopes, 2020). BRCA2 functions are essential for homologous recombination (HR) repair of DNA double-strand breaks (DSBs) (Chang *et al.*, 2017; Scully *et al.*, 2019). Therefore, loss of BRCA2 leads to the accumulation of mutations and fuels tumorigenesis (Wooster *et al.*, 1994; Wooster *et al.*, 1995). Several studies have contributed to a better understanding of the consequences of BRCA2 abrogation. For example, DDR-deficiency caused by BRCA2 abrogation sensitizes cancer cells to DNA damaging therapies, such as IR (Sharan *et al.*, 1997). Moreover, PARP inhibition is synthetic lethal with BRCA2-deficiency (Bryant *et al.*, 2005; Farmer *et al.*, 2005; Lord and Ashworth, 2017). However, how cells respond to BRCA2 abrogation is yet not fully understood. In particular, why germline *BRCA2* mutations predispose to breast, ovarian or prostate cancers remains unknown . We hypothesised that the accumulation of stalled replication forks and DNA damage in BRCA2-depleted cells may impact on gene expression and therefore contribute to their tumorigenicity. We therefore sought to investigate deregulated gene expression following loss of BRCA2 function.

Based on RNA-sequencing (RNA-seq) analyses performed in two distinct cellular models for BRCA2 inactivation, we identified differentially expressed genes at early and late timepoints after BRCA2 abrogation, which brought new insights into the signalling triggered by BRCA2 abrogation.

3.2 Characterisation of the inducible models for BRCA2 inactivation

To investigate the mechanisms of adaptation following BRCA2 abrogation, we analysed changes in gene expression by RNA-seq. For this purpose, we used two inducible models of BRCA2 abrogation: human non-small cell lung carcinoma H1299 cells and invasive ductal breast cancer MDA-MB-231 cells expressing a doxycycline (DOX)-inducible short hairpin RNA (shRNA) against *BRCA2* (H1299+sh*BRCA2*^{DOX} and MDA-MB-231+sh*BRCA2*^{DOX}). DOX addition to the growth medium effectively inhibited BRCA2 expression in both H1299+sh*BRCA2*^{DOX} and MDA-MB-231+sh*BRCA2*^{DOX} cells (Fig. 3.1A, B).

We then compared gene expression upon short-term (acute, 4 days) or long-term (chronic, 28 days) BRCA2 abrogation. We grew cells in the presence of doxycycline for 4 or 28 days to trigger acute or chronic BRCA2 abrogation, respectively and performed RNA-seq analyses in triplicate to detect transcriptional changes at each timepoint relative to BRCA2-expressing control cells.

Importantly, loss of BRCA2 expression resulted in a mild proliferation defect in both H1299+sh*BRCA2*^{DOX} and MDA-MB-231+sh*BRCA2*^{DOX}, as observed by resazurin-based population doublings assay. However, short-term and long-term BRCA2-depleted cells exhibited the same proliferation rate (Fig. 3.1B, C). Although we did not observe obvious signs of increased cell death over the course of the experiment, we measured apoptosis by Annexin V staining on cells grown in the absence or presence of DOX for 4 or 28 days. We observed a small, yet significant increase in the Annexin V-positive population at day 4 of DOX treatment in H1299+sh*BRCA2*^{DOX} cells (Fig. 3.1E, F). A small increase was

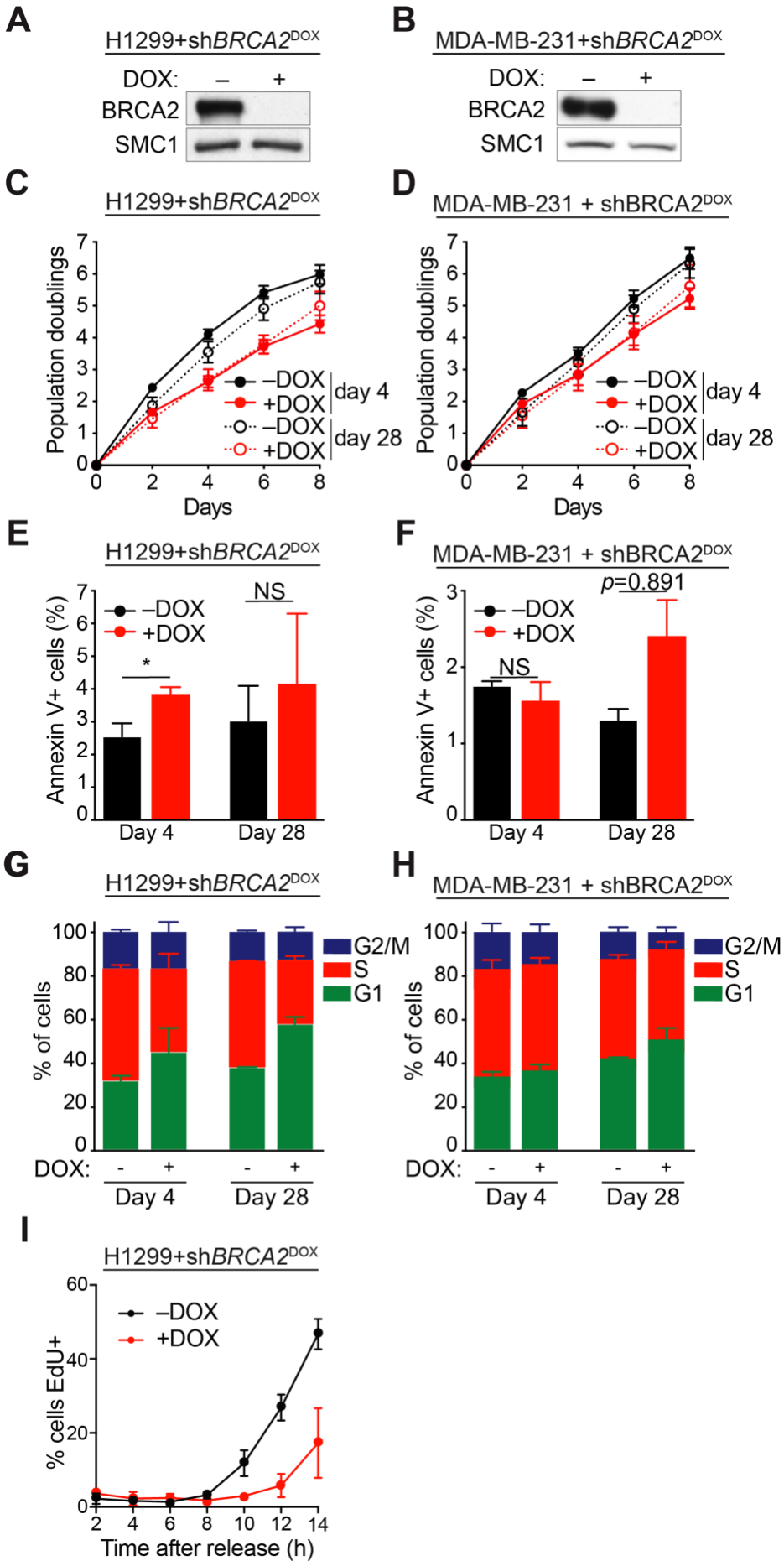

A
H1299+shBRCA2DOX
DOX: – +
BRCA2
SMC1
B
MDA-MB-231+shBRCA2DOX
DOX: – +
BRCA2
SMC1
C
H1299+shBRCA2DOX
Population doublings
Days
–DOX
+DOX
day 4
–DOX
+DOX
day 28
D
MDA-MB-231 + shBRCA2DOX
Population doublings
Days
–DOX
+DOX
day 4
–DOX
+DOX
day 28
E
H1299+shBRCA2DOX
Annexin V+ cells (%)
–DOX
+DOX
*
NS
Day 4
Day 28
F
MDA-MB-231 + shBRCA2DOX
p=0.891
Annexin V+ cells (%)
–DOX
+DOX
NS
Day 4
Day 28
G
H1299+shBRCA2DOX
% of cells
G2/M
S
G1
DOX: - + - +
Day 4
Day 28
H
MDA-MB-231 + shBRCA2DOX
% of cells
G2/M
S
G1
DOX: - + - +
Day 4
Day 28
I
H1299+shBRCA2DOX
% cells EdU+
–DOX
+DOX
Time after release (h)

Fig. 3.1. Time-dependent activation of the cGAS-STING-IRF3 and JAK-STAT pathways upon BRCA2 depletion.

H1299+sh*BRCA2*^{DOX} cells or MDA-MB-231+sh*BRCA2*^{DOX} cells were grown with or without DOX for 29 days. (**A, B**) Whole-cell extracts were immunoblotted as indicated at day 2 of DOX treatment. SMC1 was used as a loading control. (**C, D**) Populations doublings were measured using a resazurin-based assay starting at day 4 or day 28 of DOX treatment. (**E, F**) Percentage of Annexin V-positive cells as determined by flow cytometry at day 4 or day 28 of DOX treatment. (**G, H**) Flow cytometry-based cell cycle analysis at day 4 or day 28 of DOX treatment. (**I**) Percentage of EdU-positive H1299+sh*BRCA2*^{DOX} cells grown with or without DOX for 2 days and at indicated timepoint after release from nocodazole arrest. Graphs represent mean values and SD of n = 2 independent experiments.

also observed at day 28 of DOX treatment in both cell line studied, yet without statistical significance. Moreover, cell cycle analysis revealed that BRCA2 abrogation altered cell cycle distribution, independently of the duration of DOX treatment. Indeed, BRCA2-depleted cells accumulated in the G1-phase (Fig. 3.1G, H), (Lai *et al.*, 2017)). Flow cytometry analysis following nocodazole-induced mitotic arrest and release revealed that BRCA2-depleted H1299+sh*BRCA2*^{DOX} exhibit slow rate S phase entry compared to control cells (Fig. 3.1I). Altogether, this shows that BRCA2 abrogation in our models leads to a mild proliferation defect, which is characterised by slow cell cycle progression rather than increased cell death. Notably, this phenotype is not enhanced nor diminished upon long-term BRCA2 abrogation.

In brief, our RNA-seq analyses revealed limited alteration to gene expression in MDA-MB-231+sh*BRCA2*^{DOX} cells upon acute BRCA2 abrogation. In contrast, acute BRCA2 abrogation in H1299+sh*BRCA2*^{DOX} cells was

characterised by the downregulation of genes involved in processes such as cell cycle, chromosome segregation, DNA replication and DNA repair (data not shown; Reisländer *et al.* (2019)). Chronic BRCA2 abrogation led to deregulation of a high number of genes in both cell lines studied. In H1299+sh*BRCA2*^{DOX} cells, 194 genes were significantly downregulated (Log_2(Fold Change) < -0.5; FDR < 0.05) and 213 genes were significantly upregulated (Log_2(Fold Change) > 0.5; FDR < 0.05) (Fig. 3.1A) whilst 75 and 96 genes were significantly down- and upregulated, respectively, in MDA-MB-231+sh*BRCA2*^{DOX} cells (Fig. 3.1B). The work presented here focuses on transcriptional changes observed upon chronic BRCA2 abrogation.

3.3 Long-term BRCA2 abrogation triggers innate immune response signalling

Gene set enrichment analysis of significantly upregulated genes, using annotations from the Gene Ontology (GO) for biological processes, showed that in H1299+sh*BRCA2*^{DOX} chronic BRCA2 abrogation upregulated genes involved in the immune response, innate immune response, cytokine signalling, immune effector process, and type I interferon (IFN) response (Fig. 3.1C). GO analysis of significantly upregulated genes upon chronic BRCA2 abrogation in MDA-MB-231+sh*BRCA2*^{DOX} revealed that these genes belong to extracellular matrix organisation, IFN signalling, degradation of the extracellular matrix, cytokine signalling in immune system, haemostasis, and fatty acid metabolism processes (Fig. 3.1D).

Immune response genes were upregulated in both cell lines (Fig. 3.1C,D). Therefore, we next compared upregulated genes in H1299+sh*BRCA2*^{DOX} and

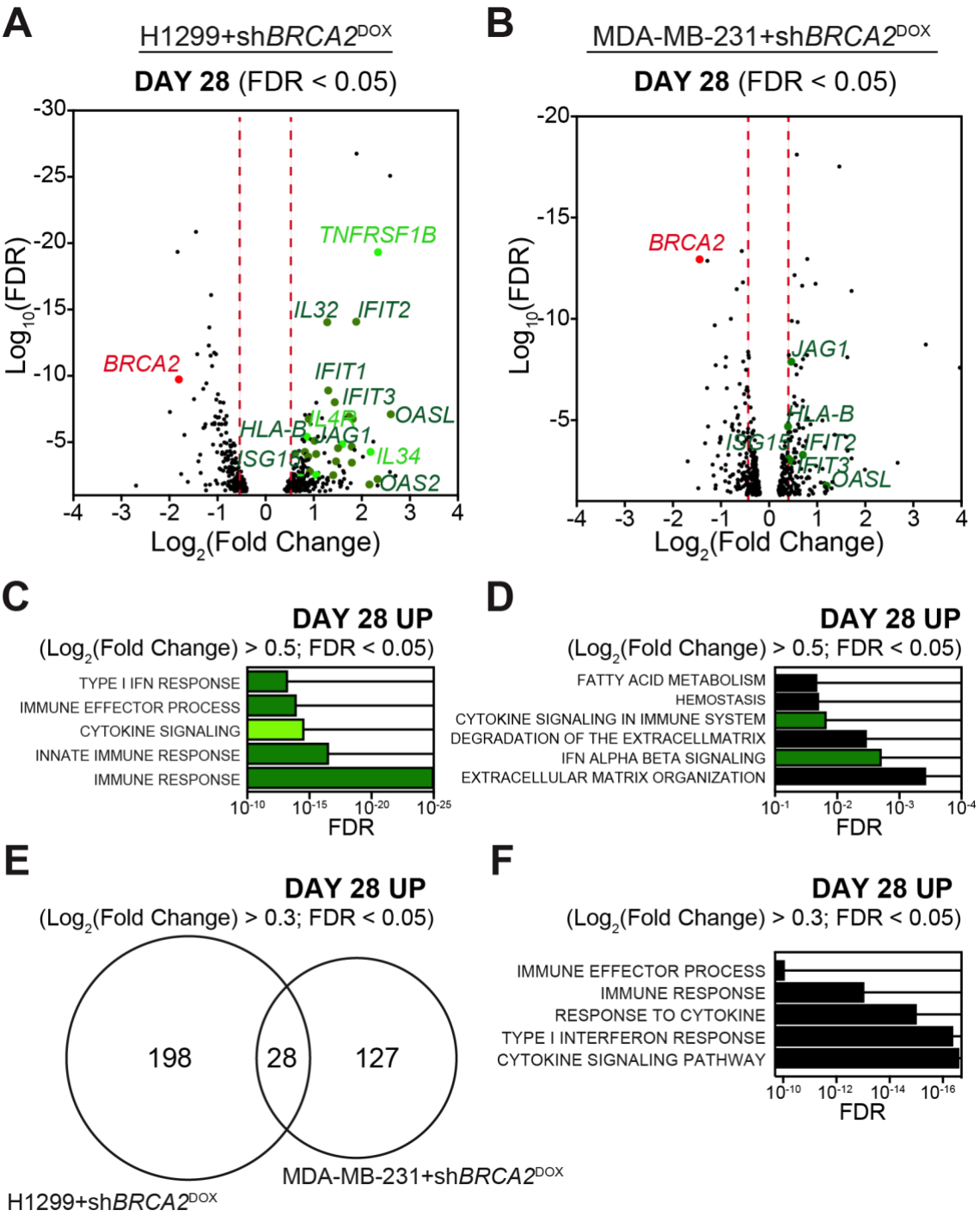


Fig. 3.2. RNA-seq analysis reveals upregulation of immune response signalling upon long-term BRCA2 depletion.

(**A**) Volcano plot shows changes in gene expression in H1299+sh*BRCA2*^{DOX} after 28 days of doxycycline (DOX) treatment. Genes with Log_2(Fold Change) > 0.5 (red dashed lines) and a false discovery rate (FDR) < 0.05 were considered significantly deregulated. (**B**) Volcano plot shows changes in genes expression in MDA-MB-

231+sh*BRCA2*^{DOX} after 28 days of DOX treatment. (**C**) Gene Ontology (GO) pathway analysis of significantly upregulated genes identified in (A) for H1299+sh*BRCA2*^{DOX}. (**D**) GO pathway analysis of significantly upregulated genes identified in (B) for MDA-MB-231+sh*BRCA2*^{DOX}. (**E**) Venn diagram shows upregulated genes (Log_2(Fold change) >0.3, FDR < 0.05) in H1299+sh*BRCA2*^{DOX} and MDA-MB-231+sh*BRCA2*^{DOX} after 28 days of DOX treatment. (**F**) GO pathway analysis of upregulated genes common to H1299+sh*BRCA2*^{DOX} and MDA-MB-231+sh*BRCA2*^{DOX} identified in (E).

MDA-MB-231+sh*BRCA2*^{DOX} upon chronic BRCA2 abrogation, in order to determine genes in common between the data sets. To increase the relevance of our results and to account for differences in expression due to cell line specificity, we considered upregulated genes with a Log_2(Fold Change) > 0.3 and FDR < 0.05 for this analysis. Our analysis revealed 28 genes common to both datasets (Fig. 3.1E). GO annotations showed that these commonly upregulated genes belong to cytokine signalling, type I IFN response, response to cytokine, immune response and immune effector process pathways (Fig. 3.1F). As an example, *IFIT2* and *IFIT3* are coding for proteins involved in type I IFN response and were significantly upregulated in both H1299+sh*BRCA2*^{DOX} and MDA-MB-231+sh*BRCA2*^{DOX} cells. Hence, we concluded that chronic BRCA abrogation leads to immune response signalling.

3.4 Long-term BRCA2 abrogation activates the cGAS-STING-IRF3 and the JAK-STAT pathways

To understand the differences between chronic and acute BRCA2 inactivation on immune response signalling, we then monitored gene expression over a 28-day period using quantitative reverse transcription PCR (RT-qPCR). Selected genes

included *IFIT1*, *IFIT2*, *IFI6*, *OAS1*, *OAS2* and *ISG15*. Whilst the expression of these genes remained stable over the 28-day period in BRCA2-proficient H1299+sh*BRCA2*^{DOX} cells, we observed a constant increase with time in their expression upon BRCA2 abrogation (Fig. 3.3A). Strikingly, *OAS2* mRNA levels were 40-fold increased at day 28 compared to day 2 of doxycycline treatment (Fig. 3.3A). Similar trends were observed in most tested ISGs following BRCA2 abrogation in MDA-MB-231+sh*BRCA2*^{DOX} cells, but to a smaller extent. Indeed,

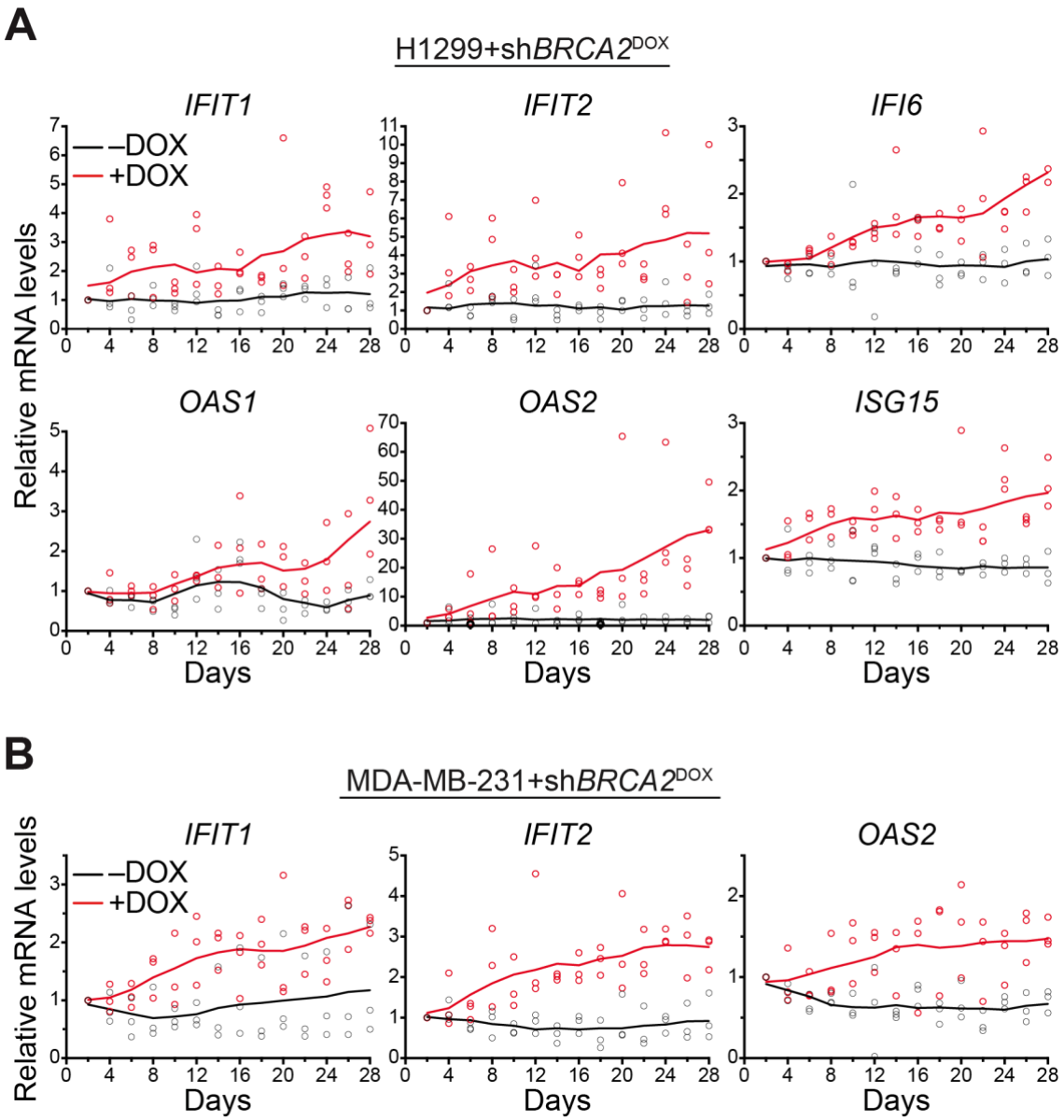


Fig. 3.3. Time-dependent expression of interferon-stimulated genes (ISGs) upon BRCA2 depletion.

(**A**) H1299+sh*BRCA2*^{DOX} cells were grown with or without DOX for 28 days. At indicated days, gene expression was analysed by RT-qPCR using primers specific for a subset of ISGs. mRNA levels are expressed relative to *ACTB* mRNA (encoding β-actin) and normalised to day 2 of DOX treatment. Dots represent the value obtained from an individual experiment. Lines represent the rolling average of n = 3 independent repeats. (**B**) MDA-MB-231+sh*BRCA2*^{DOX} were grown with or without DOX for 28 days. Gene expression was analysed and is expressed as in (A).

IFIT1, *IFIT2* and *OAS2* mRNA levels increased over the time course of the experiments (Fig. 3.3B). Altogether, these data suggest that whilst upregulation of the immune response pathways were only detected upon chronic BRCA2 abrogation, the underlying signalling is activated at an earlier stage of BRCA2 abrogation.

The upregulated genes are known to mediate a type I IFN response. In particular, they belong to a category of genes called interferon-stimulated genes (ISGs), whose expression is activated in the presence of extracellular IFNα or IFNβ. Indeed, the interaction between the IFNα or IFNβ ligands and the IFNAR1-IFNAR2 heterodimeric receptor (Schindler *et al.*, 1992; Velazquez *et al.*, 1992) triggers activation of a signalling cascade ultimately leading to JAK-mediated phosphorylation of STAT1 and STAT2 (Shuai *et al.*, 1993; Silvennoinen *et al.*, 1993; Schneider, Chevillotte and Rice, 2014). These proteins, together with IRF9, form the ISGF3 complex and bind to IFN-stimulated response elements (ISRE) in ISG promoters to initiate transcription (Fu *et al.*, 1990; Improta *et al.*, 1994; Schneider, Chevillotte and Rice, 2014). Therefore, we decided to test whether activation of the JAK-STAT pathway could explain the expression of ISGs upon chronic BRCA2 abrogation.

We monitored the phosphorylation of STAT1 at tyrosine 701 (Y701; (Shuai *et al.*, 1993)) over the 28-day period in both H1299+sh*BRCA2*^{DOX} and MDA-MB-231+sh*BRCA2*^{DOX} by immunoblotting (Fig. 3.4A,B). We observed a strong phosphorylation of STAT1 in BRCA2-deficient H1299+sh*BRCA2*^{DOX} cells compared to their BRCA2-proficient counterparts. Moreover, phosphorylated STAT1 was detected early after BRCA2 abrogation (Fig. 3.4A, day 4 of doxycycline treatment) and further increased upon long-term BRCA2 abrogation

(Fig. 3.4A, days 24 and 28 of doxycycline treatment). We found the same trend in MDA-MB-231+sh*BRCA2*^{DOX} (Fig. 3.4B), although the increase in STAT1 phosphorylation upon BRCA2 abrogation was less pronounced than in H1299+sh*BRCA2*^{DOX} cells (Fig. 3.4A). This is consistent with the weaker upregulation of ISGs observed by RT-qPCR in this cell line (Fig. 3.3B). Taken together, these data demonstrate that BRCA2 abrogation leads to activation of the JAK-STAT pathway, which is responsible for the upregulation of ISGs observed in our RNA-seq experiments.

Next, we sought to elucidate the mechanisms underlying the activation of the JAK-STAT pathway. Whilst secreted IFNs are known to activate this pathway, the *IFNA* and *IFNB* genes (which encode IFNα and IFNβ, respectively), did not appear significantly upregulated in our RNA-seq analysis upon chronic BRCA2 abrogation (Fig. 3.1A,B). We assessed the activation of the cGAS-STING-IRF3 pathway, which is an upstream regulator of IFNα and IFNβ expression (Ishikawa, Ma and Barber, 2009; Burdette *et al.*, 2011; Ablasser *et al.*, 2013; Gao *et al.*, 2013; Sun *et al.*, 2013; Wu *et al.*, 2013). The cGAS-STING-IRF3 pathway was recently found to be activated by defects in DNA damage repair pathways (Reisländer, Groelly and Tarsounas, 2020). Moreover, IR was shown to induce micronuclei formation, followed by detection by cGAS upon rupture of the micronuclear membrane. Thus, we monitored the phosphorylation of the transcription factor IRF3 at serine 386 (S386; (Tanaka and Chen, 2012)), which controls the transcription of IFN genes. We detected an increase in phosphorylated IRF3 upon BRCA2 abrogation from day 4 of doxycycline treatment onward, in both H1299+sh*BRCA2*^{DOX} and MDA-MB-231+sh*BRCA2*^{DOX} (Fig. 3.4A,B).

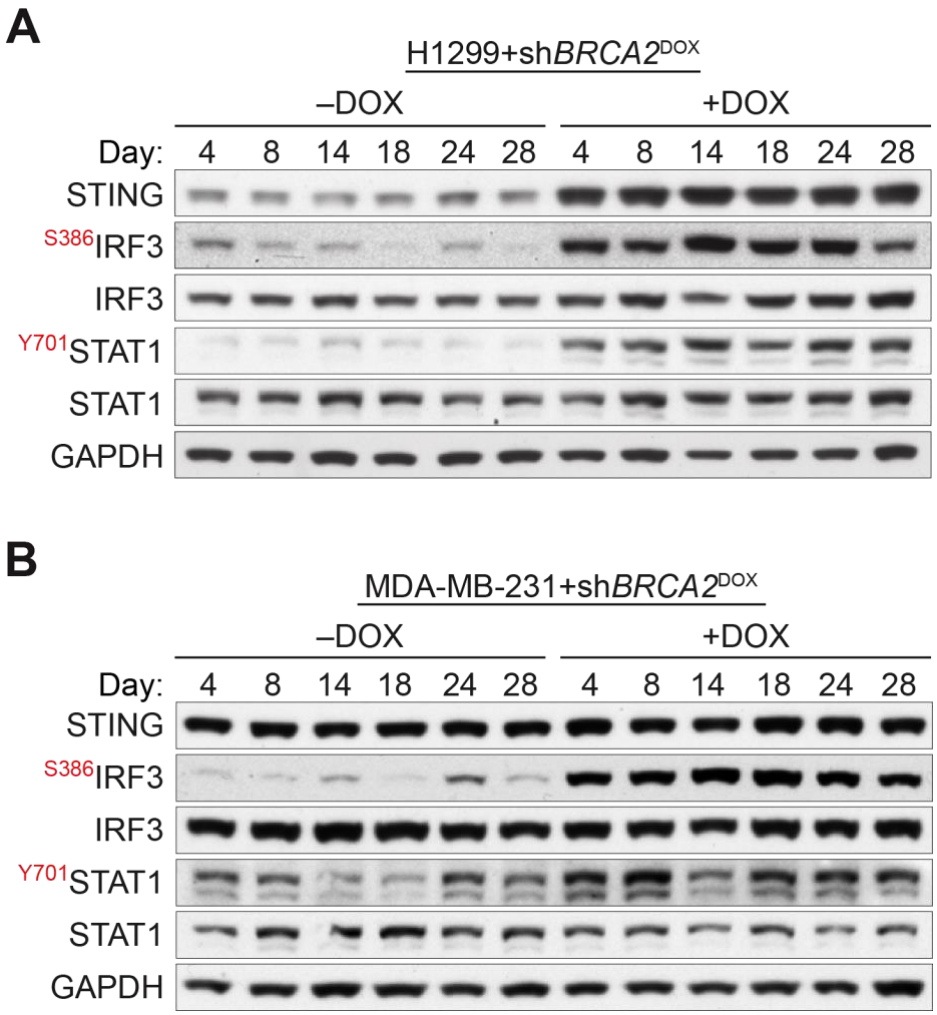


Fig. 3.4. Time-dependent activation of the cGAS-STING-IRF3 and JAK-STAT pathways upon BRCA2 depletion.

(**A**) H1299+sh*BRCA2*^{DOX} cells or (**B**) MDA-MB-231+sh*BRCA2*^{DOX} were grown with or without DOX for 28 days. At indicated days, whole-cell extracts were immunoblotted as indicated. Phosphorylation sites are indicated in red. GAPDH was used as a loading control.

BRCA1 or BRCA2 deficiencies correlate with increased micronuclei formation (Ban et al., 2001). Therefore, we tested whether micronuclei formation and cGAS surveillance underlies the activation of the type I IFN response upon BRCA2 abrogation. We performed immunofluorescence to monitor cGAS association with micronuclei in BRCA2-proficient and BRCA2-deficient

H1299+sh*BRCA2*^{DOX} cells at day 4 and 28 of DOX treatment. We observed an increase in cGAS-positive micronuclei over time upon BRCA2 abrogation in H1299+sh*BRCA2*^{DOX} (data not shown; (Reisländer *et al.*, 2019)). Moreover, small interfering RNA (siRNA)-mediated knock-down of *STING* inhibited the phosphorylation of IRF3 and STAT1 as well as the expression of ISGs in the same cell line (data not shown; (Reisländer *et al.*, 2019)).

Following up on our initial RNA-seq results (Fig. 3.1), we demonstrated that BRCA2 abrogation results in micronuclei formation that accumulate cGAS and in activation of the cGAS-STING-IRF3 pathway (Fig. 3.4). This, in turn, leads to the activation of the JAK-STAT pathway (Fig. 3.4) and activation of a type I IFN response, which is characterised by the expression of ISGs (Fig. 3.1A,B; Fig. 3.3).

3.5 PARP inhibitors enhance the type I innate immune response in BRCA2-deficient cells

We next tested the clinical significance of these findings and addressed whether the synthetic lethal interaction between *BRCA2* deficiency and PARP inhibition impacts on the immune response signalling. Indeed, PARP inhibition leads to the accumulation of DNA damage and mitotic abnormalities (Schoonen *et al.*, 2017). Moreover, identifying ways to turn ‘‘cold’’ tumours into ‘‘hot’’ tumours which respond to immunotherapy is a particularly pressing clinical challenge (Sharma and Allison, 2015).

We used two PARP inhibitors, olaparib and talazoparib, both of which have recently been approved for treatment of cancers with loss of HR repair or *BRCA1/2* genes (Lord and Ashworth, 2017). We first evaluated the effect of PARP inhibition in our models of BRCA2-deficiency. Consistent with previous

data (Tacconi *et al.*, 2017), olaparib was found to be specifically toxic to BRCA2-deficient H1299+sh*BRCA2*^{DOX} cells, as measured by a resazurin-based viability assay (Fig. 3.5A). Similar results were obtained upon treatment with talazoparib (Fig. 3.5B). To further characterise our model's response to PARP inhibition, we performed cell cycle analysis of H1299+sh*BRCA2*^{DOX} treated with olaparib. Whilst olaparib treatment did not further enhance the G1 arrest observed in BRCA2-deficient cells, it decreased the fraction of S phase cells and increased the fraction of G2/M-phase cells (Fig. 3.5B,C). For instance, S phase gated cells dropped from 31% in mock-treated cells to 19% upon treatment with 10 µM olaparib. This further confirms that PARP inhibition negatively impacts on the proliferation of BRCA2-deficient cells.

We next used phosphorylated IRF3 and phosphorylated STAT1 as markers of the activation of type I IFN response. Treatment with olaparib induced a dose-dependent phosphorylation of both IRF3 and STAT1 in BRCA2-deficient H1299+sh*BRCA2*^{DOX} cells (Fig. 3.6). Importantly, this correlated with a dose-dependent increase in DNA damage, as shown by KAP1 phosphorylation at serine 824 (S824; (White *et al.*, 2006)). Treatment with 10 µM olaparib but not with 1 µM olaparib caused phosphorylation of IRF3 or STAT1 in BRCA2-proficient H1299+sh*BRCA2*^{DOX} cells, to a lesser extent than in their BRCA2-deficient counterparts (Fig. 3.6). Again, activation of the immune response signalling was associated with KAP1 phosphorylation, which is consistent with the fact that DNA damage results in micronuclei formation and cGAS-STING activation in replicating cells (Reisländer, Groelly and Tarsounas, 2020).

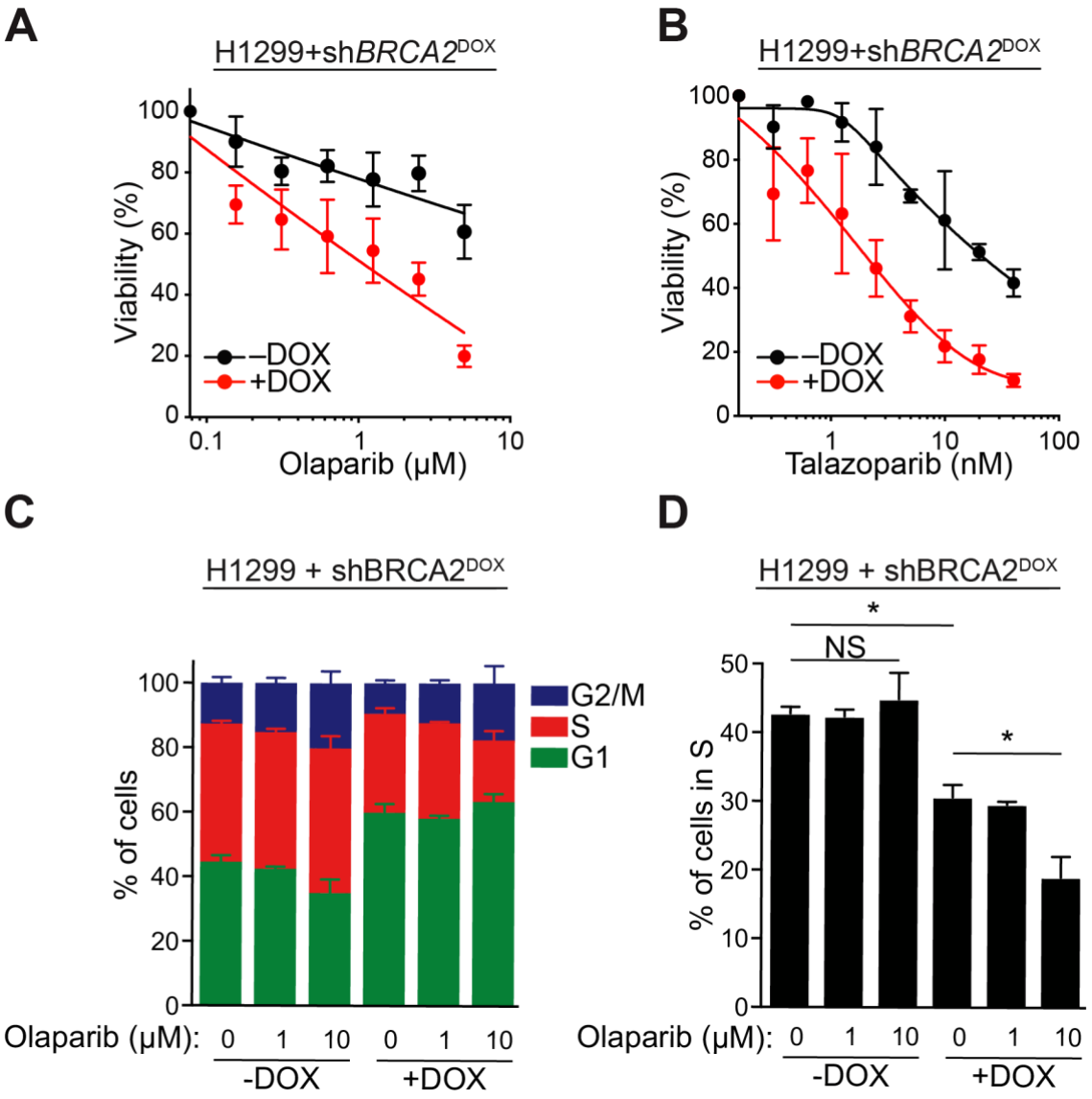


Fig. 3.5. Olaparib-treatment affects growth and survival of BRCA2-deficient H1299+sh*BRCA2*^{DOX} cells.

Dose-dependent viability assays of BRCA2-proficient (-DOX) or -deficient (+DOX) H1299+shBRCA2^{DOX} cells treated with (**A**) olaparib or (**B**) talazoparib at the indicated concentrations for six days. Graphs represent mean values and SEM of $n = 3$ independent experiments, each performed in technical triplicate. (**C**) Flow cytometry-based cell cycle analysis of BRCA2-proficient (-DOX) or -deficient (+DOX) H1299+sh*BRCA2*^{DOX} cells treated with olaparib at the indicated concentrations for three days. (**D**) S phase fraction of cells shown in (C). Graphs represent mean values and SEM of $n = 3$ independent experiments. p-values were calculated using an unpaired two-tailed t-test. $p \leq 0.05$, * ; $p > 0.5$, NS.

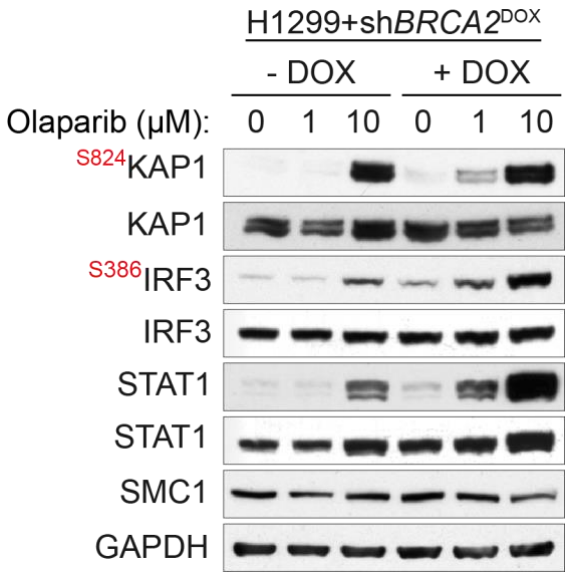


Fig. 3.6. Olaparib-treatment activates the cGAS-STING-IRF3 and JAK-STAT pathways in BRCA2-deficient H1299+sh*BRCA2*^{DOX} cells. H1299+sh*BRCA2*^{DOX} were grown in the presence or absence of DOX for four days and subsequently treated with olaparib at the indicated concentrations for three days. Whole-cell extracts were immunoblotted as indicated. Phosphorylation sites are indicated in red. GAPDH and SMC1 were used as loading controls.

Activation of a type I IFN response upon PARP inhibition was recapitulated in BRCA1-deficient and BRCA2-deficient xenograft tumour models. Indeed, RT-qPCR analysis showed that treatment with talazoparib upregulates the expression of ISGs in *BRCA1*-mutated MDA-MB-436 xenografts (data not shown; (Reisländer *et al.*, 2019)). Moreover, treatment talazoparib specifically increased the expression of ISGs in BRCA2$^{-/-}$ HCT116 xenograft models compared to their BRCA2$^{+/+}$ counterparts.

Altogether, this demonstrates that the PARP inhibitors are not only specifically toxic to BRCA1- and BRCA2-deficient cells and tumours by inflicting DNA lesions, but they also trigger a type I IFN response in these cells and tumours.

3.6 DNA damaging agents targeting BRCA2-deficiency trigger a type I IFN response

Endogenous and exogenous DNA damage is associated with immune response signalling (Reisländer, Groelly and Tarsounas, 2020). As we subsequently found olaparib-induced immune response signalling to be associated with DSB signalling, we tested whether other DNA damaging agents could trigger a type I IFN response. In particular, we focused on agents which have been reported to specifically induce DNA damage in HR repair-deficient cells.

G-quadruplex stabilizers, such as pyridostatin, are known to be specifically toxic to BRCA1- or BRCA2-deficient cells (Zimmer *et al.*, 2016; Xu *et al.*, 2017a; De Magis *et al.*, 2019). Whilst it has been suggested that pyridostatin's cytotoxic activity also involves R-loop formation (De Magis *et al.*, 2019; Miglietta, Russo and Capranico, 2020) or topoisomerase II poisoning (Olivieri *et al.*, 2020), it was shown to bind to G-quadruplex forming sequences and cause DNA damage (Rodriguez *et al.*, 2008; Rodriguez *et al.*, 2012). Pyridostatin treatment induced DNA damage in a dose-dependent manner, and we observed a greater effect in BRCA2-deficient than in BRCA2-proficient cells (Fig. 3.7A). Moreover, we observed an increase in IRF3 phosphorylation upon treatment with 10 µM pyridostatin, primarily in cells in which BRCA2 has been abrogated (Fig. 3.7A). Consistent with this finding, pyridostatin treatment caused micronuclei formation in U2OS transfected with an siRNA targeting *BRCA2* (De Magis *et al.*, 2019).

We then evaluated the effect of the alkylating agent chlorambucil on the immune response signalling. Whilst widely used to treat chronic lymphocytic leukaemia, chlorambucil was also proposed as a potential clinical candidate to target *BRCA2*-mutated tumours (Tacconi *et al.*, 2019). Indeed, chlorambucil-

induced DNA crosslinks lead to DNA damage accumulation and have been shown to be particularly toxic to BRCA2-deficient cells and tumours, including those with acquired PARP inhibitor resistance.

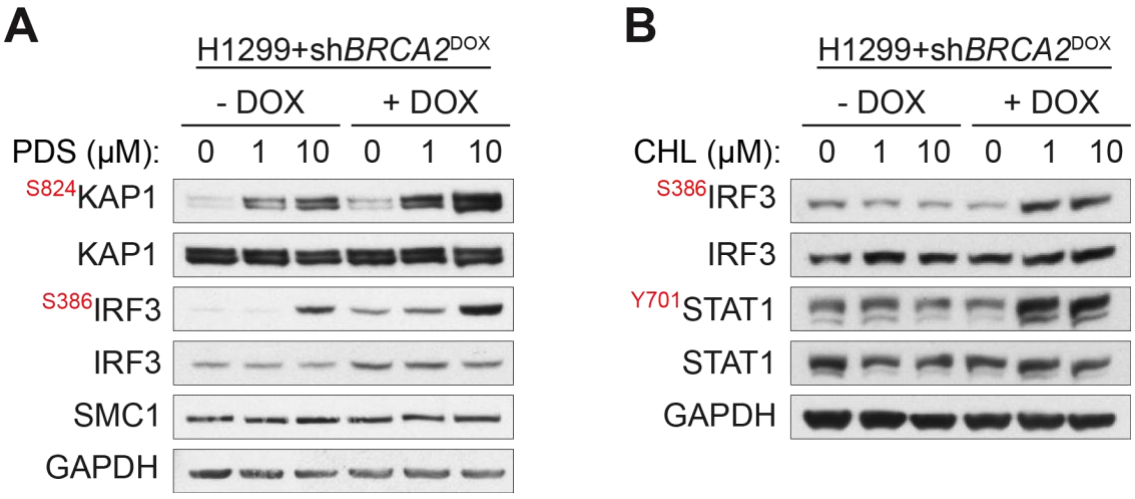


Fig. 3.7. DNA damaging agents activate the cGAS-STING-IRF3 and JAK-STAT pathways in BRCA2-deficient H1299+sh*BRCA2*^{DOX} cells. H1299+sh*BRCA2*^{DOX} were grown in the presence or absence of DOX for four days and subsequently treated with (**A**) pyridostatin (PDS) or (**B**) chlorambucil (CHL) at the indicated concentrations for three days. Whole-cell extracts were immunoblotted as indicated. Phosphorylation sites are indicated in red. GAPDH and SMC1 were used as loading controls.

Treatment of BRCA2-deficient H1299+sh*BRCA2*^{DOX} cells with 1 or 10 μM chlorambucil caused activation of the cGAS-STING-IRF3 and JAK-STAT pathways, as indicated by the phosphorylation of IRF3 and STAT1, respectively (Fig. 3.7B). Thus, chlorambucil triggers a type I IFN response in cells lacking functional BRCA2.

This suggests that DNA damage, and in particular DSBs, is associated with immune response signalling. We demonstrate that DNA damaging agents with specific activity against BRCA2-deficient cells, such as PARP inhibitors, G-

quadruplex stabilisers, or alkylating agents, activate a type I IFN response in these cells.

3.7 Functional up-regulation of ISG15 and its ISGylation activity

We next tested whether the increase in ISGs mRNA levels after BRCA2 abrogation can lead to an increase in protein levels. We focused on *ISG15*, which encodes the eponym ubiquitin-like protein (Skaug and Chen, 2010; Zuo *et al.*, 2016). ISG15 can covalently bind to target proteins, in a process called ISGylation (Fig. 3.8A). Moreover, we included in our analysis two other ISGs, whose products play key roles in the ISGylation pathway: the E3 ligase HERC5, and the hydrolase USP18, which catalyses the deISGylation reaction (Fig. 3.8A; (Skaug and Chen, 2010; Zuo *et al.*, 2016)). ISG15 has been linked to DNA replication and to the DNA damage response (Park *et al.*, 2014; Raso *et al.*, 2020). In particular, PCNA ISGylation has been shown to facilitate its de-ubiquitination following UV-induced DNA damage, suggesting that ISG15 negatively regulates translesion synthesis and prevents error-prone DNA replication (Park *et al.*, 2014). Moreover, *USP18* knock-out radio-sensitised HAP1 cells (Pinto-Fernandez *et al.*, 2020).

Endogenous ISG15 was detected in H1299+sh*BRCA2*^{DOX} cells independently of the BRCA2 status (Fig. 3.8B). As we were interested in ISG15 functions in response to DNA damage, we used olaparib to stimulate ISG15 expression. Treatment with 10 µM olaparib did not only activate the JAK-STAT pathway (Fig. 3.6) but also increased ISG15 levels in BRCA2-deficient cells (Fig. 3.8B). Moreover, HERC5 and USP18 levels were higher in BRCA2-deficient H1299+sh*BRCA2*^{DOX} cells than in their BRCA2-proficient counterparts (Fig. 3.8B).

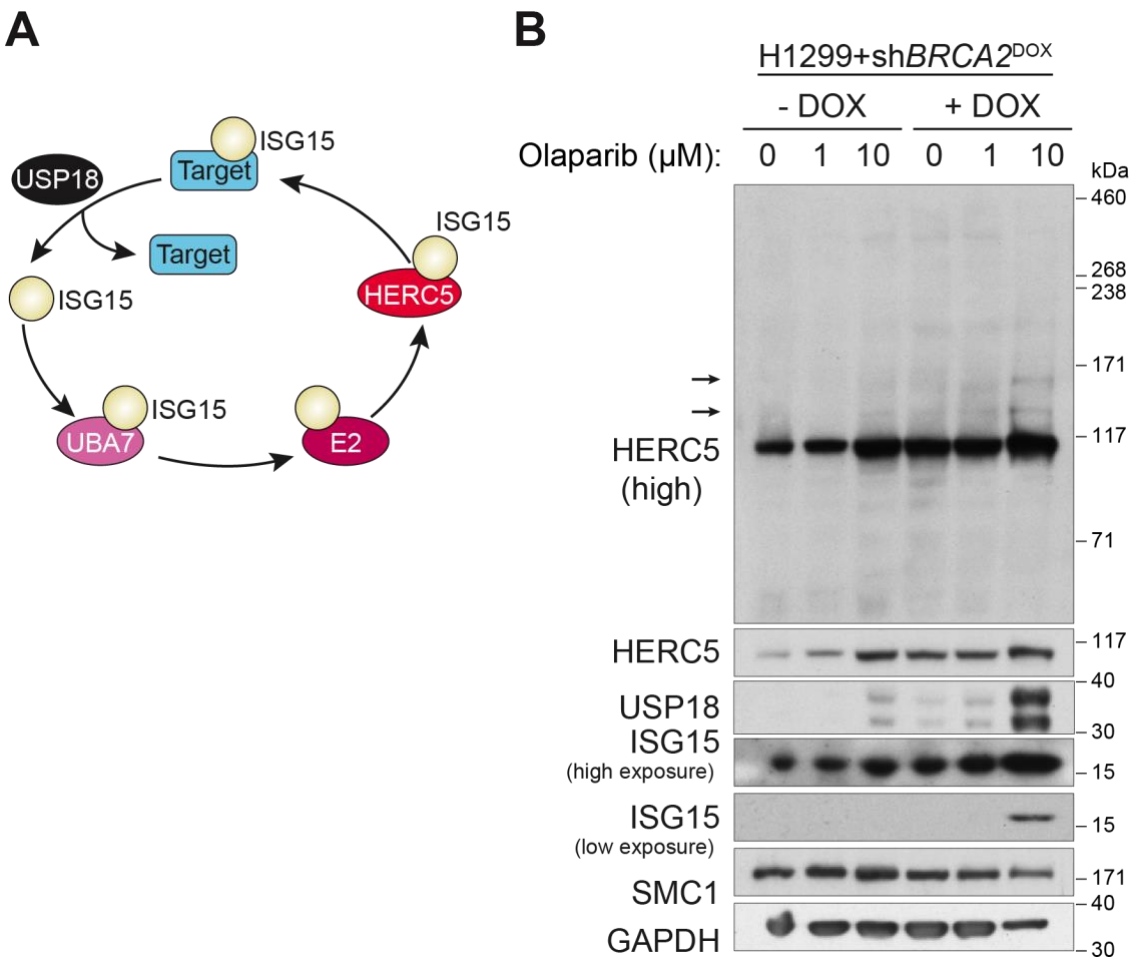


Fig. 3.8. Functional expression of ISG15 upon BRCA2 depletion and Olaparib treatment.

(**A**) Schematic representation of the ISGylation and deISGylation mechanism. Covalent binding of ISG15 to target proteins is catalysed by its sequential interaction with E1, E2 and E3 ligases, whilst conjugated-ISG15 is cleaved from target protein by the hydrolase USP18. (**B**) H1299+sh*BRCA2*^{DOX} were grown in the presence or absence of DOX for four days and subsequently treated with olaparib at the indicated concentrations for three days. Whole-cell extracts were immunoblotted as indicated. Arrows indicate ISGylated HERC5. GAPDH and SMC1 were used as loading controls.

Olaparib treatment increased ISG15, HERC5 and USP18 levels in both BRCA2-proficient and BRCA2-deficient cells, albeit a stronger effect was observed in the latter. This shows that that ISG induction observed in BRCA2-deficient cells and further enhanced by PARP inhibition leads to an increase in the levels of the encoded proteins and therefore may have a biological function.

Finally, we did not find evidence of ISGylation when detecting ISG15 by immunoblotting. Indeed, ISG15 appeared as a single band at its expected molecular weight of 18 kDa. In contrast, HERC5 appeared as three distinct bands in olaparib-treated BRCA2-deficient cells. Whilst one band is common to all tested samples, the two additional bands, less than 54 kDa above HERC5's expected molecular weight, have been reported to be ISGylated HERC5 (Fig. 3.8B; (Pinto-Fernandez *et al.*, 2020)). Hence, this suggest that the activation of a type I IFN response observed in BRCA2-deficient cells treated with olaparib, leads to a functional expression of ISG15 and increased ISGylation. Whether this impacts on the DNA damage response in the absence of BRCA2 remains to be elucidated.

3.8 Discussion

In this study we use RNA-seq analyses to identify genes which expression was altered upon long-term (chronic), but not short-term (acute) BRCA2 abrogation. Indeed, we found that genes mediating immune response signalling are upregulated upon chronic BRCA2 abrogation. Whilst this phenotype was more pronounced in H1299+sh*BRCA2*^{DOX} than in MDA-MB-231+sh*BRCA2*^{DOX} cells, our analysis revealed 28 genes to be commonly upregulated in both cell lines. Because these genes are ISGs, we concluded that BRCA2 abrogation triggers a type I IFN response. We showed that BRCA2 abrogation leads to micronuclei

formation, which activates the cGAS-STING-IRF3 and JAK-STAT pathways. Similar findings were reported in a recent study (Heijink *et al.*, 2019). Using stable isotope labelling by amino acids in cell culture (SILAC) coupled to mass spectrometry, the authors observed an upregulation of immune response proteins upon shRNA-mediated BRCA2 abrogation in BT-549 and HCC38 cells (Heijink *et al.*, 2019). Unlike what we observed in H1299 and MDA-MB-231 cells, the authors found that loss of BRCA2 expression resulted in a strong decrease in cell viability. In particular, p53-negative KBM-7 cells died within a week of BRCA2 abrogation. Strikingly, BRCA2 abrogation led to the production of pro-inflammatory cytokines, including TNFα, and activation of a pro-apoptotic signalling cascade via its receptor, TNFR1. In contrast, we found the pro-survival receptor TNFR2 (*TNFRSF1B*, Fig. 3.2) as a highly upregulated hit after 28 days of DOX treatment in H1299 cells. Whilst we have not tested whether TNFR2-mediated signalling underlies the long-term survival of our BRCA2-deficient models, these findings elegantly demonstrate that inactivation of *TP53* is not sufficient to promote the survival of *BRCA1/2*-mutated cells. Whether the tissue-specific tumorigenesis observed in patient carrying deleterious BRCA1/2 mutations relies on such transcriptional changes remains to be elucidated (Elledge and Amon, 2002).

Other recent studies have associated the loss of other DNA repair genes with micronuclei formation and immune response signalling (Reisländer, Groelly and Tarsounas, 2020). For instance, loss of *RNASE2H* or *SAMHD1*, which are associated with the autoinflammatory disorder Aicardi-Goutières syndrome, leads to micronuclei formation or release of genomic DNA into the cytosol,

respectively, which activates the cGAS-STING axis (Mackenzie *et al.*, 2016; Mackenzie *et al.*, 2017; Coquel *et al.*, 2018).

We also demonstrated that treatment with DNA damaging agents further enhance the innate immune response. In particular, we used drugs specifically targeting BRCA2-deficient cells and tumours, such as PARP inhibitors, G-quadruplex stabilisers and DNA crosslinking molecules. We showed that these agents preferentially trigger an immune response in BRCA2-deficient cells, which correlated with accumulation of DSBs and activation of the cGAS-STING-IRF3 axis. Similar results were obtained in BRCA1-deficient tumour models treated with PARP inhibitors (Ding *et al.*, 2018; Pantelidou *et al.*, 2019; Reisländer *et al.*, 2019). These findings are in line with reports associating IR-induced DNA damage with micronuclei formation or release of genomic DNA into the cytosol, and subsequent activation of an immune response signalling (Mackenzie *et al.*, 2016; Erdal *et al.*, 2017).

Finally, we showed that the activation of a type I IFN response leads to functional upregulation of proteins catalysing ISGylation reactions, especially in BRCA2-deficient cells treated with PARP inhibitors. We detected an increase in ISG15, USP18 and HERC5 protein levels, as well as in ISGylated HERC5. How increased ISGylation affects the survival and drug response of BRCA2-deficient cells is as yet unknown. However, given previously described functions of ISG15 in DNA replication and repair (Park *et al.*, 2014; Pinto-Fernandez *et al.*, 2020; Raso *et al.*, 2020), this post-translational modification could be of clinical significance for the treatment of *BRCA2*-mutated cancers. Because loss of USP18 radio-sensitises cells to IR (Pinto-Fernandez *et al.*, 2020), ISGyation reactions may play role in therapy resistance. It will therefore be crucial to assess

whether the upregulation of ISGs observed upon long-term BRCA2 inactivation impacts on the cell's intrinsic response to therapies. Moreover, establishing the "ISGylome" (Pinto-Fernandez *et al.*, 2020) of BRCA2-deficient cells may bring new insights into the role of the ISGs. Finally, with the increased use of CRISPR/Cas9 screens to identify mechanisms of resistance or sensitivity to anti-tumoural compounds (Olivieri *et al.*, 2020), our findings indicate that context-specific transcriptional changes must be taken into account. For instance, a dropout screen with PARP inhibitors may show different outcome depending on the level of expressed ISGs in the cell line studied, and may therefore identify novel synthetic lethal interactions.

Whilst we did not investigate whether immune response signalling impacts on the host's immune system, other studies brought insights into this interplay. Increased CD4+ and CD8+ T cell infiltration was observed in DDR-deficient, including *BRCA1* and *BRCA2*-mutated, breast cancer tumours (Parkes *et al.*, 2017). Moreover, PARP inhibitors' *in vivo* anti-tumour activity relies, in part, on STING activation and the consequent lymphocyte infiltration within the tumour micro-environment (Ding *et al.*, 2018; Pantelidou *et al.*, 2019). Accordingly, synergistic anti-tumour effects were observed in mice harbouring BRCA1-deficient tumours and treated with PARP inhibitors in combination with anti-PD-1 antibody (Ding *et al.*, 2018; Wang *et al.*, 2019) or anti-CTLA-4 antibody (Higuchi *et al.*, 2015). Such combinations are currently being extensively explored in clinical contexts (Reisländer, Groelly and Tarsounas, 2020). Finally, the fact that other DNA damaging agents (e.g. alkylating agents) trigger an immune response signalling in BRCA2-deficient cells suggests that they may also have synergistic

anti-tumour activity when combined to immune checkpoint inhibitors (Reisländer, Groelly and Tarsounas, 2020).

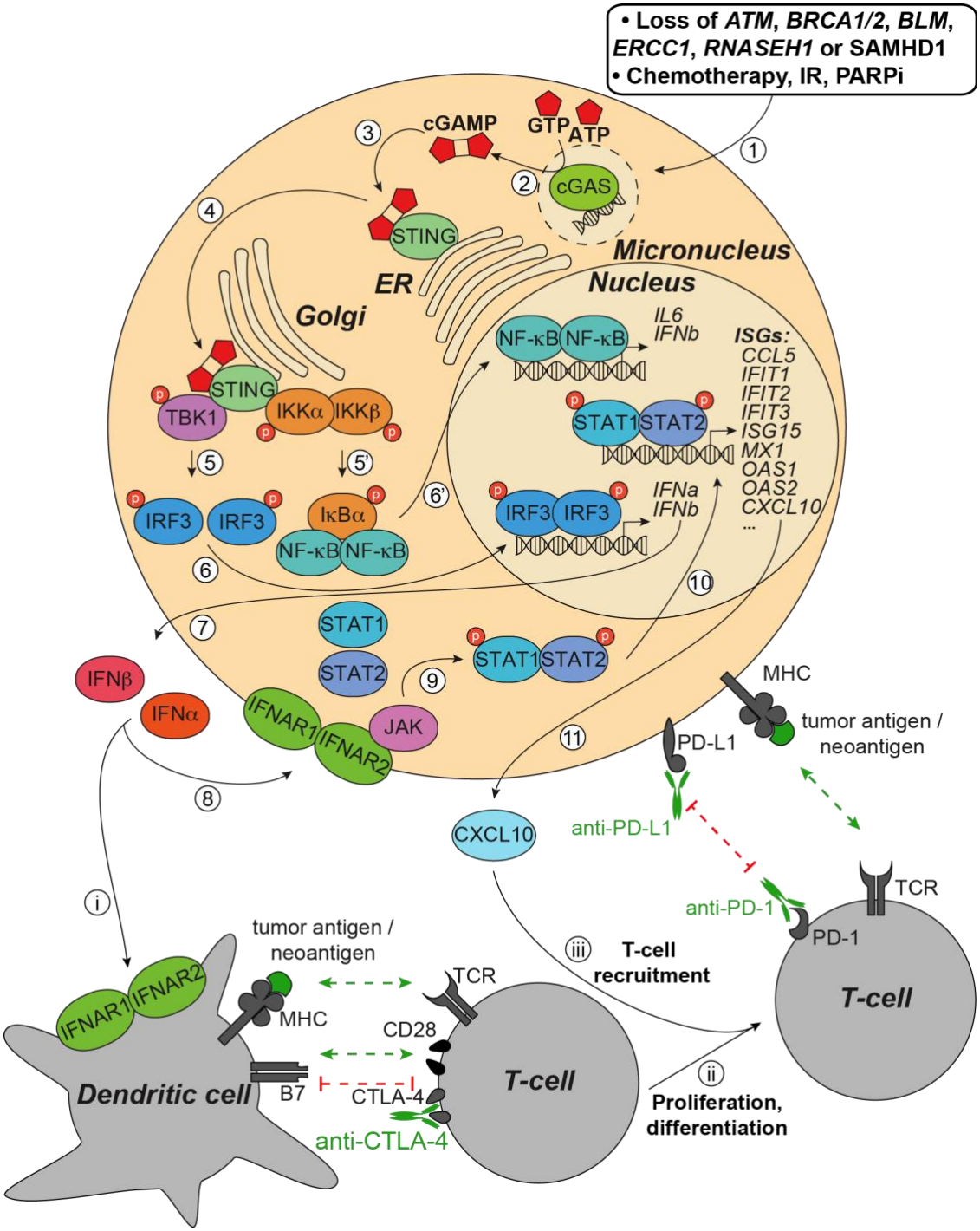


Fig. 3.9. Interplay between the DNA damage response and the innate immune response for cancer (immuno-)therapy.

Top: Endogenous (e.g., BRCA2 abrogation) or exogenous (e.g. PARP inhibition, IR) DNA damaging factors can lead to micronuclei formation and activation of the cGAS-STING pathway. Alternatively, DNA damage can lead to accumulation of mutations in protein coding sequences and expression of neoantigens. The cGAS-STING axis trigger the nuclear translocation of the dimeric IRF3 or NF-kB transcription factors which triggers secretion of IFNα and IFNβ. In cancer cells, autocrine IFN signalling activates the JAK/STAT pathway and causes expression of interferon-stimulated genes (ISGs), which is known as a type I IFN response. **Bottom**: Type I IFN signalling facilitates the recruitment of immune effector cells by promoting tumour antigen/neo-antigen presentation on the major histocompatibility complex (MHC) of dendritic cells. T-cell activation depends on the balance between the MHC:T cell receptor (TCR) stimulatory signal (green), B7:CD28 stimulatory signals (green) and B7:CTLA-4 inhibitory signals (red). T cells tumour infiltration is stimulated by chemokines (e.g., CXCL10). The immune effectors' anti-tumour activity depends on the balance between the MHC:TCR stimulatory signal (green), and the PD-1:PD-L1 inhibitory signal (red). Inhibition of immunosuppressive signals (red) by anti-CTLA-4, anti-PD-1, or anti-PD-L1 antibodies (green) potentiates the anti-tumorigenic immune responses. (Figure adapted from Reisländer, Groelly and Tarsounas, 2020).

Chapter 4

Protocols for high-resolution detection of mitotic DNA synthesis (MiDAS) using mitotic EdU-seq.

4.1 Introduction

Chromosome fragility is often detected as the breakage of condensed chromosomes in mitosis, observed by microscopy. Similarly, MiDAS is detected using fluorescence microscopy of EdU incorporation during mitosis. In order to facilitate the analysis and increase the number of detected events, mitotic cells are enriched by drug-induced mitotic arrest, often preceded by drug-induced G2-arrest and release into mitosis. However, there are limitations to these strategies, the most important being that whilst chromosome breaks can be detected throughout mitosis, MiDAS occurs early after mitotic entry. Indeed, addition of a thymidine analogue at early but not late M-phase stages allowed detection of aphidicolin-induced MiDAS in U2OS (Minocherhomji *et al.*, 2015). Hence, the timing of nascent DNA labelling needs to be tightly controlled and MiDAS detection would preferentially take place upon synchronised mitotic entry.

To ensure that the MiDAS events detected in each single experiment originate from a homogenous cell population (e.g., is not affected by the position within the cell cycle of individual cells at the start of the experiment), we used the double synchronisation strategy described below.

4.2 Synchronous S phase progression

Cells were blocked at the G1/S transition by a single thymidine block. Thymidine concentration and treatment duration were optimised to obtain the best synchronisation upon release into S phase, for both BRCA2-proficient and BRCA2-deficient H1299+sh*BRCA2*^{DOX} cells, as measured by propidium iodide-based flow cytometry. Treatment with 1.5 mM thymidine for 16 h efficiently blocked cells at the G1/S transition, independently of the BRCA2 status (Fig.

4.1A). Flow cytometry analysis showed that cells entered S phase and initiated DNA replication 2-7 h after release from the thymidine block (Fig. 4.1A). Moreover, a large fraction of cells appeared to have duplicated their genome 8 h after release from the thymidine block (Fig. 4.1A). Finally, passage through mitosis and cytokinesis took place 9 h to 11 h after S phase entry (Fig. 4.1A). Importantly, S phase progression occurred in a synchronous manner in both BRCA2-proficient and BRCA2-deficient H1299+sh*BRCA2*^{DOX} cells with no detectable difference between the two conditions (Fig. 4.1A).

To confirm these results, we next monitored Cyclin B levels and phosphorylation of Histone H3 at serine 10 (S10), markers of S and M phases progression, respectively. Cyclin B levels are known to increase in late S and G2 phases to promote mitotic entry and its degradation in anaphase promotes mitotic exit (Jin, Hardy and Morgan, 1998; Saldivar *et al.*, 2018). Consistently with DNA content analysis, we observed a time-dependant increase in Cyclin B levels 7 to 9 h after release from thymidine block in both BRCA2-proficient and BRCA2-deficient H1299+sh*BRCA2*^{DOX} (Fig. 4.1B). Phosphorylated Histone H3 levels increased throughout the analysed time period with higher levels detected 9 h and 10 h after release from thymidine block (Fig. 4.1B). Finally, we observed a drop in Cyclin B levels 10 h after release from thymidine block (Fig. 4.1B), which is consistent with the large fraction of cell undergoing cytokinesis observed by flow cytometry at the same timepoint (Fig. 4.1A).

Altogether, these data demonstrate that a single thymidine block is sufficient to ensure synchronous S phase progression in H1299+sh*BRCA2*^{DOX}. Moreover, S phase progression and mitotic entry are not affected by the BRCA2 status under these conditions.

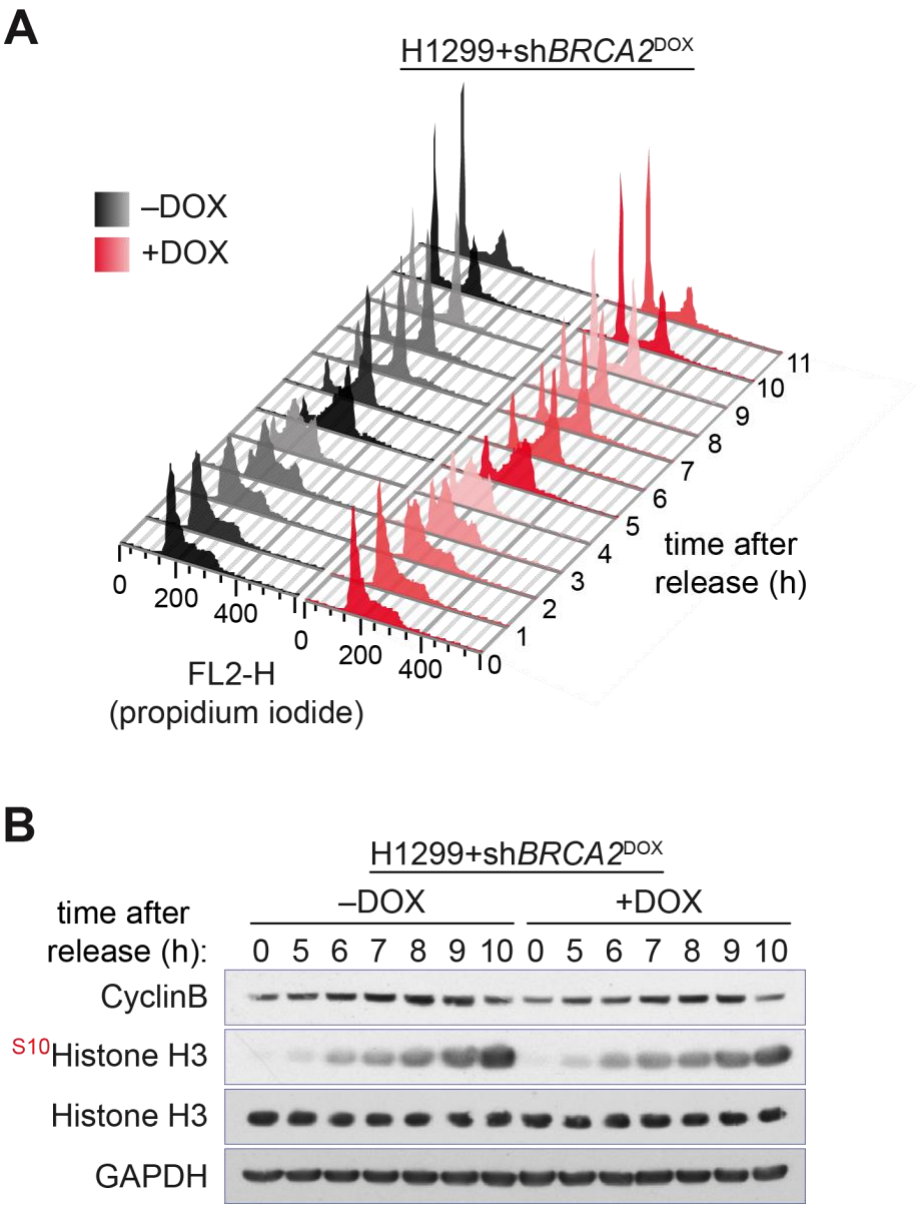


Fig. 4.1. Cell cycle progression after thymidine block and release. BRCA2-proficient (-DOX) or -deficient (+DOX) H1299+sh*BRCA2*^{DOX} cells were blocked at the G1/S transition using 1.5 mM thymidine for 16 h and released in fresh medium. (**A**) At indicated timepoints, cells were subject to flow cytometry analysis and their total DNA content was determined using propidium iodide staining. (**B**) At indicated timepoints, whole-cell extracts were immunoblotted as shown. Phosphorylation sites are indicated in red. GAPDH and Histone H3 were used as loading controls.

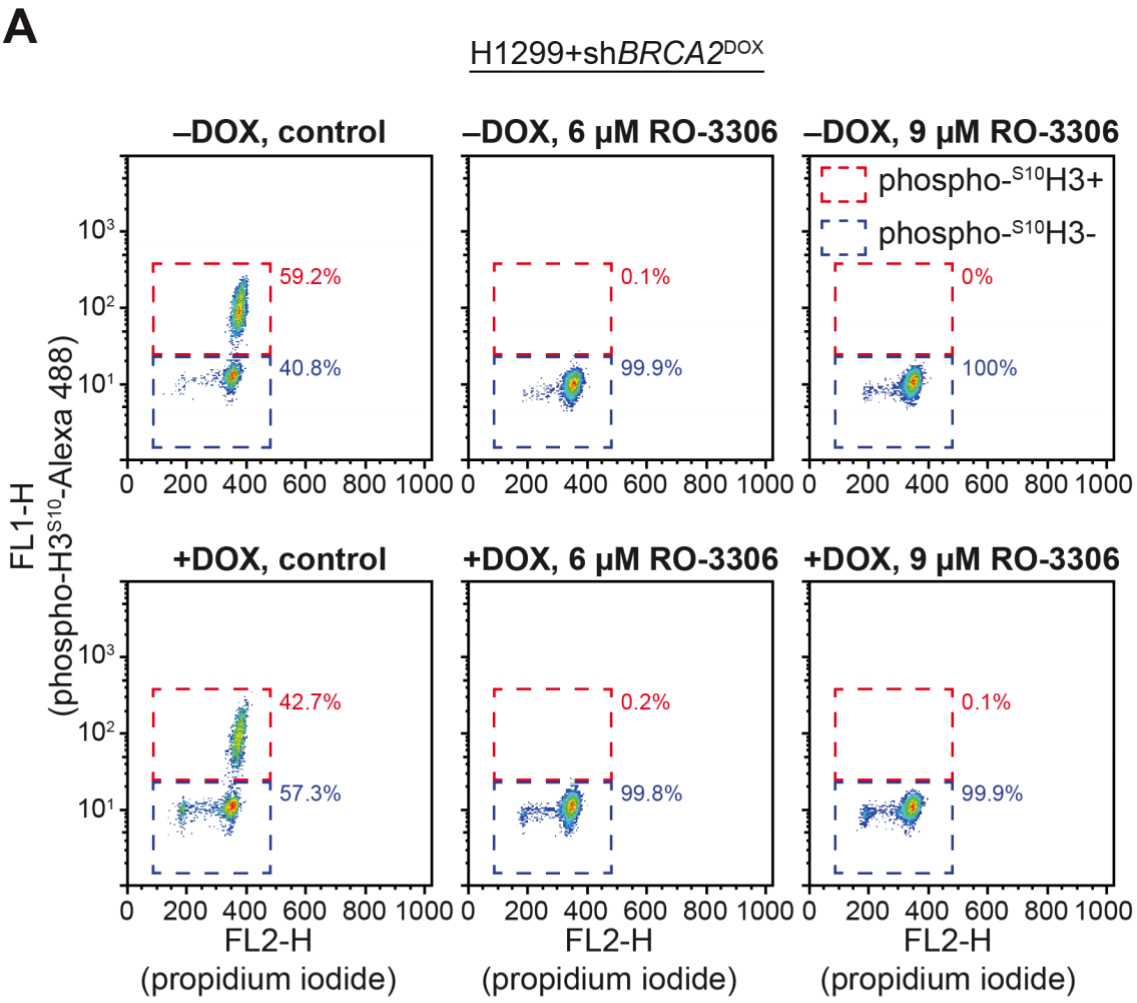
4.3 Cell synchronisation in G2/M

To ensure that cells enter mitosis synchronously, we synchronised the cells in G2/M using the CDK1 inhibitor RO-3306. We performed flow cytometry and detected mitotic cells based on Histone H3 phosphorylation at serine 10 and propidium iodide staining. Whilst 59% of the BRCA2-proficient cells and 43% of the BRCA2-deficient cells were in mitosis 12 h after release from thymidine block, incubation with 6 or 9 μM RO-3306 abrogated mitotic entry (Fig. 4.2A).

Next, we tested if addition of RO-3306 impacted on S phase progression. DNA content analysis by flow cytometry confirmed that treatment with 6 μM RO-3306 does not impair S phase progression (Fig. 4.2B).

4.4 Protocol for detection of MiDAS under untreated conditions using mitotic EdU-seq

To detect MiDAS by mitotic EdU-seq, we synchronised cells using a combination of thymidine and RO-3306 blocks, optimised as above. As an initial starting point, we allowed synchronised cells to progress through S phase in the presence of 6 μM RO-3306 for 10.5 h after release from the thymidine block. Cells were then released from the G2 arrest and allowed to enter mitosis for 90 min. This corresponded to the time required for about half of the cells (40% to 60%) to reach mitosis (Fig. 4.2A; Fig. 4.3A). Nascent DNA was labelled with EdU in order to detect MiDAS. Moreover, we used the microtubule poison nocodazole to prevent mitotic exit. Of note, MiDAS takes place in early M-phase and hence, can still be captured in nocodazole arrested cells (Minocherhomji *et al.*, 2015). Finally, mitotic cells were collected by mitotic shake-off (Fig. 4.3B) and EdU-labelled DNA was purified as described in the material and methods section (chapter 2).


A
H1299+shBRCA2DOX
–DOX, control
–DOX, 6 μM RO-3306
–DOX, 9 μM RO-3306
+DOX, control
+DOX, 6 μM RO-3306
+DOX, 9 μM RO-3306
phospho-S10H3+
phospho-S10H3-
59.2%
40.8%
0.1%
99.9%
0%
100%
42.7%
57.3%
0.2%
99.8%
0.1%
99.9%
FL1-H
(phospho-H3S10-Alexa 488)
FL2-H
(propidium iodide)

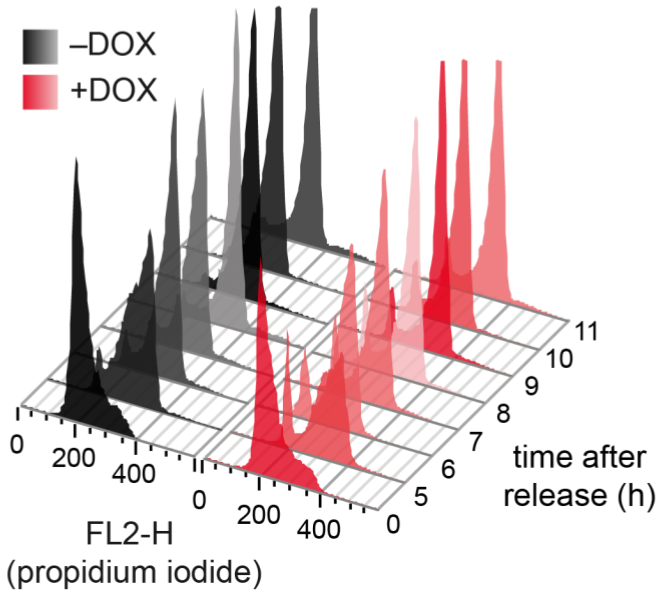

B
H1299+shBRCA2DOX
–DOX
+DOX
time after release (h)
FL2-H
(propidium iodide)

Fig. 4.2. RO-3306-induced G2 block does not stop S phase progression.

BRCA2-proficient (-DOX) or -deficient (+DOX) H1299+sh*BRCA2*^{DOX} cells were blocked at the G1/S transition using 1.5 µM thymidine for 16 h and released in fresh medium containing 6 or 9 µM RO-3306 for 12h. (**A**) Cells were subject to flow cytometry analysis and mitotic cells were detected using propidium iodide and phosphorylated Histone H3 (S10) staining. (**B**) At indicated timepoints, cells were subject to flow cytometry analysis and their total DNA content was determined using propidium iodide staining.

Importantly, we added 2 mM hydroxyurea (HU) to the growth medium for 3 h prior to the mitotic shake-off. This prevented contamination of the EdU-labelled mitotic DNA with EdU-labelled S phase DNA. Whilst HU depletes the dNTP pool and stalls DNA replication in S phase, it does not prevent MiDAS ((Macheret *et al.*, 2020); Chapter 5). Moreover, the presence or absence of HU prior to the mitotic shake-off did not impact on aphidicolin-induced MiDAS foci in U2OS (Macheret *et al.*, 2020).

An overview of the protocol used to detect MiDAS under untreated conditions is shown in Fig. 4.3B.

4.5 Low dose aphidicolin delays S phase progression

Low dose aphidicolin partially inhibits DNA polymerases Pol α, δ, and ϵ, as well as Pol ζ (Baranovskiy *et al.*, 2014), and therefore slows down replication rates (Glover et al., 1984). Hence, treatment with low dose aphidicolin induces common fragile sites expression and activates MiDAS at these sites (Glover *et al.*, 1984; Minocherhomji *et al.*, 2015; Macheret *et al.*, 2020). To map common fragile sites in H1299+sh*BRCA2*^{DOX} cells, we used a variation of the previously described protocol where we treated S phase cell with aphidicolin.

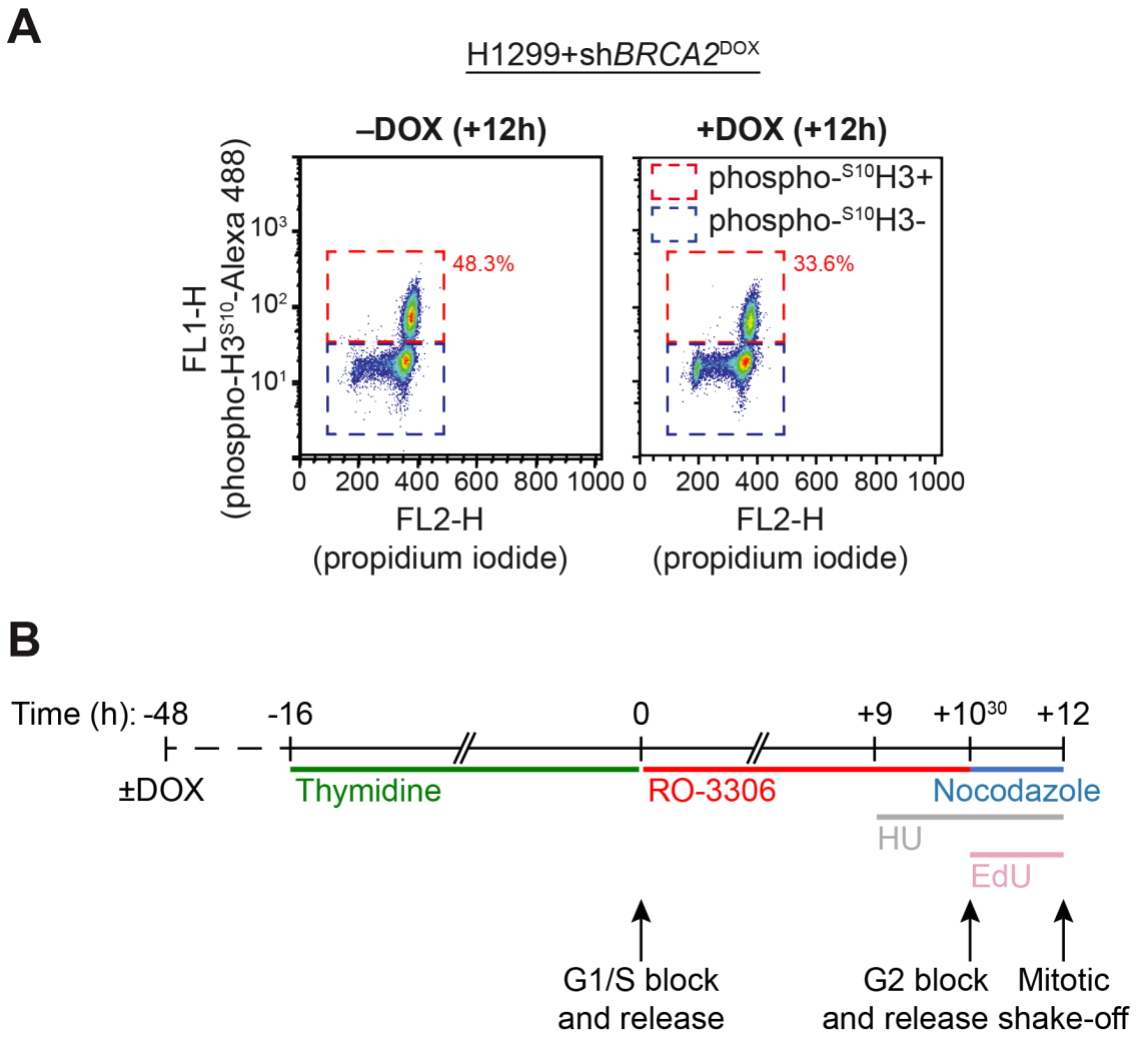


Fig. 4.3. Mitotic EdU-seq protocol for H1299+sh*BRCA2*^{DOX} cells.
(**A**) BRCA2-proficient (-DOX) or -deficient (+DOX) H1299+sh*BRCA2*^{DOX} cells were blocked at the G1/S transition using 1.5 µM thymidine for 16 h, subsequently released in medium containing 6 µM RO-3306 for 10.5 h and released in medium containing 100 ng/ml nocodazole for 90 min. Cells were subject to flow cytometry analysis and mitotic cells were detected using propidium iodide and phosphorylated Histone H3 staining. (**B**) Overview of the protocol for detection of MiDAS under untreated conditions by mitotic EdU-seq in BRCA2-proficient (-DOX) or -deficient (+DOX) H1299+sh*BRCA2*^{DOX} cells.

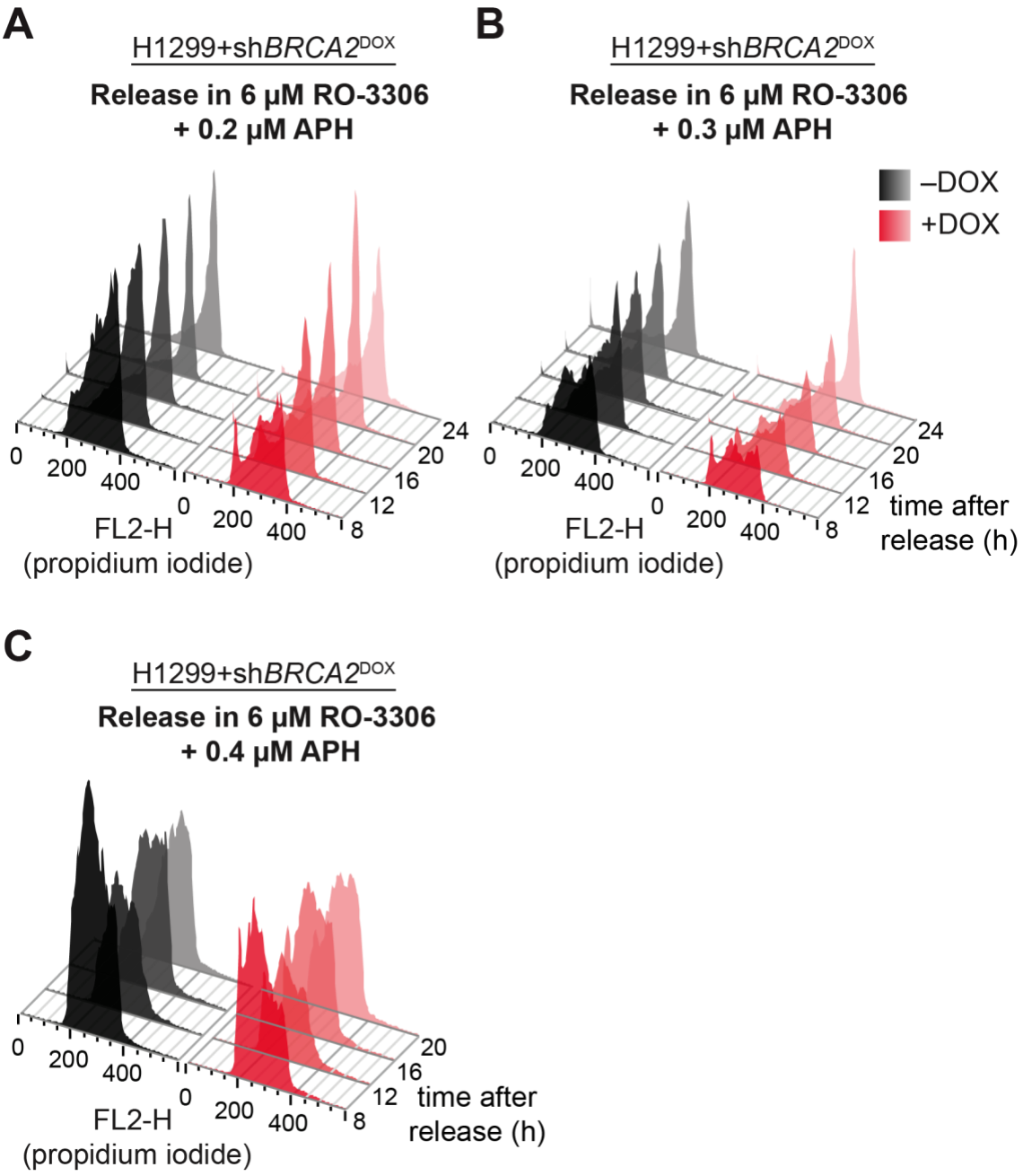


Fig. 4.4. S phase progression upon aphidicolin treatment.
BRCA2-proficient (-DOX) or -deficient (+DOX) H1299+sh*BRCA2*^{DOX} cells were blocked at the G1/S transition using 1.5 µM thymidine for 16 h and released in medium containing (**A**) 0.2 µM, (**B**) 0.3 µM or (**C**) 0.4 µM aphidicolin (APH). At indicated timepoints, cells were subject to flow cytometry analysis and their total DNA content was determined using propidium iodide staining.

We assessed the effect of a range of aphidicolin concentrations on S phase progression following release from thymidine block and in the presence of RO-3306. Unlike untreated cells which had completed DNA duplication (Fig. 4.1A), aphidicolin-treated cells were mainly in S phase 8 h after release from the thymidine block (Fig. 4.4A-C). Indeed, cells treated with 0.2 µM or 0.3 µM aphidicolin required 20 or 24 h, respectively, to duplicate their genome (Fig. 4.4A,B). Cells treated with 0.4 µM aphidicolin only reached mid- to late S phase 20 h after release from thymidine block (Fig. 4.4C). We did not observe obvious disparities in S phase progression between BRCA2-proficient and BRCA2-deficient H1299+sh*BRCA2*^{DOX} treated with aphidicolin. Since 0.2 µM aphidicolin was sufficient to double the time needed for genome duplication, we decided to continue using these conditions.

4.6 Protocol for detection of MiDAS events induced by low dose aphidicolin

We next assessed mitotic entry of aphidicolin-treated cells. After an initial thymidine block, cells were allowed to progress through S phase in the presence of 0.2 µM aphidicolin and 6 µM RO-3306 for 17.5 or 20.5 h, and subsequently released into mitosis for 90 min. Surprisingly, we detected more mitotic cells at the earliest timepoint (e.g., cells collected after 19 h compared to cells collected after 22 h, Fig. 4.5A). Moreover, floating cells we observed in the growth medium 20 h after release in aphidicolin- and RO-3306-containing medium, suggesting that prolonged treatment is toxic to the cells. We could not see any rounded cells characteristic of mitosis when the duration of the aphidicolin and RO-3306 treatment was reduced to 15.5 or 16.5 h (data not shown). We decided to collect cells for mitotic EdU-seq at 19 h post-thymidine.

An overview of the protocol used to detect aphidicolin-induced MiDAS is shown in Fig. 4.5B.

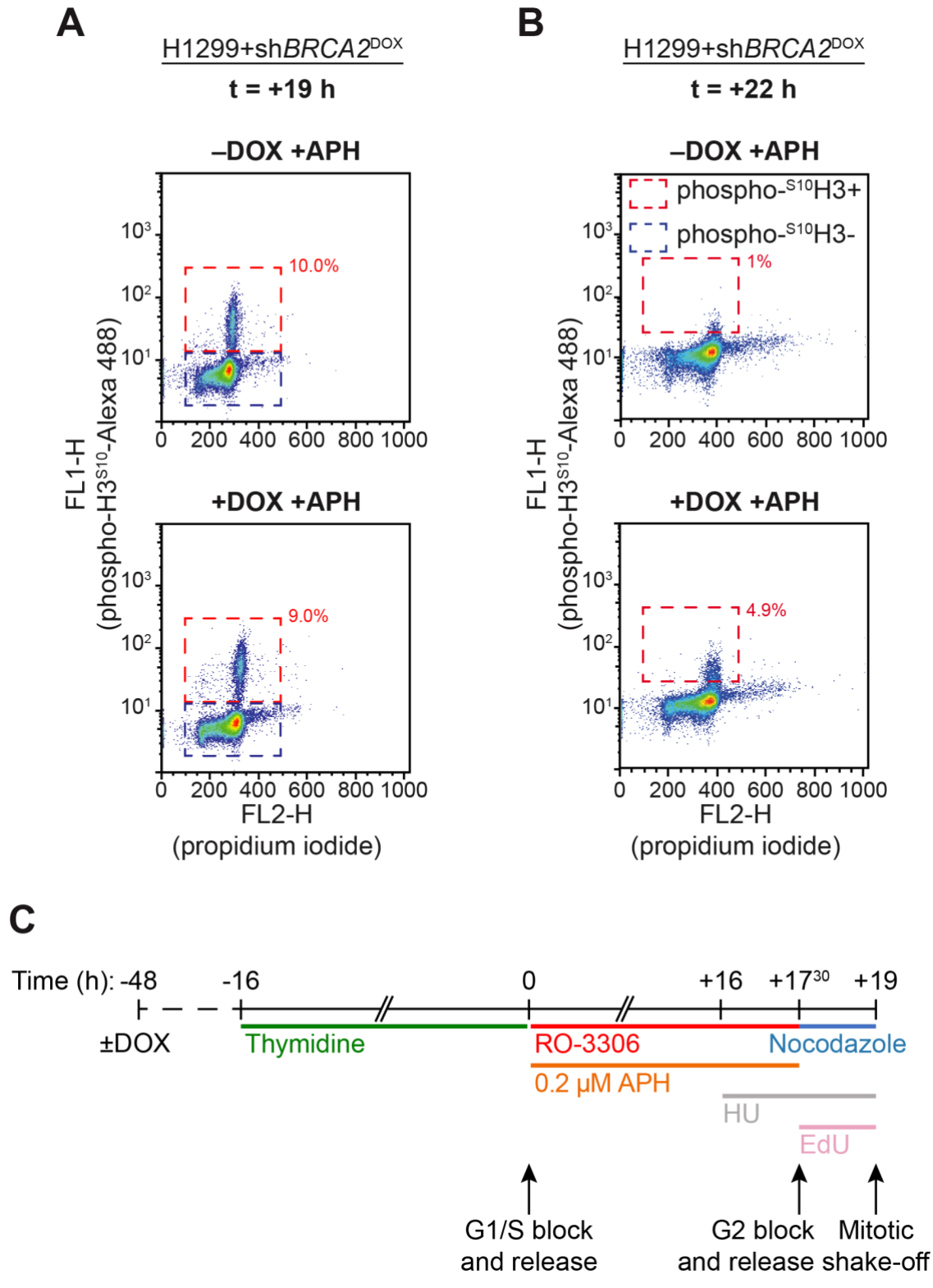


Fig. 4.5. Mitotic EdU-seq protocol for aphidicolin-treated H1299+sh*BRCA2*^{DOX} cells.

BRCA2-proficient (-DOX) or -deficient (+DOX) H1299+sh*BRCA2*^{DOX} cells were blocked at the G1/S transition using 1.5 µM thymidine for 16 h, subsequently released in medium containing 6 µM RO-3306 and 0.2 µM aphidicolin (APH) for (**A**) 17.5 or (**B**) 20.5 h and released in medium containing 100 ng/ml nocodazole for 90 min. Cells were subject to flow cytometry analysis and mitotic cells were detected using propidium iodide and phosphorylated Histone H3 staining. (**C**) Overview of the protocol for detection of aphidicolin-induced MiDAS by mitotic EdU-seq in BRCA2-proficient (-DOX) or -deficient (+DOX) H1299+sh*BRCA2*^{DOX} cells.

4.7 Discussion

In this chapter we describe optimisation of a protocol for MiDAS high-resolution detection using mitotic EdU-seq. Two distinct versions of the protocol permit detection of MiDAS induced by aphidicolin treatment or by BRCA2 inactivation. MiDAS can be detected upon shRNA-mediated knock-down of *BRCA2*, as well as in control, *BRCA2*-expressing cells in the absence of exogenous replication stress. In contrast, MiDAS occurring at common fragile sites can be identified in cells grown in the presence of the DNA polymerase inhibitor, aphidicolin ((Macheret *et al.*, 2020); see Chapter 5). Both protocols were developed around two main requirements: a) synchronous S phase progression and b) synchronous mitotic entry in the presence of EdU.

To ensure synchronous S phase progression, we arrested cells at the G1/S transition using a single thymidine block. Optimal conditions (1.5 mM thymidine for 16 h) were identified experimentally, although alternative synchronisation approaches, such as serum-starvation or lovastatin-induced G1 arrest, may also be considered. We then confirmed that S phase entry and

progression were synchronous, and measured the time required for genome duplication for both BRCA2-proficient and BRCA2-deficient cells, treated or not with aphidicolin. Whilst S phase progression was delayed by aphidicolin treatment in a dose-dependent manner, it was largely unaffected by BRCA2 abrogation relative to BRCA2-expressing cells.

To ensure synchronous mitotic entry, S phase progressing cells were treated with the CDK1 inhibitor RO-3306 and subsequently released into mitosis. The release from G2 block as performed by RO-3306 removal was timed to obtain the maximum number of mitotic cells as possible, without causing extensive G2 arrest. Of note, only one tenth of the aphidicolin-treated cells entered mitosis under these conditions. Whilst RO-3306 inhibits CDK1-mediated mitotic entry without stopping S phase progression (Fig.4.2 and 4.4), the consequences of CDK1 inhibition on DNA replication, origin firing, or DNA damage repair are not fully understood (Johnson *et al.*, 2011; Moiseeva *et al.*, 2019; Brison *et al.*, 2020). In the future, it will be important to ensure that the described chromosome fragility and MiDAS phenotypes are independent of the methods used for cell synchronisation, namely thymidine-induced G1/S arrest and RO-3306-mediated G2 block.

Finally, mitotic cells were collected and subjected to mitotic EdU-seq. Importantly, HU was added 3 h prior to the mitotic shake-off to avoid contamination from S phase DNA synthesis, without affecting MiDAS (Macheret *et al.*, 2020).

Of note, a fraction of the untreated cell population was arrested in G1 (Fig. 4.2 A, B) and a larger part of the aphidicolin-treated cell population was in G1 and S phases (Fig. 4.5A) at the end of the final timepoint. Because S phase DNA

replication was inhibited by addition of HU, and because mitotic cells were selectively collected by mitotic shake-off, the presence of G1 and S phases cells is, however, unlikely to affect the sequencing results. This is in line with the site-specific detection of MiDAS at common fragile sites in aphidicolin-treated cells (see Chapter 5) rather than detection of EdU incorporation throughout the genome. Importantly, this protocol may not allow to directly distinguish between DNA synthesis in late G2 or early mitosis. Indeed, we cannot exclude that DNA synthesis in G2 cells and their progression to mitosis during the 90-minute EdU pulse accounts for part of the captured signal. Detection of EdU incorporation in G2 cells, released or not from RO-3306-induced G2 block, will allow to confirm whether DNA synthesis in late G2 may account for part of the signal detected using the protocol developed here. Moreover, depletion of SMC2, which is required for chromosome condensation and subsequent activation of MiDAS, would permit to confirm whether this protocol specifically captures mitotic EdU incorporation.

Chapter 5

High-resolution detection of MiDAS upon BRCA2 abrogation

5.1 Introduction

BRCA2 promotes HR repair by loading the RAD51 recombinase at sites of DSBs (Chang *et al.*, 2017; Scully *et al.*, 2019). Moreover, BRCA2 protects stalled replication forks from nucleolytic degradation and promotes their restart in RAD51-dependent manner (Saldivar, Cortez and Cimprich, 2017; Berti, Cortez and Lopes, 2020). Although these functions of BRCA2 are confined to the S- and G2-phases of the cell cycle, when DNA replication occurs (Hustedt and Durocher, 2016), the DNA replication and repair defects caused by BRCA2 abrogation have consequences beyond the S and G2-phases of cell cycle. BRCA2 abrogation also leads to genome under-replication, which causes mitotic abnormalities such as DNA bridges, chromosome mis-segregation or cytokinesis failure (Feng and Jasin, 2017; Lai *et al.*, 2017). These lesions can be transmitted to daughter cells, in the form of aneuploidy, multinucleation, or 53BP1 nuclear bodies(Feng and Jasin, 2017; Lai *et al.*, 2017). MiDAS is activated in early mitosis at under-replicated loci and suppresses these DNA lesions, enabling correct segregation of BRCA2-deficient chromosomes (Feng and Jasin, 2017; Lai *et al.*, 2017).

Several studies have identified difficult to replicate genomic regions, such as common fragile sites, ribosomal DNA, telomeres or centromeres (Gadaleta and Noguchi, 2017; Ozer and Hickson, 2018; Lezaja and Altmeyer, 2020). Failure to complete DNA replication at common fragile sites triggers MiDAS or causes chromosome breaks (Minocherhomji *et al.*, 2015; Bhowmick, Minocherhomji and Hickson, 2016). DNA replication and repair defects caused by BRCA2 abrogation result in similar mitotic abnormalities (Feng and Jasin, 2017; Lai *et al.*, 2017). Hence, we proposed that BRCA2 is required for the replication of certain genomic regions, which are intrinsically difficult-to-replicate. Our hypothesis is that these

genomic regions will remain under-replicated upon BRCA2 abrogation, and hence, will be sites where MiDAS takes place. We therefore set out to map MiDAS sites by mitotic EdU-seq in order to identify genomic regions which require BRCA2 for their replication.

5.2 Detection of aphidicolin-induced MiDAS at common fragile sites

We first analysed untreated and aphidicolin-treated BRCA2-proficient H1299+sh*BRCA2*^{DOX} cells for MiDAS activation using our protocols of EdU incorporation in mitosis (Chapter 4), followed by sequencing, sequence mapping to human genome and peak-finding algorithms (Macheret *et al.*, 2020). MiDAS is a rare event under normal, unperturbed growth conditions, whilst aphidicolin-treatment triggers MiDAS at common fragile sites (Minocherhomji *et al.*, 2015; Macheret *et al.*, 2020). Using this approach, we found MiDAS to take place at 17 loci in untreated cells (Fig. 5.1A, +BRCA2) and 347 loci in aphidicolin-treated cells (Fig. 5.1B, +BRCA2 +APH). The maximal EdU-seq peak height (σ-value) was 5-fold lower and the median peak height was 2-fold lower in the absence of aphidicolin. This is consistent with MiDAS occurring at a low frequency in these cells.

We classified MiDAS sites depending on whether the EdU-seq signal was detected as a single-peak or as a double-peak (Fig. 5.1A,B). Mitotic EdU-seq was used to demonstrate that MiDAS at common fragile sites is initiated at the border of the under-replicated regions (Macheret *et al.*, 2020). Therefore, MiDAS at larger under-replicated regions appears as double-peaks, whilst it appears as single-peaks in shorter under-replicated regions. In the same report, the authors

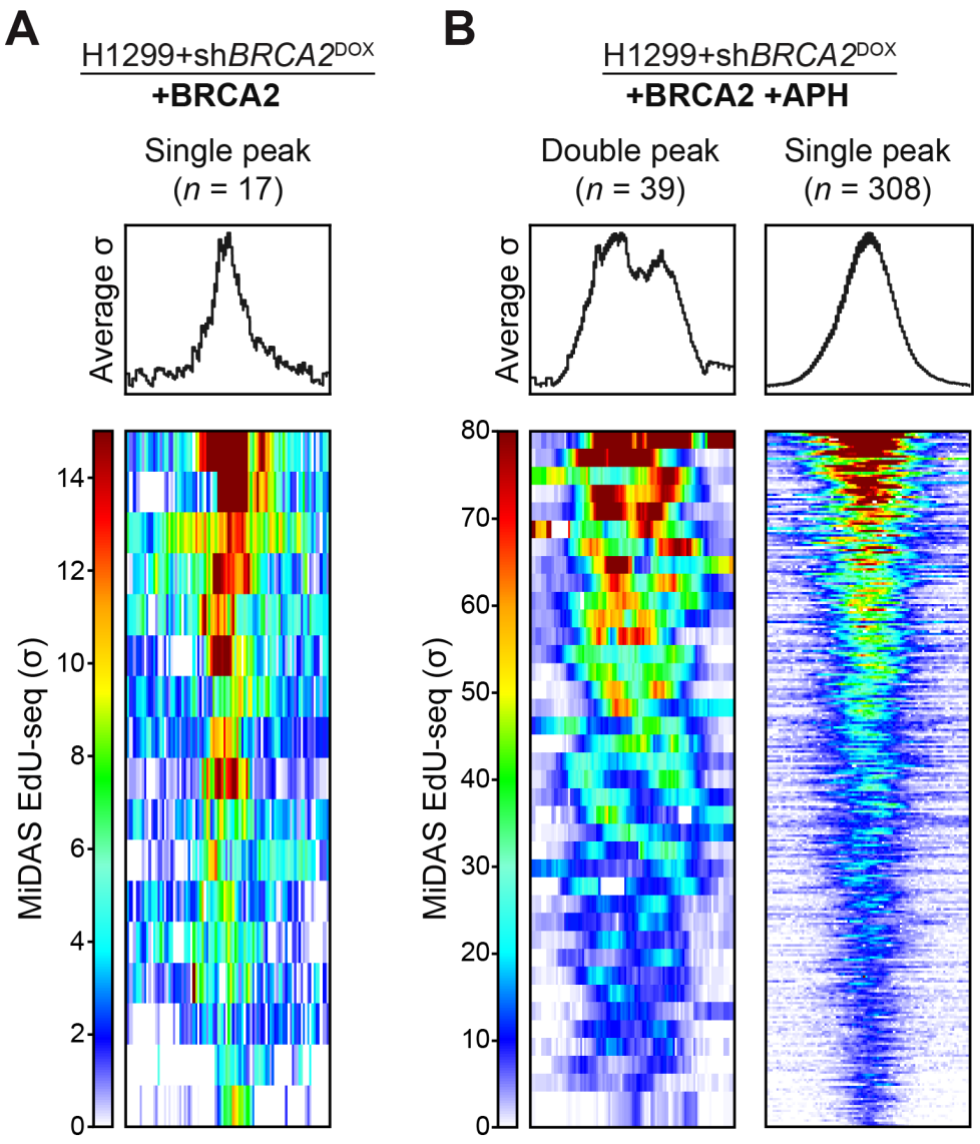


Fig. 5.1. Detection of MiDAS in BRCA2-proficient H1299+sh*BRCA2*^{DOX} treated or not with aphidicolin.

Top: Genome-wide average sigma value of (**A**) all MiDAS peaks for H1299+sh*BRCA2*^{DOX} or (**B**) of all double- or single MiDAS peaks for H1299+sh*BRCA2*^{DOX} treated with 0.2 µM aphidicolin (+APH). The height of the peaks is adjusted so that each MiDAS region contributes equally to the plot. **Bottom**: Heatmaps showing MiDAS signal, each line corresponding to one MiDAS region. Span of genomic regions is 0.7 Mb.

showed that increased aphidicolin concentration in S phase-progressing cells leads to larger under-replicated regions upon mitotic entry and thus, an increase in the number of MiDAS regions classifying as double-peaks. Consistent with this,

we detected double-peak MiDAS sites in H1299+sh*BRCA2*^{DOX} cells treated with aphidicolin, albeit less frequently than single-peaks (Fig. 5.1B), but not in control untreated cells (Fig. 5.1A).

We next compared our results with previously identified MiDAS sites in aphidicolin-treated U2OS cells (Macheret *et al.*, 2020). In this study, the authors used mitotic EdU-seq to detect MiDAS at 373 distinct sites across three cell lines, which encompassed all 73 known common fragile sites mapped to large genes (Wilson *et al.*, 2015). MiDAS sites exhibited common fragile site-specific features. In particular, these regions were found to replicate in mid- or late S phase, to be actively transcribed, to lack replication origins and to correlate with chromosome rearrangements present in cancers. Hence, mitotic EdU-seq can be used as a high-resolution surrogate to map common fragile sites. We confirmed that the MiDAS sites identified in aphidicolin-treated H1299+sh*BRCA2*^{DOX} cells correspond to known common fragile sites. As an example, MiDAS was detected in both H1299+sh*BRCA2*^{DOX} and U2OS cells within the *FHIT* and the *WWOX* genes (Fig. 5.2A), which encompass the FRA3B and the FRA16D common fragile sites, respectively (Ohta *et al.*, 1996; Bednarek *et al.*, 2000). This was also confirmed by genome-wide analysis of all MiDAS sites in H1299+sh*BRCA2*^{DOX} or U2OS cells treated with aphidicolin. Indeed, amongst the 293 MiDAS sites identified in aphidicolin-treated U2OS cells, 162 (55%) were also found in aphidicolin-treated H1299+sh*BRCA2*^{DOX} cells (Fig. 5.2B). The partial overlap between the two cells lines is consistent with the heterogeneity of common fragile sites observed in different cell types by both cytogenetic and DNA sequencing methods (Le Tallec *et al.*, 2013; Macheret *et al.*, 2020). Finally, double-peaks

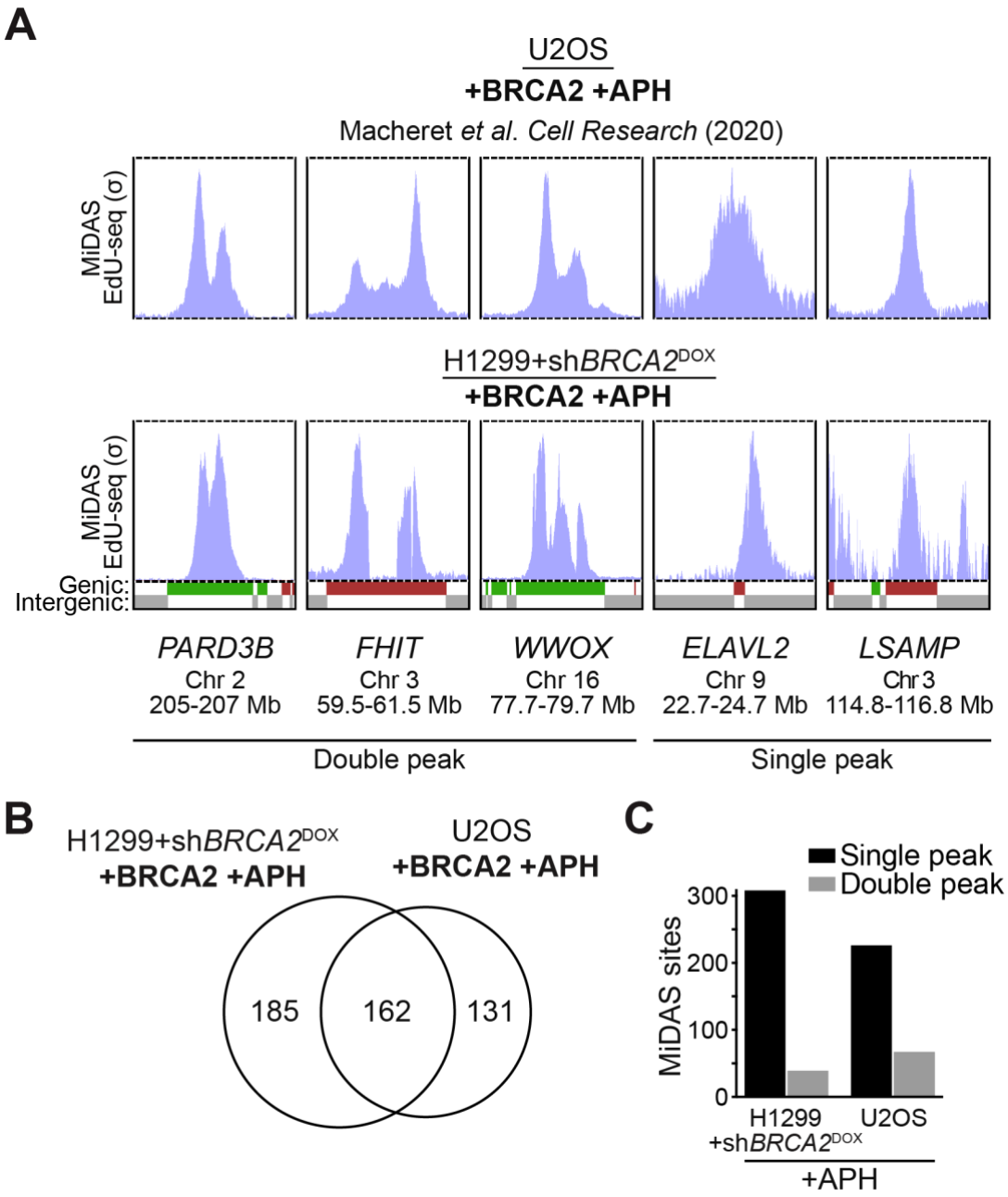


Fig. 5.2. MiDAS upon aphidicolin treatment takes place at known common fragile sites.

(**A**) MiDAS signal (sigma value) detected at representative common fragile sites in BRCA2-proficient U2OS treated with 0.4 µM aphidicolin (+APH) (Macheret *et al*., *Cell Research* 2020) and H1299+sh*BRCA2*^{DOX} treated with 0.2 µM aphidicolin. Gene names and genomic coordinates are indicated below. Genic regions coloured in green or red indicate forward or reverse direction of transcription, respectively. Maximal peak height detected in H1299+sh*BRCA2*^{DOX} +APH cells (in sigma units):

PARD3B: 131.4; *FHIT*: 237.9; *WWOX*:63.3; *ELAVL2*: 24.6; LSAMP: 6.4. Bin resolution: 10 kb. (**B**) Venn diagram shows common MiDAS regions between BRCA2-proficient U2OS treated with aphidicolin (+APH) (Macheret *et al*., 2020) and H1299+sh*BRCA2*^{DOX} treated with aphidicolin. (**C**) Genome-wide classification of MiDAS as single or double peaks in BRCA2-proficient U2OS treated with aphidicolin (Macheret *et al*., 2020) and H1299+sh*BRCA2*^{DOX} treated with aphidicolin.

were observed less frequently than single-peaks in both cells line (Fig. 5.2C) and corresponded to larger, known common fragile sites (Fig. 5.2A; (Macheret *et al.*, 2020). We therefore concluded that aphidicolin-induced MiDAS maps to common fragile sites in H1299+sh*BRCA2*^{DOX}.

Of note, we did not include EdU-unlabelled samples as negative control. These samples would allow to confirm the specificity of the pull-down method for EdU-labelled DNA. However, the quasi-absence of EdU incorporation in BRCA2-proficient cells and the detection of MiDAS at common fragile site in aphidicolin-treated cells are in good agreement with previously published data and suggest that the EdU-seq assay specifically detects nascent DNA.

5.3 Detection of MiDAS in BRCA2-deficient cells

Next, we performed mitotic EdU-seq to detect MiDAS in BRCA2-deficient H1299+sh*BRCA2*^{DOX} cells using the previously described protocols (Chapter 4). We detected MiDAS at 150 loci (Fig.5.3, -BRCA2), which we classified depending on their EdU-seq signal. Whilst 108 (72%) sites were classified as single-peaks, 42 sites exhibited multiple EdU-seq peaks. The EdU-seq signal detected at the latter did not classify as double-peak such as those observed in aphidicolin-treated cells (Fig. 5.1B) and consequently were labelled as multiple peaks

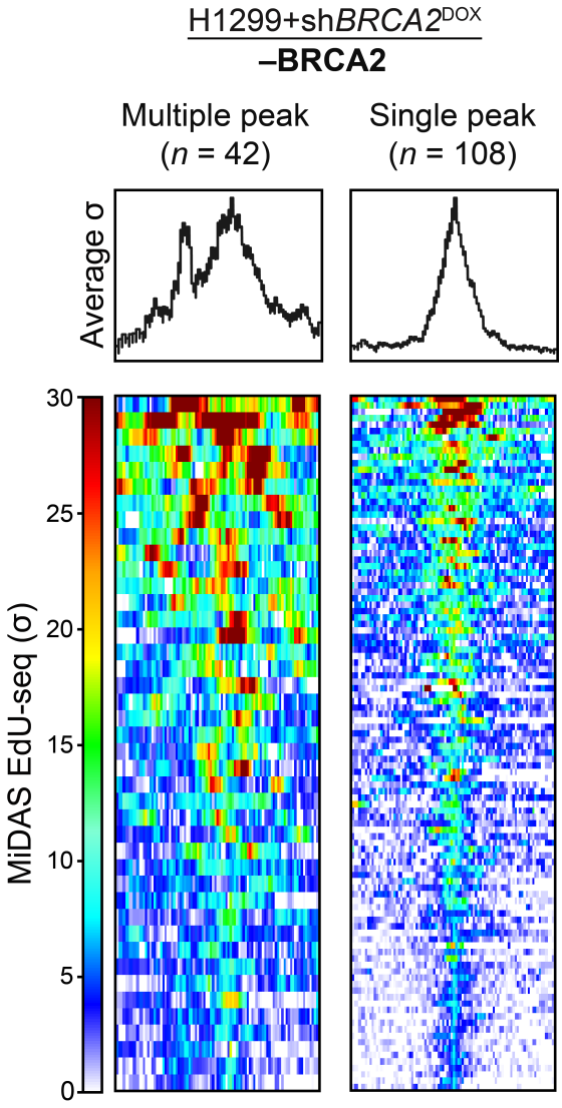


Fig. 5.3. Detection of MiDAS in BRCA2-deficient H1299+sh*BRCA2*^{DOX} cells.

Top: Genome-wide average sigma value of all multiple- or single MiDAS peaks for BRCA2-deficient H1299+sh*BRCA2*^{DOX}. The height of the peaks is adjusted so that each MiDAS region contributes equally to the plot. **Bottom**: Heatmaps showing MiDAS signal, each line corresponding to one MiDAS region. Span of genomic regions is 0.7 Mb.

(Fig.5.3). The median EdU-seq peak height (σ-value) was 2-fold lower in BRCA2-deficient cells (Fig.5.3, -BRCA2) than in aphidicolin-treated BRCA2-proficient cells (Fig. 5.1B, +BRCA2 +APH). The maximal peak height in BRCA2-deficent

cells (Fig.5.3, -BRCA2) was 2-fold lower than in aphidicolin-treated cells (Fig. 5.1B, +BRCA2 +APH), yet 2-fold higher than in untreated BRCA2-proficient cells (Fig. 5.1A, +BRCA2). Altogether this shows that BRCA2-inactivation (BRCA2i)-induced MiDAS can be detected by mitotic EdU-seq in the absence of exogenous stress.

5.4 BRCA2 abrogation does not activate MiDAS at common fragile sites

We then compared MiDAS sites triggered by BRCA2 abrogation with common fragile sites induced by aphidicolin treatment identified by mitotic EdU-seq in the same cell line. Surprisingly, we did not detect MiDAS at common fragile sites in BRCA2-deficient H1299+sh*BRCA2*^{DOX} cells (-BRCA2), as illustrated at the FRA1E or 3p12 common fragile sites, found within the *DPYD* (Hormozian *et al.*, 2007) or *CADM2* genes (Le Tallec *et al.*, 2011), respectively (Fig. 5.4A). Conversely, we did not detect aphidicolin-induced MiDAS at the sites identified upon BRCA2 abrogation (Fig. 5.4A). Genome-wide comparison of MiDAS events in BRCA2-deficient cells (Fig.5.3, -BRCA2) and in aphidicolin-treated BRCA2-proficient cells (Fig. 5.1B, +BRCA2 +APH) confirmed this observation. Indeed, amongst the 487 unique MiDAS sites identified, only 6 were common to both datasets (Fig. 5.4B). We concluded that BRCA2 abrogation triggers MiDAS at genomic loci that are distinct from common fragile sites.

5.5 BRCA2 abrogation activates MiDAS within genomic regions that replicate during early S phase

To investigate the differences between BRCA2i-induced MiDAS and

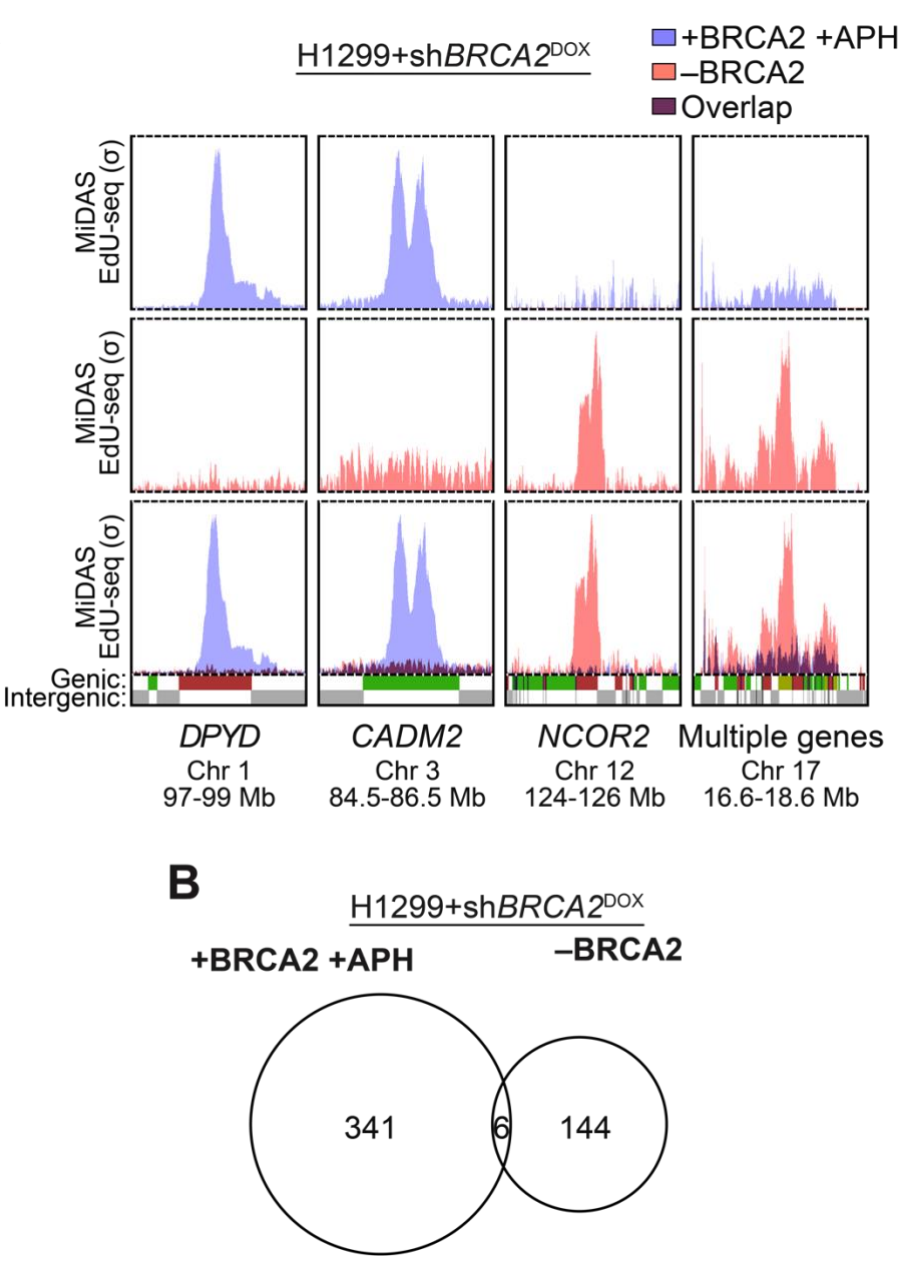


Fig. 5.4. BRCA2 inactivation and aphidicolin-treatment trigger MiDAS at distinct genomic regions.

(**A**) MiDAS signal (sigma value) detected at representative sites in BRCA2-proficient H1299+sh*BRCA2*^{DOX} cells treated with aphidicolin (+BRCA2 +APH) and BRCA2-deficient H1299+sh*BRCA2*^{DOX} cells (-BRCA2). The plot showing overlay of the two conditions is scale 1:1. Gene names and genomic coordinates are indicated below. Maximal peak height detected in H1299+sh*BRCA2*^{DOX} +BRCA2 +APH cells (in sigma units): *DPYD*: 102.8; *CADM2*: 38.1. Maximal peak height detected in H1299+sh*BRCA2*^{DOX} -BRCA2 cells (in sigma units): *NCOR2*: 20.8;

Multiple genes: 13.5. Bin resolution: 10 kb. (**B**) Venn diagram shows common MiDAS regions between BRCA2-proficient H1299+sh*BRCA2*^{DOX} treated with aphidicolin (+BRCA2 +APH) and BRCA2-deficient H1299+sh*BRCA2*^{DOX} (-BRCA2).

aphidicolin-induced MiDAS, we decided to characterise MiDAS sites relative to their replication timing in S phase. We used publicly available replication timing data from asynchronous U2OS cells (Macheret and Halazonetis, 2018) generated by REPLI-seq (Hansen *et al.*, 2010).

Common fragile sites replicate in late S phase (Le Beau *et al.*, 1998; Debatisse and Rosselli, 2019; Macheret *et al.*, 2020). Indeed, aphidicolin-treatment triggered MiDAS within the late S phase replicating *CADM2* gene (Fig. 5.5A). Genome-wide analysis of all common fragile sites identified by mitotic EdU-seq in aphidicolin-treated H1299+sh*BRCA2*^{DOX} indicated that 54% (188) and 41% (142) of the MiDAS sites mapped to mid- and late S phase replicating domains, respectively (Fig. 5.5B, +BRCA2 +APH). Compared to

early- and late- S replicating domains, mid-S replicating domains are over-represented in REPLI-seq data (Fig. 5.5C). To test if aphidicolin-induced MiDAS was preferentially activated at regions harbouring a particular replication timing, we normalised the number of MiDAS events observed within each replication timing group against its genomic size. This confirmed that aphidicolin-induced MiDAS sites occurred with higher frequency in mid- or late-S phase replicating domains (Fig. 5.5D. +BRCA2 +APH).

We then applied the same method to analyse the replication timing of the MiDAS sites detected upon BRCA2 abrogation. We found that MiDAS sites were not randomly distributed across the genome in BRCA2-deficient cells but preferentially map to early S phase replicating domains (70%; Fig. 5.5D, -BRCA2)

whilst only one third (29%) mapped to mid-S phase replicating domains (Fig. 5.5B, -BRCA2). As an example, MiDAS was triggered within the early replicating *NCOR2* gene (Fig. 5.5A). This demonstrates that aphidicolin-treatment or BRCA2 abrogation do not only trigger MiDAS at distinct sets of genomic loci, but that these loci differ in their replication timing.

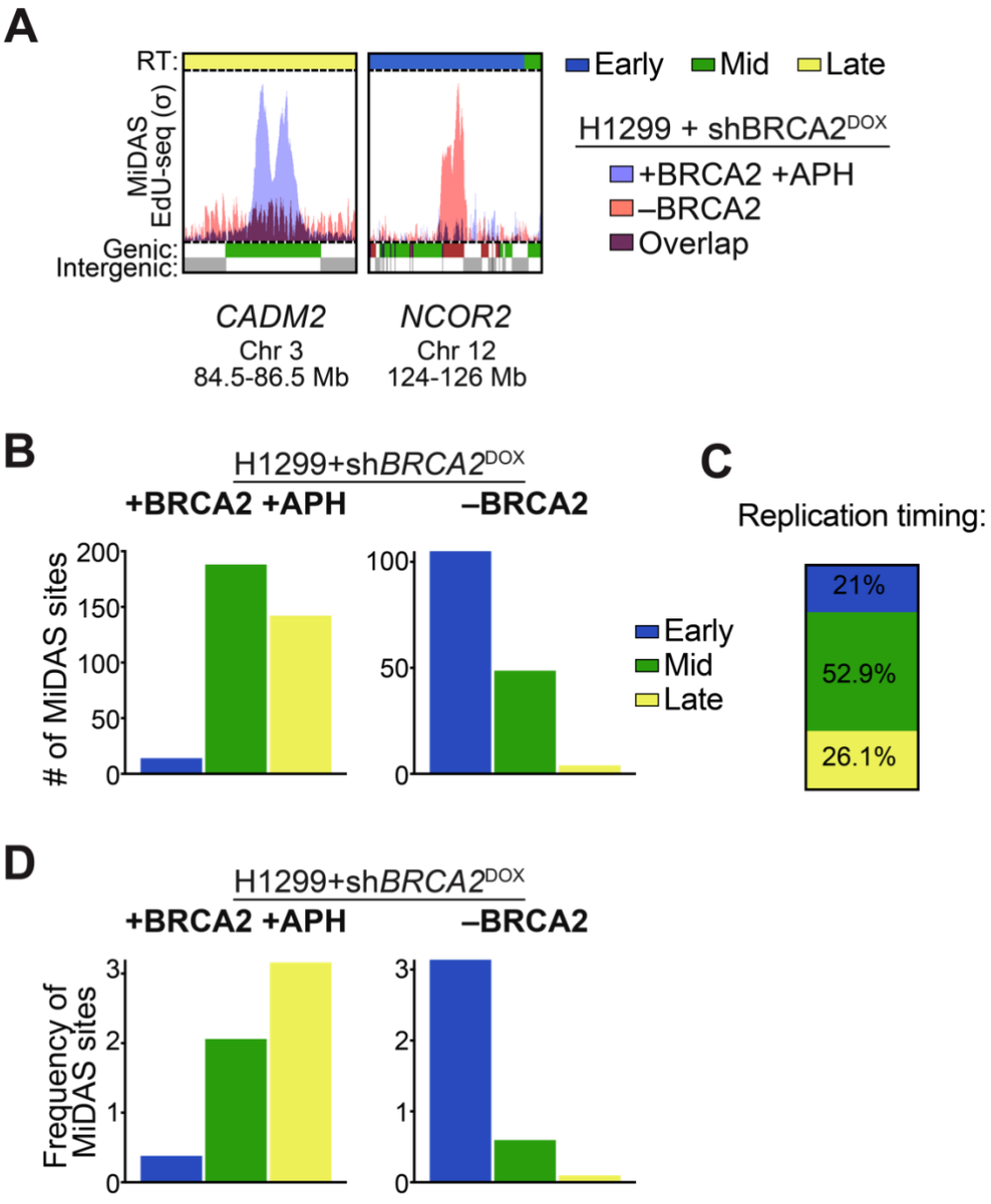


Fig. 5.5. BRCA2 inactivation triggers MiDAS at early S phase replicating domains.

(**A**) MiDAS signal (sigma value) detected at representative sites in BRCA2-proficient H1299+sh*BRCA2*^{DOX} treated with aphidicolin (+BRCA2

+APH) and BRCA2-deficient H1299+sh*BRCA2*^{DOX} cells (-BRCA2). Replication timing are data from U2OS cells (Macheret and Halazonetis, 2018). Blue, green or yellow colours indicate early, mid or late S phase, respectively. (**B**) Number of MiDAS regions within early, mid or late S phase replicating domains for in BRCA2-proficient H1299+sh*BRCA2*^{DOX} cells treated with aphidicolin (+BRCA2 +APH) and BRCA2-deficient H1299+sh*BRCA2*^{DOX} cells (-BRCA2). (**C**) Fraction of the genome classified as early, mid or late S phase replicating domain. (**D**) Frequency of MiDAS regions shown in (B) corrected for the replicating domain size shown in (C).

5.6 Resemblance between the aphidicolin-induced MiDAS pattern in BRCA2-proficient and BRCA2-deficient cells

We then compared the effect of BRCA2 abrogation in the context of aphidicolin-induced replication stress. Under these conditions, we detected MiDAS at 290 loci, which we classified as double- or single-peaks (Fig. 5.6A, C). Next, we examined the replication timing of the genomic regions where MiDAS was detected. Consistent with aphidicolin causing chromosome fragility in late-S phase replicating regions of the genome, we found that aphidicolin-induced MiDAS in BRCA2-deficient H1299+sh*BRCA2*^{DOX} cells mapped to mid- or late-S phase replicating domains (Fig. 5.6B). In contrast, only few regions mapped to early-S phase replicating domain. Indeed, 94% of the aphidicolin-induced sites detected upon BRCA2 abrogation overlapped with aphidicolin-induced MiDAS sites found in control cells (Fig. 5.6D). Yet, we have not tested whether the 17 remaining MiDAS sites were also detected in non-treated BRCA2-deficient cells. We therefore concluded that, under these conditions, aphidicolin-treatment in BRCA2-deficient H1299+sh*BRCA2*^{DOX} cells triggers MiDAS at common fragile sites and not at the previously identified BRCA2i-induced MiDAS sites (Fig. 5.4).

Why BRCA2i-induced MiDAS is not detected when upon combination of aphidicolin-treatment and BRCA2 abrogation is yet unclear. More careful analysis

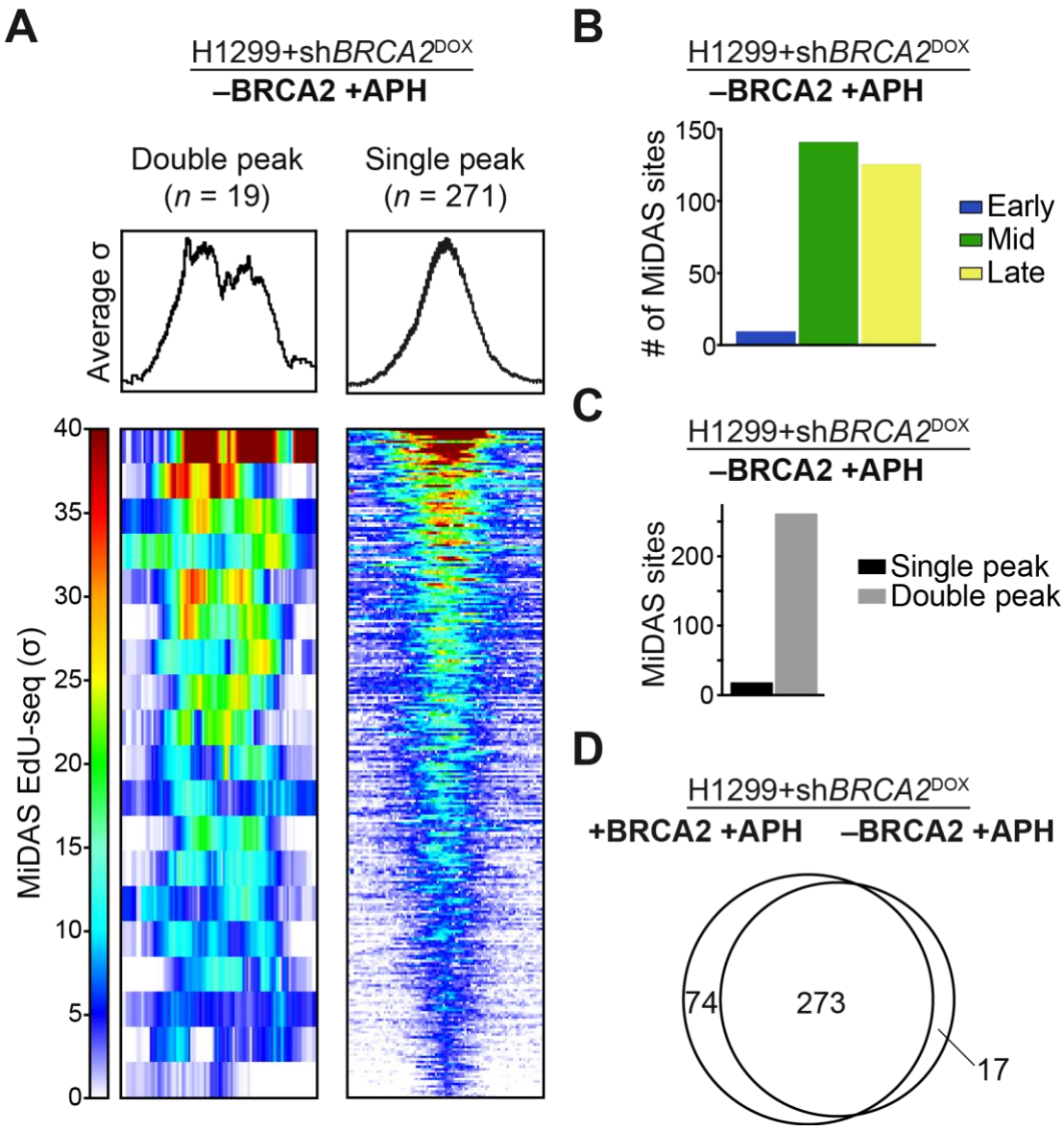


Fig. 5.6. Comparison of aphidicolin-induced MiDAS in BRCA2-proficient and BRCA2-deficient cells.

(**A**) **Top**: Genome-wide average sigma value of all double- or single MiDAS peaks for BRCA2-deficient H1299+sh*BRCA2*^{DOX} cells treated with 0.2 µM aphidicolin (-BRCA2 +APH). The height of the peaks is adjusted so that each MiDAS region contributes equally to the plot. **Bottom**: Heatmaps showing MiDAS signal, each line corresponding to one MiDAS region. Span of genomic regions is 0.7 Mb. (**B**) Number of MiDAS regions within early, mid or late S phase replicating domains for in BRCA2-

deficient H1299+sh*BRCA2*^{DOX} cells treated with aphidicolin (-BRCA2 +APH). (**C**) Genome-wide classification of MiDAS as single or double peaks in BRCA2-deficient H1299+sh*BRCA2*^{DOX} treated with aphidicolin (-BRCA2 +APH). (**D**) Venn diagram shows common MiDAS regions between BRCA2-proficient H1299+sh*BRCA2*^{DOX} cells treated with aphidicolin (+BRCA2 +APH) and BRCA2-deficient H1299+sh*BRCA2*^{DOX} treated with aphidicolin (-BRCA2 +APH).

will be required to ensure that high levels of EdU incorporation at common fragile sites does not mask the BRCA2i-induced MiDAS signal within early-S phase replicating domains. However, the slower mitotic entry in aphidicolin-treated cells compared to untreated cells (17.5 and 10.5 hours after release from thymidine, respectively) could permit the repair of early-S phase under-replicated regions. Alternatively, one could hypothesis that reduced fork speed may prevent the accumulation under-replicated DNA during early-S phase in the absence of BRCA2.

5.7 Discussion

In this thesis chapter we used mitotic EdU-seq (Chapter 4; (Macheret *et al.*, 2020)) to detect MiDAS events. Using this approach, we detected MiDAS at 347 loci in aphidicolin-treated, BRCA2-proficient H1299+sh*BRCA2*^{DOX} cells, including within the FRA3B, FRA16D, FRA1E, FRA3p12 and FRA3q13.3 common fragile sites (Fig.5.2A and Fig. 5.4A). In contrast, we detected very low levels of MiDAS activation in untreated control cells (Fig. 5.1). Consistent with the concept that low doses of aphidicolin decrease replication rates and obstruct common fragile sites replication in mid- and late S phase, we found that 95% of the aphidicolin-induced MiDAS sites mapped to mid or late S phase replicating domains. We concluded that these 347 MiDAS sites represent the common fragile sites of

H1299+sh*BRCA2*^{DOX} cells. These common fragile sites partially overlapped with MiDAS sites identified in aphidicolin-treated U2OS cells (Macheret *et al.*, 2020). We applied the same analysis to BRCA2-deficient H1299+sh*BRCA2*^{DOX} cells and detected MiDAS at 150 loci (Fig.5.3). Importantly, these loci did not correspond to common fragile sites identified in these cells (Fig. 5.4B) and instead mapped to regions replicating during early S phase (Fig. 5.5A-C). Our EdUseq-HU experiments showed that BRCA2 abrogation does not alter early replication origin firing (Dagg *et al.*, under revision). It is therefore unlikely that under-replication of early S phase replicating regions is due to changes in the replication timing program upon BRCA2 abrogation. Moreover, BRCA2 abrogation results in a mild decrease in replication fork speed (Dagg *et al.*, under revision), yet not to the same extent as aphidicolin treatment. Our flow cytometry analysis confirmed that the time required for DNA duplication following release from thymidine block was not affected by the BRCA2 status (Chapter 4). Taken together, this suggests that BRCA2i-induced genome under-replication and MiDAS do not originate from reduced replication speed or premature mitotic entry, but from yet unknown mechanisms.

DNA replication is tightly controlled to ensure that the genome is replicated once (and only once) per cell cycle (Petropoulos *et al.*, 2019). Whilst loading of the MCM machinery is restricted to G1 phase, deregulation of origin licensing factors (e.g., loss of geminin) cause *de novo* origin firing in G2 phase and therefore lead to re-replication (Wohlschlegel *et al.*, 2000; Yanow, Lygerou and Nurse, 2001). Because BRCA2 has not been reported to regulate origin licensing and BRCA2 abrogation has not been associated with over-replicated genome

before mitotic entry, the EdU-signal detected in BRCA2-deficient cells is unlikely to result from de novo origin firing in late G2.

In contrast, several lines of evidence suggest a link between DNA synthesis in mitosis and stalled replication forks in S phase. First, BRCA2-deficient cells accumulate mitotic abnormalities, such as FANCD2 foci or DNA bridges, the latter requiring MUS81 activity for their resolution (Feng and Jasin, 2017; Lai *et al.*, 2017). Second, these cells accumulated G1 abnormalities following mitotic progression, such as multinucleation and 53BP1 nuclear bodies (Feng and Jasin, 2017; Lai *et al.*, 2017), which have been shown to arise at under-replicated loci (Lukas *et al.*, 2011). Third, BRCA2i-induced MiDAS regions replicated in early S phase, a feature shared with ERFSs (Barlow *et al.*, 2013). Indeed, HU-induced fork stalling caused fragile site expression at these genomic loci.

To test whether replication fork stalling underlies the activation of MiDAS in BRCA2-deficient cells, one could identify sites of stalled replication forks using chromatin immunoprecipitation followed by sequencing (ChIP-seq). In the absence of BRCA2, ssDNA is rapidly coated by RPA, which is subsequently phosphorylated at serine 33 (S33) by ATR (Zeman and Cimprich, 2014). Hence, ChIP-seq of RPA or RPA (S33) may be used as a marker of stalled replication forks in BRCA2-deficient cells. The exact experimental conditions will have to be determined. For example, ChIP of RPA (S33) can be done in asynchronous or synchronous cells or following HU treatment. To determine the optimal conditions, quantitative image-based cytometry (QIBC) could permit to monitor the accumulation of ssDNA (e.g., RPA or RPA (S33) foci) at the different stages of S phase.

Microscopy-based detection of EdU foci in mitosis could bring mechanistic insights into the possible functions of BRCA2 at stalled replication forks. Indeed, modulation of the fork stability (e.g., depletion or inhibition of MRE11), plasticity (e.g., depletion of HLTF or SMARCAL) or restart (e.g. depletion of PrimPol or POLQ) could inform on how BRCA2 promotes chromosome integrity.

Finally, why early replicating regions require BRCA2 for their replication remains unknown. A possible explanation is the increase in replication-transcription conflicts in early S phase (Barlow *et al.*, 2013; Macheret and Halazonetis, 2018). For example, aberrant origin firing within transcribed regions leads to fork stalling and collapse (Macheret and Halazonetis, 2018). To test this hypothesis, one could assess the proximity of BRCA2i-induced MiDAS sites to constitutive or to oncogene-induced origins. Moreover, mapping of newly synthesised RNA using EU-seq in early S phase could whether transcription in S phase impacts on DNA synthesis in mitosis.

Chapter 6

Discussion and conclusion

6.1 Micronuclei formation and innate immune response signalling

We performed RNA-seq to identify transcriptional changes upon BRCA2 abrogation, using shRNA-mediated *BRCA2* silencing in H1299+sh*BRCA2*^{DOX} and MDA-MB-231+sh*BRCA2*^{DOX}cells. We compared both the immediate, short-term, and the long-term response between BRCA2-proficient and -deficient cells. Our analysis revealed a two-stage adaptation to BRCA2 abrogation.

Upon short-term BRCA2 abrogation, the expression of genes participating in cell cycle, organelle fission, chromosome segregation, DNA replication and DNA repair pathways was significantly down-regulated (Reisländer *et al.*, 2019). Consistent with previous reports (Lai *et al.*, 2017; Tacconi *et al.*, 2017), these cells also exhibited slower proliferation rates (Reisländer *et al.*, 2019), characterised by an extended G1 phase. Therefore, the DNA replication and repair defects associated with BRCA2 abrogation cause growth defects even in p53-deficient cells. This suggests that *TP53* mutation is not sufficient to promote cell survival upon BRCA2 loss (Hakem *et al.*, 1997; Heijink *et al.*, 2019).

Long-term BRCA2 abrogation was associated with a type I interferon signature, where ISGs were significantly up-regulated. We performed RT-qPCR and found that the expression of these genes increased over time in BRCA2-deficient cells. Detection of ruptured micronuclei by cGAS was shown to activate the innate immune response signalling. We found that the number of cGAS-infiltrated micronuclei increased in a time-dependant manner after BRCA2 abrogation (Reisländer *et al.*, 2019), which was in line with other studies (Ban *et al.*, 2001; Heijink *et al.*, 2019). Moreover, cGAS surveillance resulted in

phosphorylation of IRF3 and STAT1, two effectors of the type I IFN response. This demonstrates that BRCA2 loss is immunogenic.

Whether the immune system only acts as a barrier against tumorigenesis or whether inflammation promotes cancer onset is still unclear (Zitvogel *et al.*, 2015; Gonzalez, Hagerling and Werb, 2018). Also unknown is whether tissue-specific cancer predisposition is regulated by immune response signalling. Additionally, the innate and adaptive immunity could be modulated to reduce the risk of developing cancer. It would therefore be particularly interesting to assess the potential role of immune response signalling in pre-cancerous cells in the context germline heterozygous *BRCA2* mutations. A recent study demonstrated that aldehyde-induced *BRCA2* haploinsufficiency is associated with chromosome instability (Tan *et al.*, 2017). Whilst this may, in part, explain how monoallelic BRCA2 mutations promotes genomic instability, it also suggests that induced haploinsufficiency may trigger an immune response signalling. It will therefore be important to assess whether this haploinsufficiency is immunogenic and whether this promotes tumorigenesis or can, alternatively, be targeted therapeutically to prevent cancer onset in heterozygous carriers of *BRCA2* mutations.

BRCA2-deficient cells are sensitive to DNA damaging drugs, prominently PARP inhibitors (Bryant *et al.*, 2005; Farmer *et al.*, 2005; Lord and Ashworth, 2017), and exposure to DNA damaging agents was shown to trigger an immune response signalling (Reisländer, Groelly and Tarsounas, 2020). We found that treatment with the PARP inhibitor olaparib, the G-quadruplex stabilizer pyridostatin or the alkylating agent chlorambucil induced DSBs and increased the type I IFN signalling in BRCA2-deficient cells. Similarly, olaparib-induced eradication of BRCA1-deficient tumours relied, in part, on activation of the hosts'

immune system (Ding *et al.*, 2018; Pantelidou *et al.*, 2019) and PARP inhibitors synergised with immune checkpoint inhibitors (Higuchi *et al.*, 2015; Ding *et al.*, 2018; Pantelidou *et al.*, 2019; Sen *et al.*, 2019; Wang *et al.*, 2019). Loss of other DNA damage response proteins, such as ATM (Hartlova *et al.*, 2015), BLM (Gratia *et al.*, 2019) or ERCC1 (Chabanon *et al.*, 2019) have been associated with activation of the innate immunity and this may inform novel therapy combinations in the clinic (Reisländer, Groelly and Tarsounas, 2020). In contrast, loss of MMR factors does not trigger a type I IFN system but is associated with neoantigen presentation (Germano *et al.*, 2017) and response to immunotherapy (Le *et al.*, 2015; Schumacher, Scheper and Kvistborg, 2019). Future studies will be necessary to unveil the role of ISGs, for example those mediating ISGylation reactions, and determine whether their expression can be therapeutically exploited.

6.2 Replication defects and mitotic DNA synthesis (MiDAS)

Loss of BRCA2 results in mitotic abnormalities characterised by chromosome bridges, chromosome mis-segregation and cytokinesis failure (Feng and Jasin, 2017; Lai *et al.*, 2017). MiDAS is activated in BRCA2-deficient cells and facilitates chromosome segregation. This prompted us to identify genomic regions which remain under-replicated upon mitotic entry in the absence of BRCA2. Hence, we performed mitotic EdU-seq (Macheret *et al.*, 2020) in BRCA2-proficient and BRCA2-deficient H1299+sh*BRCA2*^{DOX} cells treated or not with low-dose aphidicolin and identified loci where MiDAS occurs.

Treatment with aphidicolin induced MiDAS at common fragile sites, independently of the BRCA2 status. Most of the regions presented a single MiDAS peak, and double-peaks corresponded to cytogenetically-defined

common fragile sites, including within the *FHIT* and *WWOX* genes. The numbers of MiDAS sites observed is likely to reflect the higher resolution of EdU-seq methods. Indeed, chromosome gaps may only be observed at large under-replicated loci which were not fully repaired by MiDAS (Macheret *et al.*, 2020).

BRCA2 abrogation triggered MiDAS at 150 sites, which were distinct from aphidicolin-induced common fragile sites. These loci corresponded to early S phase replicating regions, hence shared similarities with ERFSs (Barlow *et al.*, 2013). Further analysis will be required to determine the mechanisms underlying the instability of ERFSs and BRCA2i-induced fragile sites. ERFSs are sensitive to HU-induced fork stalling (Barlow *et al.*, 2013) and are contain sequences prone to harbour unusual structures (Tubbs *et al.*, 2018). Moreover, ATR orchestrates stalled fork protection (Saldivar, Cortez and Cimprich, 2017) and its inhibition caused ERFSs and common fragile sites expression (Barlow *et al.*, 2013). In contrast, HR-deficient but not fork protection-deficient *BRCA2* mutants caused mitotic abnormalities (Feng and Jasin, 2017). However, BRCA2-mediated fork restart relies on the formation of stable RAD51 nucleofilament and template switch reactions. Accordingly, failure to inactive intragenic origins and subsequent fork collapse may underlie chromosome fragility in early S phase replicating regions (Debatisse and Rosselli, 2019; Macheret *et al.*, 2020). Indeed, oncogene-induced origin firing results in lethal DNA replication defects in BRCA2-deficient cells (Dagg *et al.*, under revision).

We did not detect MiDAS within regions replicating in early S phase in BRCA2-deficient cells treated with aphidicolin. Whilst this may be a consequence of longer S phase in these cells, it may also result from reduced fork speed. Indeed, deregulated replication fork speed causes DNA damage (Maya-Mendoza

et al., 2018). Accordingly, slower rate of replication after initial replication defects may prevent fragility of regions replicating in late S phase.

6.3 The role of BRCA2 for genome and chromosome stability

BRCA2 mediates HR, which prevents mutagenic DSB repairs (Chang *et al.*, 2017; Scully *et al.*, 2019). Moreover, BRCA2 acts at stalled replication fork, where it protects nascent DNA from nucleolytic degradation (Saldivar, Cortez and Cimprich, 2017; Berti, Cortez and Lopes, 2020). The tumour suppressor also restarts stalled replication forks via template switch, which promotes continuous replication and is an alternative to error-prone DNA translesion synthesis (Quinet *et al.*, 2021). Altogether, this shows that BRCA2 promotes genome integrity.

BRCA2 ensures chromosome integrity, possibly by facilitating replication of certain genomic regions which replicate in early S phase. In the absence of BRCA2, these loci remain under-replicated upon mitotic onset and require MUS81 activity to trigger MiDAS and ensure chromosome segregation. Why early-replicating regions require BRCA2 for their replication is yet unknown. In mitosis, BRCA2 ensures chromosome alignment prior to their segregation (Ehlen *et al.*, 2020). Hence, BRCA2 abrogation is associated with micronuclei formation, although it is likely that a subset of the micronuclei observed in these cells originates from DNA repair or replications defects. Micronuclei formation links BRCA2 abrogation to activation of the innate immunity. Therefore, whilst loss of BRCA2 causes loss of chromosome integrity, which is tumorigenic, it also triggers immune responses required for tumour elimination.

References

Abbotts, R., and Wilson, D.M., 3rd (2017). Coordination of DNA single strand break repair. Free Radic Biol Med 107, 228-244.

Ablasser, A., Goldeck, M., Cavlar, T., Deimling, T., Witte, G., Rohl, I., Hopfner, K.P., Ludwig, J., and Hornung, V. (2013). cGAS produces a 2'-5'-linked cyclic dinucleotide second messenger that activates STING. Nature 498, 380-384.

Aparicio, T., Baer, R., Gottesman, M., and Gautier, J. (2016). MRN, CtIP, and BRCA1 mediate repair of topoisomerase II-DNA adducts. J Cell Biol 212, 399-408.

Arana, M.E., Seki, M., Wood, R.D., Rogozin, I.B., and Kunkel, T.A. (2008). Low-fidelity DNA synthesis by human DNA polymerase theta. Nucleic Acids Res 36, 3847-3856.

Bai, G., Kermi, C., Stoy, H., Schiltz, C.J., Bacal, J., Zaino, A.M., Hadden, M.K., Eichman, B.F., Lopes, M., and Cimprich, K.A. (2020). HLTF Promotes Fork Reversal, Limiting Replication Stress Resistance and Preventing Multiple Mechanisms of Unrestrained DNA Synthesis. Mol Cell 78, 1237-1251 e1237.

Balmus, G., Pilger, D., Coates, J., Demir, M., Sczaniecka-Clift, M., Barros, A.C., Woods, M., Fu, B., Yang, F., Chen, E., Ostermaier, M., Stankovic, T., Ponstingl, H., Herzog, M., Yusa, K., Martinez, F.M., Durant, S.T., Galanty, Y., Beli, P., Adams, D.J., Bradley, A., Metzakopian, E., Forment, J.V., and Jackson, S.P. (2019). ATM orchestrates the DNA-damage response to counter toxic non-homologous end-joining at broken replication forks. Nat Commun 10, 87.

Ban, S., Shinohara, T., Hirai, Y., Moritaku, Y., Cologne, J.B., and MacPhee, D.G. (2001). Chromosomal instability in BRCA1- or BRCA2-defective human cancer

cells detected by spontaneous micronucleus assay. Mutation Research/Fundamental and Molecular Mechanisms of Mutagenesis 474, 15-23.

Banin, S., Moyal, L., Shieh, S., Taya, Y., Anderson, C.W., Chessa, L., Smorodinsky, N.I., Prives, C., Reiss, Y., Shiloh, Y., and Ziv, Y. (1998). Enhanced phosphorylation of p53 by ATM in response to DNA damage. Science 281, 1674-1677.

Baranovskiy, A.G., Babayeva, N.D., Suwa, Y., Gu, J., Pavlov, Y.I., and Tahirov, T.H. (2014). Structural basis for inhibition of DNA replication by aphidicolin. Nucleic Acids Res 42, 14013-14021.

Barazas, M., Annunziato, S., Pettitt, S.J., de Krijger, I., Ghezraoui, H., Roobol, S.J., Lutz, C., Frankum, J., Song, F.F., Brough, R., Evers, B., Gogola, E., Bhin, J., van de Ven, M., van Gent, D.C., Jacobs, J.J.L., Chapman, R., Lord, C.J., Jonkers, J., and Rottenberg, S. (2018). The CST Complex Mediates End Protection at Double-Strand Breaks and Promotes PARP Inhibitor Sensitivity in BRCA1-Deficient Cells. Cell Rep 23, 2107-2118.

Barlow, J.H., Faryabi, R.B., Callen, E., Wong, N., Malhowski, A., Chen, H.T., Gutierrez-Cruz, G., Sun, H.W., McKinnon, P., Wright, G., Casellas, R., Robbiani, D.F., Staudt, L., Fernandez-Capetillo, O., and Nussenzweig, A. (2013). Identification of early replicating fragile sites that contribute to genome instability. Cell 152, 620-632.

Baskar, R., Lee, K.A., Yeo, R., and Yeoh, K.W. (2012). Cancer and radiation therapy: current advances and future directions. Int J Med Sci 9, 193-199.

Bednarek, A.K., Laflin, K.J., Daniel, R.L., Liao, Q., Hawkins, K.A., and Aldaz, C.M. (2000). WWOX, a Novel WW Domain-containing Protein Mapping to Human Chromosome 16q23.3–24.1, a Region Frequently Affected in Breast Cancer. Cancer Research 60, 2140-2145.

Belotserkovskaya, R., Raga Gil, E., Lawrence, N., Butler, R., Clifford, G., Wilson, M.D., and Jackson, S.P. (2020). PALB2 chromatin recruitment restores homologous recombination in BRCA1-deficient cells depleted of 53BP1. Nat Commun 11, 819.

Berti, M., Cortez, D., and Lopes, M. (2020). The plasticity of DNA replication forks in response to clinically relevant genotoxic stress. Nat Rev Mol Cell Biol 21, 633-651.

Bhat, K.P., and Cortez, D. (2018). RPA and RAD51: fork reversal, fork protection, and genome stability. Nat Struct Mol Biol 25, 446-453.

Bhowmick, R., Minocherhomji, S., and Hickson, I.D. (2016). RAD52 Facilitates Mitotic DNA Synthesis Following Replication Stress. Mol Cell 64, 1117-1126.

Blackford, A.N., and Jackson, S.P. (2017). ATM, ATR, and DNA-PK: The Trinity at the Heart of the DNA Damage Response. Mol Cell 66, 801-817.

Boersma, V., Moatti, N., Segura-Bayona, S., Peuscher, M.H., van der Torre, J., Wevers, B.A., Orthwein, A., Durocher, D., and Jacobs, J.J.L. (2015). MAD2L2 controls DNA repair at telomeres and DNA breaks by inhibiting 5' end resection. Nature 521, 537-540.

Bracht, J.W.P., Karachaliou, N., Bivona, T., Lanman, R.B., Faull, I., Nagy, R.J., Drozdowskyj, A., Berenguer, J., Fernandez-Bruno, M., Molina-Vila, M.A., and Rosell, R. (2019). BRAF Mutations Classes I, II, and III in NSCLC Patients Included in the SLLIP Trial: The Need for a New Pre-Clinical Treatment Rationale. Cancers (Basel) 11.

Brison, O., Gnan, S., Azar, D., Schmidt, M., Koundrioukoff, S., El-Hilali, S., Jaszczyszyn, Y., Lachages, A.-M., Thermes, C., Chen, C.-L., and Debatisse, M.

(2020). Unscheduled origin building in S-phase upon tight CDK1 inhibition suppresses CFS instability. bioRxiv, 2020.2011.2019.390054.

Bryant, H.E., Schultz, N., Thomas, H.D., Parker, K.M., Flower, D., Lopez, E., Kyle, S., Meuth, M., Curtin, N.J., and Helleday, T. (2005). Specific killing of BRCA2-deficient tumours with inhibitors of poly(ADP-ribose) polymerase. Nature 434, 913-917.

Bugreev, D.V., and Mazin, A.V. (2004). Ca2+ activates human homologous recombination protein Rad51 by modulating its ATPase activity. Proc Natl Acad Sci U S A 101, 9988-9993.

Bunting, S.F., Callen, E., Wong, N., Chen, H.T., Polato, F., Gunn, A., Bothmer, A., Feldhahn, N., Fernandez-Capetillo, O., Cao, L., Xu, X., Deng, C.X., Finkel, T., Nussenzweig, M., Stark, J.M., and Nussenzweig, A. (2010). 53BP1 inhibits homologous recombination in Brca1-deficient cells by blocking resection of DNA breaks. Cell 141, 243-254.

Burdette, D.L., Monroe, K.M., Sotelo-Troha, K., Iwig, J.S., Eckert, B., Hyodo, M., Hayakawa, Y., and Vance, R.E. (2011). STING is a direct innate immune sensor of cyclic di-GMP. Nature 478, 515-518.

Byun, T.S., Pacek, M., Yee, M.C., Walter, J.C., and Cimprich, K.A. (2005). Functional uncoupling of MCM helicase and DNA polymerase activities activates the ATR-dependent checkpoint. Genes Dev 19, 1040-1052.

Caldecott, K.W. (2008). Single-strand break repair and genetic disease. Nat Rev Genet 9, 619-631.

Canman, C.E., Lim, D.S., Cimprich, K.A., Taya, Y., Tamai, K., Sakaguchi, K., Appella, E., Kastan, M.B., and Siliciano, J.D. (1998). Activation of the ATM kinase by ionizing radiation and phosphorylation of p53. Science 281, 1677-1679.

Ceccaldi, R., Rondinelli, B., and D'Andrea, A.D. (2016). Repair Pathway Choices and Consequences at the Double-Strand Break. Trends Cell Biol 26, 52-64.

Chabanon, R.M., Muirhead, G., Krastev, D.B., Adam, J., Morel, D., Garrido, M., Lamb, A., Henon, C., Dorvault, N., Rouanne, M., Marlow, R., Bajrami, I., Cardenosa, M.L., Konde, A., Besse, B., Ashworth, A., Pettitt, S.J., Haider, S., Marabelle, A., Tutt, A.N., Soria, J.C., Lord, C.J., and Postel-Vinay, S. (2019). PARP inhibition enhances tumor cell-intrinsic immunity in ERCC1-deficient non-small cell lung cancer. J Clin Invest 129, 1211-1228.

Chan, K.L., North, P.S., and Hickson, I.D. (2007). BLM is required for faithful chromosome segregation and its localization defines a class of ultrafine anaphase bridges. EMBO J 26, 3397-3409.

Chan, K.L., Palmai-Pallag, T., Ying, S., and Hickson, I.D. (2009). Replication stress induces sister-chromatid bridging at fragile site loci in mitosis. Nat Cell Biol 11, 753-760.

Chan, Y.W., Fugger, K., and West, S.C. (2018). Unresolved recombination intermediates lead to ultra-fine anaphase bridges, chromosome breaks and aberrations. Nat Cell Biol 20, 92-103.

Chang, H.H.Y., Pannunzio, N.R., Adachi, N., and Lieber, M.R. (2017). Non-homologous DNA end joining and alternative pathways to double-strand break repair. Nat Rev Mol Cell Biol 18, 495-506.

Chapman, J.R., Barral, P., Vannier, J.B., Borel, V., Steger, M., Tomas-Loba, A., Sartori, A.A., Adams, I.R., Batista, F.D., and Boulton, S.J. (2013). RIF1 is essential for 53BP1-dependent nonhomologous end joining and suppression of DNA double-strand break resection. Mol Cell 49, 858-871.

Chappidi, N., Nascakova, Z., Boleslavska, B., Zellweger, R., Isik, E., Andrs, M., Menon, S., Dobrovolna, J., Balbo Pogliano, C., Matos, J., Porro, A., Lopes, M., and Janscak, P. (2020). Fork Cleavage-Religation Cycle and Active Transcription Mediate Replication Restart after Fork Stalling at Co-transcriptional R-Loops. Mol Cell 77, 528-541 e528.

Ciccia, A., Nimonkar, A.V., Hu, Y., Hajdu, I., Achar, Y.J., Izhar, L., Petit, S.A., Adamson, B., Yoon, J.C., Kowalczykowski, S.C., Livingston, D.M., Haracska, L., and Elledge, S.J. (2012). Polyubiquitinated PCNA recruits the ZRANB3 translocase to maintain genomic integrity after replication stress. Mol Cell 47, 396-409.

Cleaver, J.E., Lam, E.T., and Revet, I. (2009). Disorders of nucleotide excision repair: the genetic and molecular basis of heterogeneity. Nat Rev Genet 10, 756-768.

Coquel, F., Silva, M.J., Techer, H., Zadorozhny, K., Sharma, S., Nieminuszczy, J., Mettling, C., Dardillac, E., Barthe, A., Schmitz, A.L., Promonet, A., Cribier, A., Sarrazin, A., Niedzwiedz, W., Lopez, B., Costanzo, V., Krejci, L., Chabes, A., Benkirane, M., Lin, Y.L., and Pasero, P. (2018). SAMHD1 acts at stalled replication forks to prevent interferon induction. Nature 557, 57-61.

Costantino, L., Sotiriou, S.K., Rantala, J.K., Magin, S., Mladenov, E., Helleday, T., Haber, J.E., Iliakis, G., Kallioniemi, O.P., and Halazonetis, T.D. (2014). Break-induced replication repair of damaged forks induces genomic duplications in human cells. Science 343, 88-91.

Couch, F.B., Bansbach, C.E., Driscoll, R., Luzwick, J.W., Glick, G.G., Betous, R., Carroll, C.M., Jung, S.Y., Qin, J., Cimprich, K.A., and Cortez, D. (2013). ATR phosphorylates SMARCAL1 to prevent replication fork collapse. Genes Dev 27, 1610-1623.

Dagg, R.A., Zonderland, G., Puig Lombardi, L., Rossetti, G.G., Groelly, F.J., Barroso, S., Tacconi, E.M.C., Wright, B., Lockstone, H., Aguilera, A., Halazonetis, T.D., and Tarsounas, M. (under revision). A transcription-based mechanism for oncogene-induced lethality in BRCA1/2-deficient cells.

Das, P.M., and Singal, R. (2004). DNA methylation and cancer. J Clin Oncol 22, 4632-4642.

De Magis, A., Manzo, S.G., Russo, M., Marinello, J., Morigi, R., Sordet, O., and Capranico, G. (2019). DNA damage and genome instability by G-quadruplex ligands are mediated by R loops in human cancer cells. Proc Natl Acad Sci U S A 116, 816-825.

Debatisse, M., and Rosselli, F. (2019). A journey with common fragile sites: From S phase to telophase. Genes Chromosomes Cancer 58, 305-316.

Deng, L., Wu, R.A., Sonneville, R., Kochenova, O.V., Labib, K., Pellman, D., and Walter, J.C. (2019). Mitotic CDK Promotes Replisome Disassembly, Fork Breakage, and Complex DNA Rearrangements. Mol Cell 73, 915-929 e916.

Dev, H., Chiang, T.W., Lescale, C., de Krijger, I., Martin, A.G., Pilger, D., Coates, J., Sczaniecka-Clift, M., Wei, W., Ostermaier, M., Herzog, M., Lam, J., Shea, A., Demir, M., Wu, Q., Yang, F., Fu, B., Lai, Z., Balmus, G., Belotserkovskaya, R., Serra, V., O'Connor, M.J., Bruna, A., Beli, P., Pellegrini, L., Caldas, C., Deriano, L., Jacobs, J.J.L., Galanty, Y., and Jackson, S.P. (2018). Shieldin complex promotes DNA end-joining and counters homologous recombination in BRCA1-null cells. Nat Cell Biol 20, 954-965.

Di Virgilio, M., Callen, E., Yamane, A., Zhang, W., Jankovic, M., Gitlin, A.D., Feldhahn, N., Resch, W., Oliveira, T.Y., Chait, B.T., Nussenzweig, A., Casellas, R., Robbiani, D.F., and Nussenzweig, M.C. (2013). Rif1 prevents resection of DNA breaks and promotes immunoglobulin class switching. Science 339, 711-715.

Ding, L., Kim, H.J., Wang, Q., Kearns, M., Jiang, T., Ohlson, C.E., Li, B.B., Xie, S., Liu, J.F., Stover, E.H., Howitt, B.E., Bronson, R.T., Lazo, S., Roberts, T.M., Freeman, G.J., Konstantinopoulos, P.A., Matulonis, U.A., and Zhao, J.J. (2018). PARP Inhibition Elicits STING-Dependent Antitumor Immunity in Brca1-Deficient Ovarian Cancer. Cell Rep 25, 2972-2980 e2975.

Duda, H., Arter, M., Gloggnitzer, J., Teloni, F., Wild, P., Blanco, M.G., Altmeyer, M., and Matos, J. (2016). A Mechanism for Controlled Breakage of Under-replicated Chromosomes during Mitosis. Dev Cell 39, 740-755.

Ehlen, A., Martin, C., Miron, S., Julien, M., Theillet, F.X., Ropars, V., Sessa, G., Beaurepere, R., Boucherit, V., Duchambon, P., El Marjou, A., Zinn-Justin, S., and Carreira, A. (2020). Proper chromosome alignment depends on BRCA2 phosphorylation by PLK1. Nat Commun 11, 1819.

Ehlen, A., Sessa, G., Zinn-Justin, S., and Carreira, A. (2021). The phospho-dependent role of BRCA2 on the maintenance of chromosome integrity. Cell Cycle 20, 731-741.

Ehrlich, M. (2002). DNA methylation in cancer: too much, but also too little. Oncogene 21, 5400-5413.

El Achkar, E., Gerbault-Seureau, M., Muleris, M., Dutrillaux, B., and Debatisse, M. (2005). Premature condensation induces breaks at the interface of early and late replicating chromosome bands bearing common fragile sites. Proc Natl Acad Sci U S A 102, 18069-18074.

Elledge, S.J., and Amon, A. (2002). The BRCA1 suppressor hypothesis: an explanation for the tissue-specific tumor development in BRCA1 patients. Cancer Cell 1, 129-132.

Erdal, E., Haider, S., Rehwinkel, J., Harris, A.L., and McHugh, P.J. (2017). A prosurvival DNA damage-induced cytoplasmic interferon response is mediated by end resection factors and is limited by Trex1. Genes Dev 31, 353-369.

Escribano-Diaz, C., Orthwein, A., Fradet-Turcotte, A., Xing, M., Young, J.T., Tkac, J., Cook, M.A., Rosebrock, A.P., Munro, M., Canny, M.D., Xu, D., and Durocher, D. (2013). A cell cycle-dependent regulatory circuit composed of 53BP1-RIF1 and BRCA1-CtIP controls DNA repair pathway choice. Mol Cell 49, 872-883.

Farmer, H., McCabe, N., Lord, C.J., Tutt, A.N., Johnson, D.A., Richardson, T.B., Santarosa, M., Dillon, K.J., Hickson, I., Knights, C., Martin, N.M., Jackson, S.P., Smith, G.C., and Ashworth, A. (2005). Targeting the DNA repair defect in BRCA mutant cells as a therapeutic strategy. Nature 434, 917-921.

Feng, W., and Jasin, M. (2017). BRCA2 suppresses replication stress-induced mitotic and G1 abnormalities through homologous recombination. Nat Commun 8, 525.

Fu, X.Y., Kessler, D.S., Veals, S.A., Levy, D.E., and Darnell, J.E., Jr. (1990). ISGF3, the transcriptional activator induced by interferon alpha, consists of multiple interacting polypeptide chains. Proc Natl Acad Sci U S A 87, 8555-8559.

Fugger, K., Mistrik, M., Neelsen, K.J., Yao, Q., Zellweger, R., Kousholt, A.N., Haahr, P., Chu, W.K., Bartek, J., Lopes, M., Hickson, I.D., and Sorensen, C.S. (2015). FBH1 Catalyzes Regression of Stalled Replication Forks. Cell Rep 10, 1749-1757.

Gadaleta, M.C., and Noguchi, E. (2017). Regulation of DNA Replication through Natural Impediments in the Eukaryotic Genome. Genes (Basel) 8.

Gao, P., Ascano, M., Wu, Y., Barchet, W., Gaffney, B.L., Zillinger, T., Serganov, A.A., Liu, Y., Jones, R.A., Hartmann, G., Tuschl, T., and Patel, D.J. (2013). Cyclic [G(2',5')pA(3',5')p] is the metazoan second messenger produced by DNA-activated cyclic GMP-AMP synthase. Cell 153, 1094-1107.

Gartler, S.M. (2006). The chromosome number in humans: a brief history. Nat Rev Genet 7, 655-660.

Genomes Project, C., Abecasis, G.R., Altshuler, D., Auton, A., Brooks, L.D., Durbin, R.M., Gibbs, R.A., Hurles, M.E., and McVean, G.A. (2010). A map of human genome variation from population-scale sequencing. Nature 467, 1061-1073.

Genomes Project, C., Auton, A., Brooks, L.D., Durbin, R.M., Garrison, E.P., Kang, H.M., Korbel, J.O., Marchini, J.L., McCarthy, S., McVean, G.A., and Abecasis, G.R. (2015). A global reference for human genetic variation. Nature 526, 68-74.

Germano, G., Lamba, S., Rospo, G., Barault, L., Magri, A., Maione, F., Russo, M., Crisafulli, G., Bartolini, A., Lerda, G., Siravegna, G., Mussolin, B., Frapolli, R., Montone, M., Morano, F., de Braud, F., Amirouchene-Angelozzi, N., Marsoni, S., D'Incalci, M., Orlandi, A., Giraudo, E., Sartore-Bianchi, A., Siena, S., Pietrantonio, F., Di Nicolantonio, F., and Bardelli, A. (2017). Inactivation of DNA repair triggers neoantigen generation and impairs tumour growth. Nature 552, 116-120.

Ghezraoui, H., Oliveira, C., Becker, J.R., Bilham, K., Moralli, D., Anzilotti, C., Fischer, R., Deobagkar-Lele, M., Sanchiz-Calvo, M., Fueyo-Marcos, E., Bonham, S., Kessler, B.M., Rottenberg, S., Cornall, R.J., Green, C.M., and Chapman, J.R. (2018). 53BP1 cooperation with the REV7-shieldin complex underpins DNA structure-specific NHEJ. Nature 560, 122-127.

Ghosh, M., Saha, S., Bettke, J., Nagar, R., Parrales, A., Iwakuma, T., van der Velden, A.W.M., and Martinez, L.A. (2021). Mutant p53 suppresses innate immune signaling to promote tumorigenesis. Cancer Cell 39, 494-508 e495.

Giannattasio, M., Zwicky, K., Follonier, C., Foiani, M., Lopes, M., and Branzei, D. (2014). Visualization of recombination-mediated damage bypass by template switching. Nat Struct Mol Biol 21, 884-892.

Gilbert, E.S. (2009). Ionising radiation and cancer risks: what have we learned from epidemiology? Int J Radiat Biol 85, 467-482.

Glover, T.W., Berger, C., Coyle, J., and Echo, B. (1984). DNA polymerase alpha inhibition by aphidicolin induces gaps and breaks at common fragile sites in human chromosomes. Hum Genet 67, 136-142.

Glover, T.W., Wilson, T.E., and Arlt, M.F. (2017). Fragile sites in cancer: more than meets the eye. Nat Rev Cancer 17, 489-501.

Gonzalez, H., Hagerling, C., and Werb, Z. (2018). Roles of the immune system in cancer: from tumor initiation to metastatic progression. Genes Dev 32, 1267-1284.

Graber-Feesl, C.L., Pederson, K.D., Aney, K.J., and Shima, N. (2019). Mitotic DNA Synthesis Is Differentially Regulated between Cancer and Noncancerous Cells. Mol Cancer Res 17, 1687-1698.

Gratia, M., Rodero, M.P., Conrad, C., Bou Samra, E., Maurin, M., Rice, G.I., Duffy, D., Revy, P., Petit, F., Dale, R.C., Crow, Y.J., Amor-Gueret, M., and Manel, N. (2019). Bloom syndrome protein restrains innate immune sensing of micronuclei by cGAS. J Exp Med 216, 1199-1213.

Gupta, R., Somyajit, K., Narita, T., Maskey, E., Stanlie, A., Kremer, M., Typas, D., Lammers, M., Mailand, N., Nussenzweig, A., Lukas, J., and Choudhary, C. (2018). DNA Repair Network Analysis Reveals Shieldin as a Key Regulator of NHEJ and PARP Inhibitor Sensitivity. Cell 173, 972-988 e923.

Hakem, R., de la Pompa, J.L., Elia, A., Potter, J., and Mak, T.W. (1997). Partial rescue of Brca1 (5-6) early embryonic lethality by p53 or p21 null mutation. Nat Genet 16, 298-302.

Hamperl, S., Bocek, M.J., Saldivar, J.C., Swigut, T., and Cimprich, K.A. (2017). Transcription-Replication Conflict Orientation Modulates R-Loop Levels and Activates Distinct DNA Damage Responses. Cell 170, 774-786 e719.

Hanada, K., Budzowska, M., Davies, S.L., van Drunen, E., Onizawa, H., Beverloo, H.B., Maas, A., Essers, J., Hickson, I.D., and Kanaar, R. (2007). The structure-specific endonuclease Mus81 contributes to replication restart by generating double-strand DNA breaks. Nat Struct Mol Biol 14, 1096-1104.

Hansen, R.S., Thomas, S., Sandstrom, R., Canfield, T.K., Thurman, R.E., Weaver, M., Dorschner, M.O., Gartler, S.M., and Stamatoyannopoulos, J.A. (2010). Sequencing newly replicated DNA reveals widespread plasticity in human replication timing. Proc Natl Acad Sci U S A 107, 139-144.

Harrigan, J.A., Belotserkovskaya, R., Coates, J., Dimitrova, D.S., Polo, S.E., Bradshaw, C.R., Fraser, P., and Jackson, S.P. (2011). Replication stress induces 53BP1-containing OPT domains in G1 cells. J Cell Biol 193, 97-108.

Hartlova, A., Erttmann, S.F., Raffi, F.A., Schmalz, A.M., Resch, U., Anugula, S., Lienenklaus, S., Nilsson, L.M., Kroger, A., Nilsson, J.A., Ek, T., Weiss, S., and Gekara, N.O. (2015). DNA damage primes the type I interferon system via the cytosolic DNA sensor STING to promote anti-microbial innate immunity. Immunity 42, 332-343.

Heijink, A.M., Talens, F., Jae, L.T., van Gijn, S.E., Fehrmann, R.S.N., Brummelkamp, T.R., and van Vugt, M. (2019). BRCA2 deficiency instigates cGAS-mediated inflammatory signaling and confers sensitivity to tumor necrosis factor-alpha-mediated cytotoxicity. Nat Commun 10, 100.

Helmrich, A., Ballarino, M., and Tora, L. (2011). Collisions between replication and transcription complexes cause common fragile site instability at the longest human genes. Mol Cell 44, 966-977.

Higuchi, T., Flies, D.B., Marjon, N.A., Mantia-Smaldone, G., Ronner, L., Gimotty, P.A., and Adams, S.F. (2015). CTLA-4 Blockade Synergizes Therapeutically with PARP Inhibition in BRCA1-Deficient Ovarian Cancer. Cancer Immunol Res 3, 1257-1268.

Hollestelle, A., Nagel, J.H., Smid, M., Lam, S., Elstrodt, F., Wasielewski, M., Ng, S.S., French, P.J., Peeters, J.K., Rozendaal, M.J., Riaz, M., Koopman, D.G., Ten Hagen, T.L., de Leeuw, B.H., Zwarthoff, E.C., Teunisse, A., van der Spek, P.J., Klijn, J.G., Dinjens, W.N., Ethier, S.P., Clevers, H., Jochemsen, A.G., den Bakker, M.A., Foekens, J.A., Martens, J.W., and Schutte, M. (2010). Distinct gene mutation profiles among luminal-type and basal-type breast cancer cell lines. Breast Cancer Res Treat 121, 53-64.

Hormozian, F., Schmitt, J.G., Sagulenko, E., Schwab, M., and Savelyeva, L. (2007). FRA1E common fragile site breaks map within a 370kilobase pair region and disrupt the dihydropyrimidine dehydrogenase gene (DPYD). Cancer Lett 246, 82-91.

Hsieh, P., and Zhang, Y. (2017). The Devil is in the details for DNA mismatch repair. Proc Natl Acad Sci U S A 114, 3552-3554.

Hustedt, N., and Durocher, D. (2016). The control of DNA repair by the cell cycle. Nat Cell Biol 19, 1-9.

Improta, T., Schindler, C., Horvath, C.M., Kerr, I.M., Stark, G.R., and Darnell, J.E., Jr. (1994). Transcription factor ISGF-3 formation requires phosphorylated Stat91 protein, but Stat113 protein is phosphorylated independently of Stat91 protein. Proc Natl Acad Sci U S A 91, 4776-4780.

Ishikawa, H., Ma, Z., and Barber, G.N. (2009). STING regulates intracellular DNA-mediated, type I interferon-dependent innate immunity. Nature 461, 788-792.

Jiang, W., Crowe, J.L., Liu, X., Nakajima, S., Wang, Y., Li, C., Lee, B.J., Dubois, R.L., Liu, C., Yu, X., Lan, L., and Zha, S. (2015). Differential phosphorylation of DNA-PKcs regulates the interplay between end-processing and end-ligation during nonhomologous end-joining. Mol Cell 58, 172-185.

Jin, P., Hardy, S., and Morgan, D.O. (1998). Nuclear localization of cyclin B1 controls mitotic entry after DNA damage. J Cell Biol 141, 875-885.

Johnson, N., Li, Y.C., Walton, Z.E., Cheng, K.A., Li, D., Rodig, S.J., Moreau, L.A., Unitt, C., Bronson, R.T., Thomas, H.D., Newell, D.R., D'Andrea, A.D., Curtin, N.J., Wong, K.K., and Shapiro, G.I. (2011). Compromised CDK1 activity sensitizes BRCA-proficient cancers to PARP inhibition. Nat Med 17, 875-882.

Kathe, S.D., Shen, G.P., and Wallace, S.S. (2004). Single-stranded breaks in DNA but not oxidative DNA base damages block transcriptional elongation by RNA polymerase II in HeLa cell nuclear extracts. J Biol Chem 279, 18511-18520.

Kile, A.C., Chavez, D.A., Bacal, J., Eldirany, S., Korzhnev, D.M., Bezsonova, I., Eichman, B.F., and Cimprich, K.A. (2015). HLTF's Ancient HIRAN Domain Binds 3' DNA Ends to Drive Replication Fork Reversal. Mol Cell 58, 1090-1100.

Kolinjivadi, A.M., Sannino, V., De Antoni, A., Zadorozhny, K., Kilkenny, M., Techer, H., Baldi, G., Shen, R., Ciccia, A., Pellegrini, L., Krejci, L., and Costanzo,

V. (2017). Smarcal1-Mediated Fork Reversal Triggers Mre11-Dependent Degradation of Nascent DNA in the Absence of Brca2 and Stable Rad51 Nucleofilaments. Mol Cell 67, 867-881 e867.

Kunkel, T.A. (2004). DNA replication fidelity. J Biol Chem 279, 16895-16898.

Kunkel, T.A., and Erie, D.A. (2015). Eukaryotic Mismatch Repair in Relation to DNA Replication. Annu Rev Genet 49, 291-313.

Lai, X., Broderick, R., Bergoglio, V., Zimmer, J., Badie, S., Niedzwiedz, W., Hoffmann, J.S., and Tarsounas, M. (2017). MUS81 nuclease activity is essential for replication stress tolerance and chromosome segregation in BRCA2-deficient cells. Nat Commun 8, 15983.

Lambert, S., Mizuno, K., Blaisonneau, J., Martineau, S., Chanet, R., Freon, K., Murray, J.M., Carr, A.M., and Baldacci, G. (2010). Homologous recombination restarts blocked replication forks at the expense of genome rearrangements by template exchange. Mol Cell 39, 346-359.

Le Beau, M.M., Rassool, F.V., Neilly, M.E., Espinosa, R., 3rd, Glover, T.W., Smith, D.I., and McKeithan, T.W. (1998). Replication of a common fragile site, FRA3B, occurs late in S phase and is delayed further upon induction: implications for the mechanism of fragile site induction. Hum Mol Genet 7, 755-761.

Le, D.T., Uram, J.N., Wang, H., Bartlett, B.R., Kemberling, H., Eyring, A.D., Skora, A.D., Luber, B.S., Azad, N.S., Laheru, D., Biedrzycki, B., Donehower, R.C., Zaheer, A., Fisher, G.A., Crocenzi, T.S., Lee, J.J., Duffy, S.M., Goldberg, R.M., de la Chapelle, A., Koshiji, M., Bhaijee, F., Huebner, T., Hruban, R.H., Wood, L.D., Cuka, N., Pardoll, D.M., Papadopoulos, N., Kinzler, K.W., Zhou, S., Cornish, T.C., Taube, J.M., Anders, R.A., Eshleman, J.R., Vogelstein, B., and Diaz, L.A., Jr. (2015). PD-1 Blockade in Tumors with Mismatch-Repair Deficiency. N Engl J Med 372, 2509-2520.

Le Tallec, B., Dutrillaux, B., Lachages, A.M., Millot, G.A., Brison, O., and Debatisse, M. (2011). Molecular profiling of common fragile sites in human fibroblasts. Nat Struct Mol Biol 18, 1421-1423.

Le Tallec, B., Millot, G.A., Blin, M.E., Brison, O., Dutrillaux, B., and Debatisse, M. (2013). Common fragile site profiling in epithelial and erythroid cells reveals that most recurrent cancer deletions lie in fragile sites hosting large genes. Cell Rep 4, 420-428.

Lemacon, D., Jackson, J., Quinet, A., Brickner, J.R., Li, S., Yazinski, S., You, Z., Ira, G., Zou, L., Mosammaparast, N., and Vindigni, A. (2017). MRE11 and EXO1 nucleases degrade reversed forks and elicit MUS81-dependent fork rescue in BRCA2-deficient cells. Nat Commun 8, 860.

Letessier, A., Millot, G.A., Koundrioukoff, S., Lachages, A.M., Vogt, N., Hansen, R.S., Malfoy, B., Brison, O., and Debatisse, M. (2011). Cell-type-specific replication initiation programs set fragility of the FRA3B fragile site. Nature 470, 120-123.

Lezaja, A., and Altmeyer, M. (2020). Dealing with DNA lesions: When one cell cycle is not enough. Curr Opin Cell Biol 70, 27-36.

Li, X., and Heyer, W.D. (2008). Homologous recombination in DNA repair and DNA damage tolerance. Cell Res 18, 99-113.

Liu, D., Keijzers, G., and Rasmussen, L.J. (2017). DNA mismatch repair and its many roles in eukaryotic cells. Mutat Res 773, 174-187.

Lomonosov, M., Anand, S., Sangrithi, M., Davies, R., and Venkitaraman, A.R. (2003). Stabilization of stalled DNA replication forks by the BRCA2 breast cancer susceptibility protein. Genes Dev 17, 3017-3022.

Lord, C.J., and Ashworth, A. (2017). PARP inhibitors: Synthetic lethality in the clinic. Science 355, 1152-1158.

Lukas, C., Savic, V., Bekker-Jensen, S., Doil, C., Neumann, B., Pedersen, R.S., Grofte, M., Chan, K.L., Hickson, I.D., Bartek, J., and Lukas, J. (2011). 53BP1 nuclear bodies form around DNA lesions generated by mitotic transmission of chromosomes under replication stress. Nat Cell Biol 13, 243-253.

Macheret, M., Bhowmick, R., Sobkowiak, K., Padayachy, L., Mailler, J., Hickson, I.D., and Halazonetis, T.D. (2020). High-resolution mapping of mitotic DNA synthesis regions and common fragile sites in the human genome through direct sequencing. Cell Res 30, 997-1008.

Macheret, M., and Halazonetis, T.D. (2018). Intragenic origins due to short G1 phases underlie oncogene-induced DNA replication stress. Nature 555, 112-116.

Mackenzie, K.J., Carroll, P., Lettice, L., Tarnauskaite, Z., Reddy, K., Dix, F., Revuelta, A., Abbondati, E., Rigby, R.E., Rabe, B., Kilanowski, F., Grimes, G., Fluteau, A., Devenney, P.S., Hill, R.E., Reijns, M.A., and Jackson, A.P. (2016). Ribonuclease H2 mutations induce a cGAS/STING-dependent innate immune response. EMBO J 35, 831-844.

Mackenzie, K.J., Carroll, P., Martin, C.A., Murina, O., Fluteau, A., Simpson, D.J., Olova, N., Sutcliffe, H., Rainger, J.K., Leitch, A., Osborn, R.T., Wheeler, A.P., Nowotny, M., Gilbert, N., Chandra, T., Reijns, M.A.M., and Jackson, A.P. (2017). cGAS surveillance of micronuclei links genome instability to innate immunity. Nature 548, 461-465.

Marston, A.L., and Amon, A. (2004). Meiosis: cell-cycle controls shuffle and deal. Nat Rev Mol Cell Biol 5, 983-997.

Maya-Mendoza, A., Moudry, P., Merchut-Maya, J.M., Lee, M., Strauss, R., and Bartek, J. (2018). High speed of fork progression induces DNA replication stress and genomic instability. Nature 559, 279-284.

Mazina, O.M., and Mazin, A.V. (2004). Human Rad54 protein stimulates DNA strand exchange activity of hRad51 protein in the presence of Ca2+. J Biol Chem 279, 52042-52051.

Mazloum, N., and Holloman, W.K. (2009). Brh2 promotes a template-switching reaction enabling recombinational bypass of lesions during DNA synthesis. Mol Cell 36, 620-630.

McFall, T., Schomburg, N.K., Rossman, K.L., and Stites, E.C. (2020). Discernment between candidate mechanisms for KRAS G13D colorectal cancer sensitivity to EGFR inhibitors. Cell Commun Signal 18, 179.

Meselson, M., and Stahl, F.W. (1958). The Replication of DNA in Escherichia Coli. Proc Natl Acad Sci U S A 44, 671-682.

Miglietta, G., Russo, M., and Capranico, G. (2020). G-quadruplex-R-loop interactions and the mechanism of anticancer G-quadruplex binders. Nucleic Acids Res 48, 11942-11957.

Mijic, S., Zellweger, R., Chappidi, N., Berti, M., Jacobs, K., Mutreja, K., Ursich, S., Ray Chaudhuri, A., Nussenzweig, A., Janscak, P., and Lopes, M. (2017). Replication fork reversal triggers fork degradation in BRCA2-defective cells. Nat Commun 8, 859.

Minocherhomji, S., Ying, S., Bjerregaard, V.A., Bursomanno, S., Aleliunaite, A., Wu, W., Mankouri, H.W., Shen, H., Liu, Y., and Hickson, I.D. (2015). Replication stress activates DNA repair synthesis in mitosis. Nature 528, 286-290.

Mirman, Z., Lottersberger, F., Takai, H., Kibe, T., Gong, Y., Takai, K., Bianchi, A., Zimmermann, M., Durocher, D., and de Lange, T. (2018). 53BP1-RIF1-shieldin counteracts DSB resection through CST- and Polalpha-dependent fill-in. Nature 560, 112-116.

Moiseeva, T.N., Qian, C., Sugitani, N., Osmanbeyoglu, H.U., and Bakkenist, C.J. (2019). WEE1 kinase inhibitor AZD1775 induces CDK1 kinase-dependent origin firing in unperturbed G1- and S-phase cells. Proc Natl Acad Sci U S A 116, 23891-23893.

Mouron, S., Rodriguez-Acebes, S., Martinez-Jimenez, M.I., Garcia-Gomez, S., Chocron, S., Blanco, L., and Mendez, J. (2013). Repriming of DNA synthesis at stalled replication forks by human PrimPol. Nat Struct Mol Biol 20, 1383-1389.

Naim, V., and Rosselli, F. (2009). The FANC pathway and BLM collaborate during mitosis to prevent micro-nucleation and chromosome abnormalities. Nat Cell Biol 11, 761-768.

Naim, V., Wilhelm, T., Debatisse, M., and Rosselli, F. (2013). ERCC1 and MUS81-EME1 promote sister chromatid separation by processing late replication intermediates at common fragile sites during mitosis. Nat Cell Biol 15, 1008-1015.

Noordermeer, S.M., Adam, S., Setiaputra, D., Barazas, M., Pettitt, S.J., Ling, A.K., Olivieri, M., Alvarez-Quilon, A., Moatti, N., Zimmermann, M., Annunziato, S., Krastev, D.B., Song, F., Brandsma, I., Frankum, J., Brough, R., Sherker, A., Landry, S., Szilard, R.K., Munro, M.M., McEwan, A., Goullet de Rugy, T., Lin, Z.Y., Hart, T., Moffat, J., Gingras, A.C., Martin, A., van Attikum, H., Jonkers, J., Lord, C.J., Rottenberg, S., and Durocher, D. (2018). The shieldin complex mediates 53BP1-dependent DNA repair. Nature 560, 117-121.

Noordermeer, S.M., and van Attikum, H. (2019). PARP Inhibitor Resistance: A Tug-of-War in BRCA-Mutated Cells. Trends Cell Biol 29, 820-834.

Ogawa, T., Yu, X., Shinohara, A., and Egelman, E.H. (1993). Similarity of the yeast RAD51 filament to the bacterial RecA filament. Science 259, 1896-1899.

Ohta, M., Inoue, H., Cotticelli, M.G., Kastury, K., Baffa, R., Palazzo, J., Siprashvili, Z., Mori, M., McCue, P., Druck, T., Croce, C.M., and Huebner, K. (1996). The FHIT Gene, Spanning the Chromosome 3p14.2 Fragile Site and Renal Carcinoma–Associated t(3;8) Breakpoint, Is Abnormal in Digestive Tract Cancers. Cell 84, 587-597.

Okamoto, Y., Iwasaki, W.M., Kugou, K., Takahashi, K.K., Oda, A., Sato, K., Kobayashi, W., Kawai, H., Sakasai, R., Takaori-Kondo, A., Yamamoto, T., Kanemaki, M.T., Taoka, M., Isobe, T., Kurumizaka, H., Innan, H., Ohta, K., Ishiai, M., and Takata, M. (2018). Replication stress induces accumulation of FANCD2 at central region of large fragile genes. Nucleic Acids Res 46, 2932-2944.

Olivieri, M., Cho, T., Alvarez-Quilon, A., Li, K., Schellenberg, M.J., Zimmermann, M., Hustedt, N., Rossi, S.E., Adam, S., Melo, H., Heijink, A.M., Sastre-Moreno, G., Moatti, N., Szilard, R.K., McEwan, A., Ling, A.K., Serrano-Benitez, A., Ubhi, T., Feng, S., Pawling, J., Delgado-Sainz, I., Ferguson, M.W., Dennis, J.W., Brown, G.W., Cortes-Ledesma, F., Williams, R.S., Martin, A., Xu, D., and Durocher, D. (2020). A Genetic Map of the Response to DNA Damage in Human Cells. Cell 182, 481-496 e421.

Ozer, O., and Hickson, I.D. (2018). Pathways for maintenance of telomeres and common fragile sites during DNA replication stress. Open Biol 8.

Ozeri-Galai, E., Lebofsky, R., Rahat, A., Bester, A.C., Bensimon, A., and Kerem, B. (2011). Failure of origin activation in response to fork stalling leads to chromosomal instability at fragile sites. Mol Cell 43, 122-131.

Palma, A., Pugliese, G.M., Murfuni, I., Marabitti, V., Malacaria, E., Rinalducci, S., Minoprio, A., Sanchez, M., Mazzei, F., Zolla, L., Franchitto, A., and Pichierri, P.

(2018). Phosphorylation by CK2 regulates MUS81/EME1 in mitosis and after replication stress. Nucleic Acids Res 46, 5109-5124.

Pantelidou, C., Sonzogni, O., De Oliveria Taveira, M., Mehta, A.K., Kothari, A., Wang, D., Visal, T., Li, M.K., Pinto, J., Castrillon, J.A., Cheney, E.M., Bouwman, P., Jonkers, J., Rottenberg, S., Guerriero, J.L., Wulf, G.M., and Shapiro, G.I. (2019). PARP Inhibitor Efficacy Depends on CD8(+) T-cell Recruitment via Intratumoral STING Pathway Activation in BRCA-Deficient Models of Triple-Negative Breast Cancer. Cancer Discov 9, 722-737.

Park, J.M., Yang, S.W., Yu, K.R., Ka, S.H., Lee, S.W., Seol, J.H., Jeon, Y.J., and Chung, C.H. (2014). Modification of PCNA by ISG15 plays a crucial role in termination of error-prone translesion DNA synthesis. Mol Cell 54, 626-638.

Parkes, E.E., Walker, S.M., Taggart, L.E., McCabe, N., Knight, L.A., Wilkinson, R., McCloskey, K.D., Buckley, N.E., Savage, K.I., Salto-Tellez, M., McQuaid, S., Harte, M.T., Mullan, P.B., Harkin, D.P., and Kennedy, R.D. (2017). Activation of STING-Dependent Innate Immune Signaling By S-Phase-Specific DNA Damage in Breast Cancer. J Natl Cancer Inst 109.

Pellegrini, L., Yu, D.S., Lo, T., Anand, S., Lee, M., Blundell, T.L., and Venkitaraman, A.R. (2002). Insights into DNA recombination from the structure of a RAD51-BRCA2 complex. Nature 420, 287-293.

Pentzold, C., Shah, S.A., Hansen, N.R., Le Tallec, B., Seguin-Orlando, A., Debatisse, M., Lisby, M., and Oestergaard, V.H. (2018). FANCD2 binding identifies conserved fragile sites at large transcribed genes in avian cells. Nucleic Acids Res 46, 1280-1294.

Petermann, E., Orta, M.L., Issaeva, N., Schultz, N., and Helleday, T. (2010). Hydroxyurea-stalled replication forks become progressively inactivated and require two different RAD51-mediated pathways for restart and repair. Mol Cell 37, 492-502.

Petropoulos, M., Champeris Tsaniras, S., Taraviras, S., and Lygerou, Z. (2019). Replication Licensing Aberrations, Replication Stress, and Genomic Instability. Trends Biochem Sci 44, 752-764.

Petukhova, G., Stratton, S., and Sung, P. (1998). Catalysis of homologous DNA pairing by yeast Rad51 and Rad54 proteins. Nature 393, 91-94.

Piberger, A.L., Bowry, A., Kelly, R.D.W., Walker, A.K., Gonzalez-Acosta, D., Bailey, L.J., Doherty, A.J., Mendez, J., Morris, J.R., Bryant, H.E., and Petermann, E. (2020). PrimPol-dependent single-stranded gap formation mediates homologous recombination at bulky DNA adducts. Nat Commun 11, 5863.

Pinto-Fernandez, A., Salio, M., Partridge, T., Chen, J., Vere, G., Greenwood, H., Olie, C.S., Damianou, A., Scott, H.C., Pegg, H.J., Chiarenza, A., Diaz-Saez, L., Smith, P., Gonzalez-Lopez, C., Patel, B., Anderton, E., Jones, N., Hammonds, T.R., Huber, K., Muschel, R., Borrow, P., Cerundolo, V., and Kessler, B.M. (2020). Deletion of the deISGylating enzyme USP18 enhances tumour cell antigenicity and radiosensitivity. Br J Cancer.

Priego Moreno, S., Jones, R.M., Poovathumkadavil, D., Scaramuzza, S., and Gambus, A. (2019). Mitotic replisome disassembly depends on TRAIP ubiquitin ligase activity. Life Sci Alliance 2.

Quinet, A., Tirman, S., Cybulla, E., Meroni, A., and Vindigni, A. (2021). To skip or not to skip: choosing repriming to tolerate DNA damage. Mol Cell.

Quinet, A., Tirman, S., Jackson, J., Svikovic, S., Lemacon, D., Carvajal-Maldonado, D., Gonzalez-Acosta, D., Vessoni, A.T., Cybulla, E., Wood, M., Tavis, S., Batista, L.F.Z., Mendez, J., Sale, J.E., and Vindigni, A. (2020). PRIMPOL-Mediated Adaptive Response Suppresses Replication Fork Reversal in BRCA-Deficient Cells. Mol Cell 77, 461-474 e469.

Ramirez, F., Ryan, D.P., Gruning, B., Bhardwaj, V., Kilpert, F., Richter, A.S., Heyne, S., Dundar, F., and Manke, T. (2016). deepTools2: a next generation web server for deep-sequencing data analysis. Nucleic Acids Res 44, W160-165.

Raso, M.C., Djoric, N., Walser, F., Hess, S., Schmid, F.M., Burger, S., Knobeloch, K.P., and Penengo, L. (2020). Interferon-stimulated gene 15 accelerates replication fork progression inducing chromosomal breakage. J Cell Biol 219.

Rastogi, R.P., Richa, Kumar, A., Tyagi, M.B., and Sinha, R.P. (2010). Molecular mechanisms of ultraviolet radiation-induced DNA damage and repair. J Nucleic Acids 2010, 592980.

Reisländer, T., Groelly, F.J., and Tarsounas, M. (2020). DNA Damage and Cancer Immunotherapy: A STING in the Tale. Mol Cell 80, 21-28.

Reisländer, T., Lombardi, E.P., Groelly, F.J., Miar, A., Porru, M., Di Vito, S., Wright, B., Lockstone, H., Biroccio, A., Harris, A., Londono-Vallejo, A., and Tarsounas, M. (2019). BRCA2 abrogation triggers innate immune responses potentiated by treatment with PARP inhibitors. Nat Commun 10, 3143.

Rodriguez, R., Miller, K.M., Forment, J.V., Bradshaw, C.R., Nikan, M., Britton, S., Oelschlaegel, T., Xhemalce, B., Balasubramanian, S., and Jackson, S.P. (2012). Small-molecule-induced DNA damage identifies alternative DNA structures in human genes. Nat Chem Biol 8, 301-310.

Rodriguez, R., Muller, S., Yeoman, J.A., Trentesaux, C., Riou, J.F., and Balasubramanian, S. (2008). A novel small molecule that alters shelterin integrity and triggers a DNA-damage response at telomeres. J Am Chem Soc 130, 15758-15759.

Rondinelli, B., Gogola, E., Yucel, H., Duarte, A.A., van de Ven, M., van der Sluijs, R., Konstantinopoulos, P.A., Jonkers, J., Ceccaldi, R., Rottenberg, S., and

D'Andrea, A.D. (2017). EZH2 promotes degradation of stalled replication forks by recruiting MUS81 through histone H3 trimethylation. Nat Cell Biol 19, 1371-1378.

Roth, D.B., and Craig, N.L. (1998). VDJ recombination: a transposase goes to work. Cell 94, 411-414.

Ruggiano, A., and Ramadan, K. (2021). The Trinity of SPRTN Protease Regulation. Trends Biochem Sci 46, 2-4.

Saldivar, J.C., Cortez, D., and Cimprich, K.A. (2017). The essential kinase ATR: ensuring faithful duplication of a challenging genome. Nat Rev Mol Cell Biol 18, 622-636.

Saldivar, J.C., Hamperl, S., Bocek, M.J., Chung, M., Bass, T.E., Cisneros-Soberanis, F., Samejima, K., Xie, L., Paulson, J.R., Earnshaw, W.C., Cortez, D., Meyer, T., and Cimprich, K.A. (2018). An intrinsic S/G2 checkpoint enforced by ATR. Science 361, 806-810.

Sale, J.E. (2013). Translesion DNA synthesis and mutagenesis in eukaryotes. Cold Spring Harb Perspect Biol 5, a012708.

Sartori, A.A., Lukas, C., Coates, J., Mistrik, M., Fu, S., Bartek, J., Baer, R., Lukas, J., and Jackson, S.P. (2007). Human CtIP promotes DNA end resection. Nature 450, 509-514.

Sasanuma, H., Tsuda, M., Morimoto, S., Saha, L.K., Rahman, M.M., Kiyooka, Y., Fujiike, H., Cherniack, A.D., Itou, J., Callen Moreu, E., Toi, M., Nakada, S., Tanaka, H., Tsutsui, K., Yamada, S., Nussenzweig, A., and Takeda, S. (2018). BRCA1 ensures genome integrity by eliminating estrogen-induced pathological topoisomerase II-DNA complexes. Proc Natl Acad Sci U S A 115, E10642-E10651.

Schatz, D.G., and Ji, Y. (2011). Recombination centres and the orchestration of V(D)J recombination. Nat Rev Immunol 11, 251-263.

Schindler, C., Shuai, K., Prezioso, V.R., and Darnell, J.E., Jr. (1992). Interferon-dependent tyrosine phosphorylation of a latent cytoplasmic transcription factor. Science 257, 809-813.

Schlacher, K. (2017). PARPi focus the spotlight on replication fork protection in cancer. Nat Cell Biol 19, 1309-1310.

Schlacher, K., Christ, N., Siaud, N., Egashira, A., Wu, H., and Jasin, M. (2011). Double-strand break repair-independent role for BRCA2 in blocking stalled replication fork degradation by MRE11. Cell 145, 529-542.

Schlacher, K., Wu, H., and Jasin, M. (2012). A distinct replication fork protection pathway connects Fanconi anemia tumor suppressors to RAD51-BRCA1/2. Cancer Cell 22, 106-116.

Schneider, W.M., Chevillotte, M.D., and Rice, C.M. (2014). Interferon-stimulated genes: a complex web of host defenses. Annu Rev Immunol 32, 513-545.

Schoonen, P.M., Talens, F., Stok, C., Gogola, E., Heijink, A.M., Bouwman, P., Foijer, F., Tarsounas, M., Blatter, S., Jonkers, J., Rottenberg, S., and van Vugt, M. (2017). Progression through mitosis promotes PARP inhibitor-induced cytotoxicity in homologous recombination-deficient cancer cells. Nat Commun 8, 15981.

Schumacher, T.N., Scheper, W., and Kvistborg, P. (2019). Cancer Neoantigens. Annu Rev Immunol 37, 173-200.

Scully, R., Panday, A., Elango, R., and Willis, N.A. (2019). DNA double-strand break repair-pathway choice in somatic mammalian cells. Nat Rev Mol Cell Biol 20, 698-714.

Sen, T., Rodriguez, B.L., Chen, L., Corte, C.M.D., Morikawa, N., Fujimoto, J., Cristea, S., Nguyen, T., Diao, L., Li, L., Fan, Y., Yang, Y., Wang, J., Glisson, B.S., Wistuba, II, Sage, J., Heymach, J.V., Gibbons, D.L., and Byers, L.A. (2019). Targeting DNA Damage Response Promotes Antitumor Immunity through STING-Mediated T-cell Activation in Small Cell Lung Cancer. Cancer Discov 9, 646-661.

Sharan, S.K., Morimatsu, M., Albrecht, U., Lim, D.S., Regel, E., Dinh, C., Sands, A., Eichele, G., Hasty, P., and Bradley, A. (1997). Embryonic lethality and radiation hypersensitivity mediated by Rad51 in mice lacking Brca2. Nature 386, 804-810.

Sharma, P., and Allison, J.P. (2015). The future of immune checkpoint therapy. Science 348, 56-61.

Shuai, K., Ziemiecki, A., Wilks, A.F., Harpur, A.G., Sadowski, H.B., Gilman, M.Z., and Darnell, J.E. (1993). Polypeptide signalling to the nucleus through tyrosine phosphorylation of Jak and Stat proteins. Nature 366, 580-583.

Silvennoinen, O., Ihle, J.N., Schlessinger, J., and Levy, D.E. (1993). Interferon-induced nuclear signalling by Jak protein tyrosine kinases. Nature 366, 583-585.

Skaug, B., and Chen, Z.J. (2010). Emerging role of ISG15 in antiviral immunity. Cell 143, 187-190.

Song, Z., Liu, F., and Zhang, J. (2017). Targeting NRAS(Q61K) mutant delays tumor growth and angiogenesis in non-small cell lung cancer. Am J Cancer Res 7, 831-844.

Sonneville, R., Bhowmick, R., Hoffmann, S., Mailand, N., Hickson, I.D., and Labib, K. (2019). TRAIP drives replisome disassembly and mitotic DNA repair synthesis at sites of incomplete DNA replication. Elife 8.

Sotiriou, S.K., Kamileri, I., Lugli, N., Evangelou, K., Da-Re, C., Huber, F., Padayachy, L., Tardy, S., Nicati, N.L., Barriot, S., Ochs, F., Lukas, C., Lukas, J., Gorgoulis, V.G., Scapozza, L., and Halazonetis, T.D. (2016). Mammalian RAD52 Functions in Break-Induced Replication Repair of Collapsed DNA Replication Forks. Mol Cell 64, 1127-1134.

Spies, J., Lukas, C., Somyajit, K., Rask, M.B., Lukas, J., and Neelsen, K.J. (2019). 53BP1 nuclear bodies enforce replication timing at under-replicated DNA to limit heritable DNA damage. Nat Cell Biol 21, 487-497.

Sun, L., Wu, J., Du, F., Chen, X., and Chen, Z.J. (2013). Cyclic GMP-AMP synthase is a cytosolic DNA sensor that activates the type I interferon pathway. Science 339, 786-791.

Sung, P. (1994). Catalysis of ATP-dependent homologous DNA pairing and strand exchange by yeast RAD51 protein. Science 265, 1241-1243.

Sutherland, G.R. (2003). Rare fragile sites. Cytogenet Genome Res 100, 77-84.

Taanman, J.-W. (1999). The mitochondrial genome: structure, transcription, translation and replication. Biochimica et Biophysica Acta (BBA) - Bioenergetics 1410, 103-123.

Tacconi, E.M., Badie, S., De Gregoriis, G., Reisländer, T., Lai, X., Porru, M., Folio, C., Moore, J., Kopp, A., Baguna Torres, J., Sneddon, D., Green, M., Dedic, S., Lee, J.W., Batra, A.S., Rueda, O.M., Bruna, A., Leonetti, C., Caldas, C., Cornelissen, B., Brino, L., Ryan, A., Biroccio, A., and Tarsounas, M. (2019).

Chlorambucil targets BRCA1/2-deficient tumours and counteracts PARP inhibitor resistance. EMBO Mol Med 11, e9982.

Tacconi, E.M., Lai, X., Folio, C., Porru, M., Zonderland, G., Badie, S., Michl, J., Sechi, I., Rogier, M., Matia Garcia, V., Batra, A.S., Rueda, O.M., Bouwman, P., Jonkers, J., Ryan, A., Reina-San-Martin, B., Hui, J., Tang, N., Bruna, A., Biroccio, A., and Tarsounas, M. (2017). BRCA1 and BRCA2 tumor suppressors protect against endogenous acetaldehyde toxicity. EMBO Mol Med 9, 1398-1414.

Tadi, S.K., Tellier-Lebegue, C., Nemoz, C., Drevet, P., Audebert, S., Roy, S., Meek, K., Charbonnier, J.B., and Modesti, M. (2016). PAXX Is an Accessory c-NHEJ Factor that Associates with Ku70 and Has Overlapping Functions with XLF. Cell Rep 17, 541-555.

Taglialatela, A., Alvarez, S., Leuzzi, G., Sannino, V., Ranjha, L., Huang, J.W., Madubata, C., Anand, R., Levy, B., Rabadan, R., Cejka, P., Costanzo, V., and Ciccia, A. (2017). Restoration of Replication Fork Stability in BRCA1- and BRCA2-Deficient Cells by Inactivation of SNF2-Family Fork Remodelers. Mol Cell 68, 414-430 e418.

Tan, S.L.W., Chadha, S., Liu, Y., Gabasova, E., Perera, D., Ahmed, K., Constantinou, S., Renaudin, X., Lee, M., Aebersold, R., and Venkitaraman, A.R. (2017). A Class of Environmental and Endogenous Toxins Induces BRCA2 Haploinsufficiency and Genome Instability. Cell 169, 1105-1118 e1115.

Tanaka, Y., and Chen, Z.J. (2012). STING specifies IRF3 phosphorylation by TBK1 in the cytosolic DNA signaling pathway. Sci Signal 5, ra20.

Tarsounas, M., and Sung, P. (2020). The antitumorigenic roles of BRCA1-BARD1 in DNA repair and replication. Nat Rev Mol Cell Biol 21, 284-299.

Tubbs, A., and Nussenzweig, A. (2017). Endogenous DNA Damage as a Source of Genomic Instability in Cancer. Cell 168, 644-656.

Tubbs, A., Sridharan, S., van Wietmarschen, N., Maman, Y., Callen, E., Stanlie, A., Wu, W., Wu, X., Day, A., Wong, N., Yin, M., Canela, A., Fu, H., Redon, C., Pruitt, S.C., Jaszczyszyn, Y., Aladjem, M.I., Aplan, P.D., Hyrien, O., and Nussenzweig, A. (2018). Dual Roles of Poly(dA:dT) Tracts in Replication Initiation and Fork Collapse. Cell 174, 1127-1142 e1119.

Vaisman, A., and Woodgate, R. (2017). Translesion DNA polymerases in eukaryotes: what makes them tick? Crit Rev Biochem Mol Biol 52, 274-303.

Velazquez, L., Fellous, M., Stark, G.R., and Pellegrini, S. (1992). A protein tyrosine kinase in the interferon αβ signaling pathway. Cell 70, 313-322.

Vujanovic, M., Krietsch, J., Raso, M.C., Terraneo, N., Zellweger, R., Schmid, J.A., Taglialatela, A., Huang, J.W., Holland, C.L., Zwicky, K., Herrador, R., Jacobs, H., Cortez, D., Ciccia, A., Penengo, L., and Lopes, M. (2017). Replication Fork Slowing and Reversal upon DNA Damage Require PCNA Polyubiquitination and ZRANB3 DNA Translocase Activity. Mol Cell 67, 882-890 e885.

Wang, Z., Sun, K., Xiao, Y., Feng, B., Mikule, K., Ma, X., Feng, N., Vellano, C.P., Federico, L., Marszalek, J.R., Mills, G.B., Hanke, J., Ramaswamy, S., and Wang, J. (2019). Niraparib activates interferon signaling and potentiates anti-PD-1 antibody efficacy in tumor models. Sci Rep 9, 1853.

Weston, R., Peeters, H., and Ahel, D. (2012). ZRANB3 is a structure-specific ATP-dependent endonuclease involved in replication stress response. Genes Dev 26, 1558-1572.

White, D.E., Negorev, D., Peng, H., Ivanov, A.V., Maul, G.G., and Rauscher, F.J., 3rd (2006). KAP1, a novel substrate for PIKK family members, colocalizes with

numerous damage response factors at DNA lesions. Cancer Res 66, 11594-11599.

Wilson, T.E., Arlt, M.F., Park, S.H., Rajendran, S., Paulsen, M., Ljungman, M., and Glover, T.W. (2015). Large transcription units unify copy number variants and common fragile sites arising under replication stress. Genome Res 25, 189-200.

Wohlschlegel, J.A., Dwyer, B.T., Dhar, S.K., Cvetic, C., Walter, J.C., and Dutta, A. (2000). Inhibition of eukaryotic DNA replication by geminin binding to Cdt1. Science 290, 2309-2312.

Wooster, R., Bignell, G., Lancaster, J., Swift, S., Seal, S., Mangion, J., Collins, N., Gregory, S., Gumbs, C., and Micklem, G. (1995). Identification of the breast cancer susceptibility gene BRCA2. Nature 378, 789-792.

Wooster, R., Neuhausen, S.L., Mangion, J., Quirk, Y., Ford, D., Collins, N., Nguyen, K., Seal, S., Tran, T., Averill, D., and et al. (1994). Localization of a breast cancer susceptibility gene, BRCA2, to chromosome 13q12-13. Science 265, 2088-2090.

Wu, J., Sun, L., Chen, X., Du, F., Shi, H., Chen, C., and Chen, Z.J. (2013). Cyclic GMP-AMP is an endogenous second messenger in innate immune signaling by cytosolic DNA. Science 339, 826-830.

Wu, X., and Zhang, Y. (2017). TET-mediated active DNA demethylation: mechanism, function and beyond. Nat Rev Genet 18, 517-534.

Xia, B., Sheng, Q., Nakanishi, K., Ohashi, A., Wu, J., Christ, N., Liu, X., Jasin, M., Couch, F.J., and Livingston, D.M. (2006). Control of BRCA2 cellular and clinical functions by a nuclear partner, PALB2. Mol Cell 22, 719-729.

Xu, G., Chapman, J.R., Brandsma, I., Yuan, J., Mistrik, M., Bouwman, P., Bartkova, J., Gogola, E., Warmerdam, D., Barazas, M., Jaspers, J.E., Watanabe, K., Pieterse, M., Kersbergen, A., Sol, W., Celie, P.H.N., Schouten, P.C., van den Broek, B., Salman, A., Nieuwland, M., de Rink, I., de Ronde, J., Jalink, K., Boulton, S.J., Chen, J., van Gent, D.C., Bartek, J., Jonkers, J., Borst, P., and Rottenberg, S. (2015). REV7 counteracts DNA double-strand break resection and affects PARP inhibition. Nature 521, 541-544.

Xu, H., Di Antonio, M., McKinney, S., Mathew, V., Ho, B., O'Neil, N.J., Santos, N.D., Silvester, J., Wei, V., Garcia, J., Kabeer, F., Lai, D., Soriano, P., Banath, J., Chiu, D.S., Yap, D., Le, D.D., Ye, F.B., Zhang, A., Thu, K., Soong, J., Lin, S.C., Tsai, A.H., Osako, T., Algara, T., Saunders, D.N., Wong, J., Xian, J., Bally, M.B., Brenton, J.D., Brown, G.W., Shah, S.P., Cescon, D., Mak, T.W., Caldas, C., Stirling, P.C., Hieter, P., Balasubramanian, S., and Aparicio, S. (2017a). CX-5461 is a DNA G-quadruplex stabilizer with selective lethality in BRCA1/2 deficient tumours. Nat Commun 8, 14432.

Xu, J., Zhao, L., Xu, Y., Zhao, W., Sung, P., and Wang, H.W. (2017b). Cryo-EM structures of human RAD51 recombinase filaments during catalysis of DNA-strand exchange. Nat Struct Mol Biol 24, 40-46.

Yang, H., Jeffrey, P.D., Miller, J., Kinnucan, E., Sun, Y., Thoma, N.H., Zheng, N., Chen, P.L., Lee, W.H., and Pavletich, N.P. (2002). BRCA2 function in DNA binding and recombination from a BRCA2-DSS1-ssDNA structure. Science 297, 1837-1848.

Yanow, S.K., Lygerou, Z., and Nurse, P. (2001). Expression of Cdc18/Cdc6 and Cdt1 during G2 phase induces initiation of DNA replication. EMBO J 20, 4648-4656.

Ying, S., Minocherhomji, S., Chan, K.L., Palmai-Pallag, T., Chu, W.K., Wass, T., Mankouri, H.W., Liu, Y., and Hickson, I.D. (2013). MUS81 promotes common fragile site expression. Nat Cell Biol 15, 1001-1007.

Zellweger, R., Dalcher, D., Mutreja, K., Berti, M., Schmid, J.A., Herrador, R., Vindigni, A., and Lopes, M. (2015). Rad51-mediated replication fork reversal is a global response to genotoxic treatments in human cells. J Cell Biol 208, 563-579.

Zeman, M.K., and Cimprich, K.A. (2014). Causes and consequences of replication stress. Nat Cell Biol 16, 2-9.

Zhang, F., Fan, Q., Ren, K., and Andreassen, P.R. (2009). PALB2 functionally connects the breast cancer susceptibility proteins BRCA1 and BRCA2. Mol Cancer Res 7, 1110-1118.

Zhao, W., Steinfeld, J.B., Liang, F., Chen, X., Maranon, D.G., Jian Ma, C., Kwon, Y., Rao, T., Wang, W., Sheng, C., Song, X., Deng, Y., Jimenez-Sainz, J., Lu, L., Jensen, R.B., Xiong, Y., Kupfer, G.M., Wiese, C., Greene, E.C., and Sung, P. (2017). BRCA1-BARD1 promotes RAD51-mediated homologous DNA pairing. Nature 550, 360-365.

Zimmer, J., Tacconi, E.M.C., Folio, C., Badie, S., Porru, M., Klare, K., Tumiati, M., Markkanen, E., Halder, S., Ryan, A., Jackson, S.P., Ramadan, K., Kuznetsov, S.G., Biroccio, A., Sale, J.E., and Tarsounas, M. (2016). Targeting BRCA1 and BRCA2 Deficiencies with G-Quadruplex-Interacting Compounds. Mol Cell 61, 449-460.

Zimmermann, M., Lottersberger, F., Buonomo, S.B., Sfeir, A., and de Lange, T. (2013). 53BP1 regulates DSB repair using Rif1 to control 5' end resection. Science 339, 700-704.

Zitvogel, L., Galluzzi, L., Kepp, O., Smyth, M.J., and Kroemer, G. (2015). Type I interferons in anticancer immunity. Nat Rev Immunol 15, 405-414.

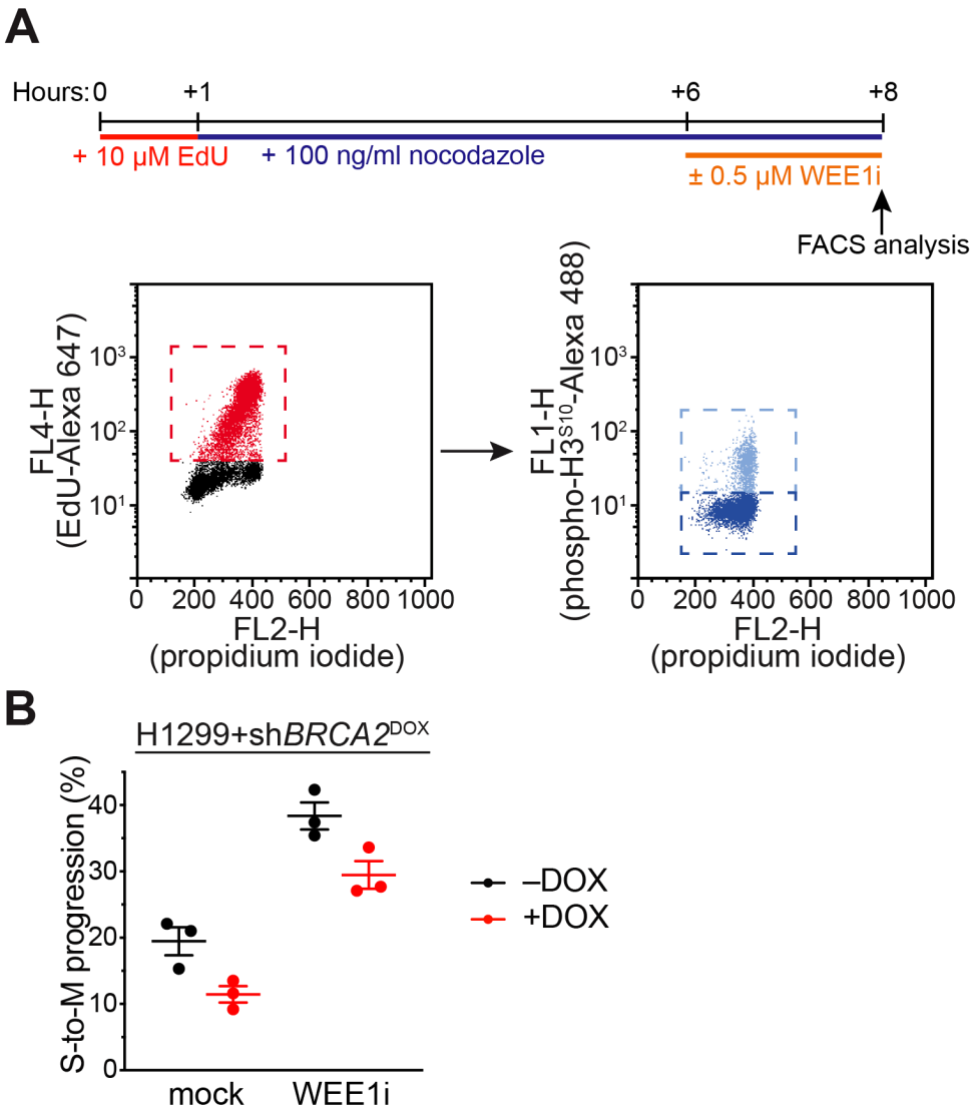
Zlotorynski, E., Rahat, A., Skaug, J., Ben-Porat, N., Ozeri, E., Hershberg, R., Levi, A., Scherer, S.W., Margalit, H., and Kerem, B. (2003). Molecular basis for expression of common and rare fragile sites. Mol Cell Biol 23, 7143-7151.

Zong, D., Adam, S., Wang, Y., Sasanuma, H., Callen, E., Murga, M., Day, A., Kruhlak, M.J., Wong, N., Munro, M., Ray Chaudhuri, A., Karim, B., Xia, B., Takeda, S., Johnson, N., Durocher, D., and Nussenzweig, A. (2019). BRCA1 Haploinsufficiency Is Masked by RNF168-Mediated Chromatin Ubiquitylation. Mol Cell 73, 1267-1281 e1267.

Zong, D., Callen, E., Pegoraro, G., Lukas, C., Lukas, J., and Nussenzweig, A. (2015). Ectopic expression of RNF168 and 53BP1 increases mutagenic but not physiological non-homologous end joining. Nucleic Acids Res 43, 4950-4961.

Zuo, C., Sheng, X., Ma, M., Xia, M., and Ouyang, L. (2016). ISG15 in the tumorigenesis and treatment of cancer: An emerging role in malignancies of the digestive system. Oncotarget 7, 74393-74409.

Appendix



Supplementary Fig. 1

(**A**) Asynchronous BRCA2-proficient (-DOX) or BRCA2-deficient (+DOX) H1299+sh*BRCA2*^{DOX} cells were treated as indicated and subject to flow cytometry analysis. The gating strategy to determine the S-to-M progression is shown. (**B**) Percentage of phosphorylated Histone H3-positive cells amongst EdU-positive cells using the strategy shown in (B). Bars represent mean values and SEM of *n* = 3 independent experiments. Dots represent value obtained from each experiment.